

**MEASUREMENT OF SINGLE-PHASE FLUID FLOW BY PULSED
ULTRASOUND TECHNIQUE USING CROSS-CORRELATION**

Thesis

submitted in partial fulfilment of the requirements
for the degree of

Doctor of Philosophy

by

Harshal B. Nemade



Department of Electrical Engineering
Indian Institute of Technology, Bombay
Powai, Mumbai 400 076, India

January 2000

Harshal B. Nemade, *Measurement of Single-Phase Fluid Flow by Pulsed Ultrasound Technique Using Cross-Correlation*, Ph.D. Thesis, Department of Electrical Engineering, Indian Institute of Technology, Bombay, 1999.

Supervisors: Prof. T. Anjaneyulu and Prof. P. C. Pandey.

ABSTRACT

In a cross-correlation flowmeter, disturbances in the flow are sensed at two locations separated by a known distance along a pipe. The transit time of the disturbances between the two locations is measured as the delay corresponding to the peak in the cross-correlation function of the two signals. Thus, the flow velocity is equal to the distance divided by the transit time. The measurement is unaffected by variations in the fluid properties and environmental factors.

The present work is aimed at applying cross-correlation principle for non-invasive flow measurement of single-phase fluid, like clean water, using ultrasonic sensing. The turbulent eddies in single-phase fluid flow cause phase modulation of a continuous wave ultrasonic beam sent across the pipe diameter. The problems of variations in the standing waves formed inside the pipe, the acoustic short circuit noise through the pipe wall, and multiple reflections within the pipe have been studied. In order to avoid the problems faced in the use of continuous wave ultrasound, the use of pulsed ultrasound has been investigated and a new technique for sensing naturally available turbulence in the flow has been developed. The turbulence patterns sensed at two locations on the pipe can be cross-correlated and flow velocity can be obtained from the position of the peak in the cross-correlation function.

The technique facilitates sensing variations in the time of flight of ultrasonic pulses, caused by the turbulent velocity components. The velocity component of turbulence perpendicular to the flow axis is sensed by two ultrasonic transducers mounted diametrically opposite on the pipe. The transducers transmit ultrasonic pulses at the same instant and in opposite directions. The pulses after passing through the fluid in the pipe are received by the same pair of transducers and are fed to a differential amplifier. In the presence of turbulence, the instants of arrival of the two pulses are different and the magnitude of differential amplifier output is a function of the turbulent velocity component. The repetition rate of pulse transmission is set higher than twice the maximum frequency component of the turbulence signal, and a sample-and-hold circuit is used after the differential amplifier to reconstruct the turbulence signal.

The technique has been supported by developing a theoretical model of the process and carrying out a numerical simulation of the flowmeter based on the theoretical model. The effect of dispersion in turbulence pattern and quantization on the peak in the cross-correlation function has been studied. The applicability of the technique has been verified experimentally by building the hardware, and employing it for the measurement of water flow non-intrusively on a PVC pipe, in a water circulation system for various sensor spacings.

CONTENTS

	ABSTRACT	i
	CONTENTS	ii
	ACKNOWLEDGMENT	iv
	LIST OF SYMBOLS AND ABBREVIATIONS	v
	LIST OF FIGURES	vii
	LIST OF TABLES	x
Chapter 1	INTRODUCTION	1
1.1	Problem Overview	2
1.2	Research Objectives	3
1.3	Scope of the Research	3
1.4	Thesis Outline	4
Chapter 2	CROSS-CORRELATION TECHNIQUE WITH CONTINUOUS WAVE ULTRASOUND	5
2.1	Flow Measurement by Cross-Correlation	5
2.2	Flow Resolution and Effect of Sensor Spacing	8
2.3	Ultrasonic Sensing Methods	10
2.4	Continuous Wave Ultrasonic Sensing Techniques	11
2.5	Investigation of Standing Waves inside the Pipe	14
2.5.1	Experiment to confirm the presence of standing waves	14
2.5.2	Effect of variation in standing wave pattern	16
2.6	Investigation of Reflections within the Pipe Wall	20
2.7	Study of Acoustic Short Circuit through the Pipe Wall	23
2.7.1	Analysis and observation of acoustic short circuit noise	23
2.7.2	Diametrically opposite mounting	25
2.7.3	Receiver displaced by $\lambda/4$	27
2.7.4	Analysis for full contact of receiver	27
2.8	Conclusions	30
Chapter 3	A NEW TECHNIQUE FOR SENSING TURBULENCE BY PULSED ULTRASOUND	31
3.1	The Technique	31
3.2	Circuit Implementation of the Technique	33
3.2.1	Transmitter-receiver circuit	34
3.2.2	Sample-and-hold	36
3.2.3	Timing block	36
3.3	Sensing Water Currents in a Tank	37

3.4	Sensing Turbulence in Pipe	42
3.5	Flow Measurement by Cross-Correlation	49
Chapter 4	MODELING AND NUMERICAL SIMULATION	51
4.1	Relationship between Turbulence and Change in Time of Flight	52
4.2	Relationship between Sampled Differential Voltage and Change in Time of Flight	54
4.3	A Theoretical Model of Pulse Transmission and Reception	56
4.4	Numerical Simulation of the Turbulence Sensing Technique and Cross-Correlation	58
4.5	Simulation of Dispersion in Turbulence Pattern	60
4.6	Simulation of Effect of Quantization	62
Chapter 5	FLOW MEASUREMENT SET-UP AND EXPERIMENTAL RESULTS	66
5.1	Experimental Set-up	66
5.2	Measurement Results	71
5.3	Discussion	71
Chapter 6	SUMMARY AND CONCLUSIONS	87
Appendix A	ABSTRACT OF DATA SHEETS	92
A.1	LM733C Differential Video Amplifier	93
A.2	SHC605 High-Speed Operational Track-And-Hold Amplifier	94
A.3	SHC5320 High Speed Bipolar Monolithic Sample/ Hold Amplifier	95
Appendix B	SPECIFICATIONS OF THE SIGNAL ANALYZER <i>(Analogic model DATA6000 with plug in module 620)</i>	96
References		98
Synopsis		S-1

ACKNOWLEDGMENT

First and foremost I would like to record my sincere feelings of gratitude towards my supervisor Professor T. Anjaneyulu, who generously granted all the facilities required for the research since the beginning, and who persistently encouraged me to undertake the research all these years. I am deeply indebted to Professor Anjaneyulu for his kind and affectionate guidance during the entire period of my research.

The true source of inspiration for my work at every stage was my co-supervisor Professor P. C. Pandey. His involvement so invaluable to me in the day-to-day progress of the research is beyond the narrow capacity of this acknowledgment. The virtues Professor Pandey has transmitted in me will be a constant source of progress in my future life.

I am grateful to Professor S. D. Agashe whose precious instructions improved the quality of the work, and to Professors T. S. Rathore and C. P. Gadgil who have gone through the entire thesis and made many valuable suggestions.

The experimental work was possible with the support from Professors D. P. Roy and Ms. Usha Pawle, Department of Mechanical Engineering, who made some of the required equipment available. Many helpful suggestions were made by Professor Roy and by the staff of Fluid Power Engineering Laboratory, particularly Mr. S. Prakash, the Laboratory Superintendent. I sincerely thank them. I thank Professor G. G. Ray, Industrial Design Center, and Professor G. R. Shevare, Department of Aerospace Engineering, for offering their generous help.

I owe many thanks to the following colleagues and friends whose constructive criticism and suggestions were helpful in bringing quality to the research:

Santosh Inamdar (R.A.), C. Sathish Kumar (M.Tech.), Bhupendra Parmar (M.Tech.), Sudhir Gokhale (M.Tech.), Mandar Chitnis (R.A.), S. Balaji (M.Tech.).

Their constant company was of immense benefit to me. I am thankful to Vilas Rokade (M.Tech.) who helped me scanning some figures, and to my brother Janamejay (M.E., presently Ph.D. student at Regina University), for making me familiar with the MSOffice and helping me drawing some of the figures.

Thanks are due to Mr. L. D. Muntode and Mr. A. D. Apte, and other members of laboratory staff for their timely help and support.

It was indeed a privilege for me to work in the department of Electrical Engineering, and I consider myself fortunate to have received all the great values of scientific research in the high I. I. T. traditions.

The basic infrastructure for experimental work was possible due to the BRNS sponsored project undertaken by my supervisors. I take this opportunity to thank the authorities of BRNS, and to Mr. V. K. Chadda and Mr. R. K. Nigam of Electronics Systems Division, BARC for their support and useful discussions in the early phases of the project.

The genuine interest in my research by several participants in the IEEE-IMT Conference 1997, at Ottawa, Canada, particularly Professor Robert Gao (University of Massachusetts Amherst) and Dr. G. P. P. Gunarathne (The Robert Gordon University, UK) boosted my spirits considerably and I am very thankful to them.

Finally I wish to recognize the debt of the researchers in the field of ultrasonic flow measurement whose published work has guided me in my research.

LIST OF SYMBOLS AND ABBREVIATIONS

SYMBOLS

A	gain of differential amplifier
A_m	peak amplitude of a sinusoid
c	acoustic velocity in water
c_s	shear velocity of acoustic wave in steel
c_L	Longitudinal velocity of acoustic wave in steel
D	diameter of pipe
D_i	internal diameter of pipe
D_m	mean diameter of pipe
d	distance
f	frequency of ultrasound
h	thickness of pipe
$h(t)$	impulse response of transducer
j	discretized delay variable for cross-correlation function
k	constant
ℓ	length of pipe
L	sensor spacing
m	discretized time variable
n	integer, discretized time variable
$n(t)$	noise
$p(t)$	pressure wave
P	pressure amplitude
$p(t)$	excitation pulse given to transducers
$q(t)$	signal obtained at the output of a transducer
Q	volumetric flow
\bar{Q}	mean volumetric flow
Q_c	volumetric flow obtained by cross-correlation
Q_v	volumetric flow measured by venturimeter
r	radial distance
$r_{xy}(\tau)$	cross-correlation function of $x(t)$ and $y(t)$ as a function of delay τ in $y(t)$
Re	Reynolds number
$s(t)$	differential amplifier output
t	time
t_w	time of flight of ultrasound through water
t_{sc}	time taken by short circuit noise to reach the receiver
T	period of integration
T_s	sampling interval
u	mean linear flow velocity in the direction of pipe axis

v	turbulent velocity component perpendicular to pipe axis
$x(n)$	discretized turbulence signal sensed at upstream location
$x(t)$	turbulence signal sensed at upstream location
$y(n)$	discretized turbulence signal sensed at downstream location
$y(t)$	turbulence signal sensed at downstream location
$z(n)$	discretized noise
α	attenuation
β	normalizing factor for noise
δ	maximum deviation
$\delta(t)$	impulse function
ϕ	nominal pipe size
λ	acoustic wavelength
ν	kinematic viscosity of water
θ	phase angle
σ	standard deviation
$\bar{\sigma}$	mean of standard deviations
τ	delay variable for cross-correlation function
τ_m	position of the peak in the cross-correlation function
ω	angular frequency of a sinusoid
ζ	damping ratio

ABBREVIATIONS

ADC	analog-to-digital converter
CST	circuit for sensing turbulence
CMRR	common mode rejection ratio
DSP	digital signal processing
GI	galvanized iron
L	liter
min	minute, minimum
max	maximum
MS	mild steel
p-p	peak-to-peak
PC	personal computer
PLL	phase-locked loop
PRF	pulse repetition frequency
S/H	sample-and-hold amplifier
TOF	time of flight of ultrasonic pulse between transmitter and receiver

LIST OF FIGURES

Fig. 2-1	Schematic of flow measurement by cross-correlation.	7
Fig. 2-2	Graph of flow resolution $\Delta u/u$ versus τ_m for sampling interval of 1 ms.	9
Fig. 2-3	Effect of sensor spacing, L , on the peak in the cross-correlation function.	9
Fig. 2-4	Block diagram of a cross-correlation flowmeter using continuous wave ultrasound.	12
Fig. 2-5	Diagram showing sources of interference in continuous wave ultrasound application.	13
Fig. 2-6	The presence of standing waves observed in the magnitude response of a continuous wave transducer pair when mounted on a PVC pipe filled with water.	15
Fig. 2-7	Effect of variation in the standing wave pattern on the cross-correlation function.	17
Fig. 2-8	Possible receiver positions obtained by a phase-locked loop.	19
Fig. 2-9	Waveforms showing reflections within a pipe wall for transducers mounted diametrically opposite on a PVC pipe filled with water.	21
Fig. 2-10	Waveforms showing reflections within pipe wall for a GI pipe of outer diameter 76 mm and wall thickness 4.5 mm.	22
Fig. 2-11	Diagram showing acoustic short circuit path through the pipe wall.	24
Fig. 2-12	Waveforms showing acoustic short circuit noise and fluid-borne signal in two cases: (a) empty pipe; (b) pipe filled with water.	24
Fig. 2-13	Position of the receiver (displaced by $\lambda/4$ along the circumference of the pipe), in order to minimize acoustic short circuit noise.	26

Fig. 2-14	Acoustic short circuit path in two cases: (a) Receiver diametrically opposite to the transmitter; (b) Receiver displaced by $\lambda/4$ along the acoustic short circuit path.	26
Fig. 2-15	The graph of pressure amplitude of acoustic short circuit versus displacement of the receiver.	28
Fig. 2-16	Acoustic short circuit waveforms for the receiver in full contact with the pipe.	28
Fig. 3-1	Block diagram of the system used to sense turbulence using pulsed ultrasound.	32
Fig. 3-2	Circuit diagram of the system used to sense turbulence using pulsed ultrasound.	35
Fig. 3-3	Diagram of the set-up for sensing water currents in a tank.	38
Fig. 3-4	Input and output waveforms of the differential amplifier for still water.	39
Fig. 3-5	Expanded waveforms of Fig. 3-4.	40
Fig. 3-6	Differential amplifier output in three cases: (a) still water; (b) water current in one direction; (c) water current in the opposite direction.	41
Fig. 3-7	Waveforms for S/H#1.	43
Fig. 3-8	Expanded waveforms for S/H#1.	44
Fig. 3-9	Waveforms for S/H#2.	45
Fig. 3-10	Expanded waveforms for S/H#2.	46
Fig. 3-11	Turbulence signal in a flow pipe sensed by the system at various flow rates.	47
Fig. 3-12	The magnitude spectra of the turbulence signals shown in Fig. 3-11.	48
Fig. 3-13	Block diagram of the cross-correlation flowmeter based on ultrasonic sensing of turbulence.	50
Fig. 4-1	Effect of turbulent velocity component $v(r)$ on the velocity of the two ultrasonic pulses traveling in opposite directions.	53

Fig. 4-2	Received pulses and differential amplifier output.	55
Fig. 4-3	Model of ultrasonic pulse transmission and reception.	57
Fig. 4-4	Simulated impulse response $h(t)$ of the transducer.	59
Fig. 4-5	Results of simulation of the model given in Fig. 4-3.	59
Fig. 4-6	Results of cross-correlator simulation.	61
Fig. 4-7	Simulation of dispersion in turbulence to study its effect on the cross-correlation function.	61
Fig. 4-8	Output of the cross-correlator with random noise added in the turbulence signal obtained at the downstream sensor.	63
Fig. 4-9	Effect of quantization noise on the cross-correlator output, for various bits of quantization, n .	65
Fig. 5-1	Placement of ultrasonic transducers in the cross-correlation flowmeter.	67
Fig. 5-2	Block diagram of the experimental set-up used to measure flow by cross-correlation technique.	67
Fig. 5-3	Schematic of water circulation system.	69
Fig. 5-4	Graphs of average flow measured by cross-correlation flowmeter (\bar{Q}_C) versus flow measured by venturimeter (Q_V) for sensor spacings of 35 mm, 50 mm, 101 mm, 187 mm, 254 mm.	73
Fig. 5-5	Graphs of standard deviation of the turbulence transit time (σ_T) and standard deviation of the flow measured by cross-correlation (σ_{Q_C}), versus mean flow measured by cross-correlation (\bar{Q}_C) for the sensor spacings of 35 mm, 50 mm, 101 mm, 187 mm, 254 mm.	78

LIST OF TABLES

Table 5-1	The lower limit of flow for which water flow through a PVC pipe is turbulent.	70
Table 5-2	Measurement results showing volumetric flow Q_v measured by the venturimeter and mean volumetric flow \bar{Q}_c (measured by cross-correlation flowmeter assuming uniform flow profile) and its standard deviation σ_{Q_c} for sensor spacing of 187 mm.	72
Table 5-3	Standard deviation (σ) and maximum deviation (δ) from the linear best fit line, in the flow measured by cross-correlation technique for various sensor spacings (L).	83
Table 5-4	Mean values of standard deviation of transit time τ and standard deviation of flow rate Q , mean values of relative errors $\sigma_\tau/\bar{\tau}$ and σ_Q/\bar{Q} , for various sensor spacings over the flow range of 300–600 L/min.	84
Table 5-5	The range of linear flow (u) and volumetric flow (Q) that can be measured by the cross-correlation flowmeter for pipes of various diameters.	86

Chapter 1

INTRODUCTION

Various types of flowmeters based on well-established principles are available commercially. The flowmeters widely used in industry are the following [1]–[7]:

- Orifice meter and venturimeter based on variable pressure drop across an obstruction.
- Rotameter based on variable area, constant pressure drop across an obstruction.
- Mechanical flowmeters like positive displacement meter, turbine flow meter.
- Hot wire anemometer based on heat loss by convection.
- Electromagnetic flowmeter using Faraday's law of electromagnetic induction [5].
- Ultrasonic flowmeters measuring Doppler frequency shift and transit time.

With the advent of fast computing microelectronic circuits, flowmeters based on cross-correlation technique have become realizable [8]. The cross-correlation technique for flow measurement is based on determination of the transit time of a measurable disturbance moving with the flow over a known distance. The measurable properties, such as the variations in temperature, pressure, and capacitance are detected by appropriate sensors at two suitable locations along the flow stream. The position of the peak in the cross-correlation function of the signals sensed at the two locations gives the transit time of the disturbance pattern between the locations. The flow velocity is computed as the distance divided by the transit time. The major advantages of cross-correlation flow measurement are that the measurement is independent of the fluid properties, and that the sensors need not be linear and calibrated.

Ultrasonic sensing facilitates non-intrusive flow measurement, as the ultrasonic transducers can be clamped on to an existing pipe. The installation does not disturb the flow, neither do they obstruct the flow during operation, and the pressure drop due to the flowmeter is nil. Their maintenance is easy, and they are durable. Therefore, ultrasonic flowmeters have distinct advantage in corrosive fluid and slurry flow measurement.

1.1 Problem Overview

The historical development of cross-correlation methods for flow measurement has been reviewed by Beck and Plaskowski [8]. The early work with ultrasonic sensing was by Coulthard at Bradford University, UK. Coulthard, in 1973, used ultrasonic transducers for cross-correlation flow measurement of two-component liquid/gas flow. Coulthard's work was extended by Wormald (1973) who designed ultrasonic systems suitable for large pipes. Ong (1975) further extended the use of ultrasonic transducers to the measurement of the flow of a range of liquids and slurries in pipes. Smith (1979) used ultrasound for single-phase gas flow measurement. However, a major problem often encountered by the early researchers was the need to adjust the frequency of the transmitted ultrasound in order to maintain the phase difference and obtain satisfactory cross-correlation function. Leach (1975) and Trivedi (1977) demonstrated that the phase shift problem was owing to the standing wave structure formed inside the pipe. Flemons (1977) first tackled this problem and used four phase sensitive demodulators supplied with references in each 90° quadrant and an automatic selection of the quadrature that would give good cross-correlation function. Batty (1976) devised a closed-loop system to maintain the phase automatically. Balachandran and Beck [9] used the closed-loop system for the flow measurement of slurry. However, the problem with phase shift was still persistent in low flow velocities and low turbulence signals [8].

Another problem arises from the presence of acoustic short circuit through the pipe wall from the transmitter to the receiver. The acoustic short circuit magnitude is often larger than the fluid-borne signal. Yet another problem inherent in continuous wave ultrasound is of multiple reflections within the pipe wall, leading to a standing wave pattern that may affect the magnitude of the received signal. In a recent development in cross-correlation flow measurement using ultrasonic sensing, Xu et al. [10] used pulsed ultrasound for the measurement of two-component (water/air) flow to avoid problems that occur in continuous wave ultrasonic applications. They detected amplitude modulation of an ultrasonic pulse train as a result of obstruction by artificially injected air bubbles in water flow through the pipe. However, cross-correlation flow measurement of single-phase flow using pulsed ultrasound to the best of author's knowledge has not been reported.

Several problems are encountered while applying pulsed ultrasound for the measurement of single-phase flow, using cross-correlation technique. In a single-phase flow the turbulence is the only disturbance that could be detected

by ultrasound. The turbulent velocity component perpendicular to the flow direction alters the velocity of ultrasonic pulses transmitted across the diameter of the pipe. Therefore, the variation in the transit time of the ultrasonic pulse is a function of the turbulent velocity component. However, the variation in transit time, which is extremely small compared with the time of flight of the pulse across the pipe diameter, is difficult to measure reliably. For example, the transit time of an ultrasonic pulse across a pipe of 90 mm diameter carrying water (acoustic velocity = 1482 m/s) is about 60 μ s and the change in the transit time caused by a turbulent velocity component of 0.1 m/s is approximately 4 ns. Besides, the instant of pulse arrival is uncertain because of initial build-up in the received pulse. These could be perhaps the main reasons why researchers had difficulty in implementing pulsed ultrasonic sensing for single-phase flow measurement.

1.2 Research Objectives

Cross-correlation technique with ultrasonic sensing has been successfully used for the measurement of multi-component flow [8], [10]. Our research is aimed at applying this non-intrusive technique for the measurement of single-phase flow.

1.3 Scope of the Research

In the initial stage of the work, we studied the problems occurring in continuous wave ultrasound application mentioned in Section 1.1, theoretically and experimentally, and concluded that continuous wave ultrasound would not be suitable for application in single-phase flow measurement using the cross-correlation technique. Consequently, the use of pulsed ultrasound was investigated in order to avoid the problems of continuous wave ultrasound. A new technique for sensing naturally available turbulence in the flow, using pulsed ultrasound was subsequently developed. The new technique facilitates sensing variations in the time of flight of ultrasonic pulses caused by the turbulent velocity components.

The velocity component of turbulence perpendicular to the flow axis is sensed by two ultrasonic transducers mounted diametrically opposite to each other on the pipe. The transducers transmit ultrasonic pulses at the same instant and in opposite directions. The pulses after passing through the fluid in the pipe are received by the same pair of transducers and are fed to a differential amplifier. In the presence of turbulence, the instants of arrival of the two pulses are different and the magnitude of differential amplifier output is a function of the turbulent velocity component. The repetition rate of pulse transmission is set

higher than twice the maximum frequency component of turbulence signal. A sample-and-hold circuit is used after the differential amplifier to reconstruct the turbulence signal. The working of the circuit has been tested by detecting water currents artificially generated in a tank.

The turbulence pattern sensed at two suitable locations on the pipe can be cross-correlated and the flow velocity can be obtained from the peak position in the cross-correlation function.

The technique has been supported by developing a theoretical model of ultrasonic pulse transmission-reception process and carrying out a numerical simulation of the flowmeter based on the theoretical model. The applicability of the technique is verified experimentally by building the hardware, and employing it for the measurement of water flow non-intrusively on a PVC pipe in a water circulation system. The results are compared with the flow rate measurements using a venturimeter for various sensor spacings.

1.4 Thesis Outline

To begin with, the cross-correlation principle is introduced in Chapter 2. The cross-correlation technique in the context of flow measurement is explained with continuous wave ultrasonic sensing. We investigated theoretically and experimentally the drawbacks of continuous wave ultrasonic application mentioned in Section 1.2. The details of the investigations are included in Chapter 2. Considering that the continuous wave ultrasound was unsuitable for single-phase flow, we investigated the viability of pulsed ultrasound and developed a new technique for sensing turbulent velocity component. The technique is described in Chapter 3. It includes the circuit details and the test results obtained by detecting artificially generated water currents in a tank. A theoretical treatment and numerical simulation of the technique for application in cross-correlation based flowmeter are given in Chapter 4. Experiments were carried out to measure water flow through a PVC pipe non-invasively. The experimental set-up and the test results are presented in Chapter 5. The concluding chapter summarizes the work and provides suggestions for future work.

Chapter 2

CROSS-CORRELATION TECHNIQUE WITH CONTINUOUS WAVE ULTRASOUND

Flow measurement by cross-correlation technique involves sensing disturbances in the flow at two locations spaced axially along the flow stream. The flow is calculated from the time required for the disturbance pattern to move between the locations, with the help of the position of the peak in the cross-correlation function of the signals sensed at the two locations. Thus the flow velocity is inversely proportional to the transit time of the disturbances between the two measurement points [11]. The principle of cross-correlation in the context of flow measurement is explained in Section 2.1. The most common method of sensing disturbances in the flow is by detecting modulation of continuous wave ultrasonic beam projected across the flow stream. Section 2.4 describes the continuous wave ultrasonic sensing techniques. The major drawback of continuous wave ultrasound is that the desired fluid-borne signal is corrupted by reflections from the inner pipe wall, the acoustic short circuit through the pipe wall, and the reflections within the pipe wall. We have investigated these sources of interference and the results of the investigations are included in this chapter.

2.1 Flow Measurement by Cross-Correlation

The cross-correlation function of two signals measures the degree of similarity between the two signals as a function of delay in one of the signals [12, p. 118]. The cross-correlation of signals $x(t)$ and $y(t)$ may be obtained, as a function of time delay τ , from the average of the product of the two signals [13, p. 434] over the observation time T as

$$r_{xy}(\tau) = \lim_{T \rightarrow \infty} \frac{1}{T} \int_0^T x(t) y(t - \tau) dt = \overline{x(t) y(t - \tau)} \quad (2.1)$$

If we interchange the signals,

$$r_{yx}(\tau) = \lim_{T \rightarrow \infty} \frac{1}{T} \int_0^T x(t - \tau) y(t) dt = \overline{x(t - \tau) y(t)} \quad (2.2)$$

In a flowmeter based on the cross-correlation technique, two sensors are mounted a known distance apart on the pipe as shown in Fig. 2-1(a). The sensors convert measurable properties such as variation of pressure, temperature, capacitance, electrical conductivity and disturbances into electrical signals [8], [14]. Let $x(t)$ and $y(t)$ be the output signals of the upstream sensor A and downstream sensor B respectively. As the disturbance pattern moves from A to B, the downstream signal is a delayed attenuated version of the upstream signal corrupted by additive noise. Therefore, we can represent the downstream signal as

$$y(t) = \alpha x(t - \tau_m) + n(t) \quad (2.3)$$

where α is the attenuation in the original disturbance pattern, τ_m is the transit time of the disturbance pattern between the sensing locations, and $n(t)$ is additive noise and other interference. From (2.2) and (2.3)

$$\begin{aligned} r_{yx}(\tau) &= \overline{x(t - \tau) [\alpha x(t - \tau_m) + n(t)]} \\ &= \overline{\alpha x(t - \tau) x(t - \tau_m)} + \overline{x(t - \tau) n(t)} \end{aligned}$$

Assuming that the noise $n(t)$ is uncorrelated with signal $x(t)$, we have

$$\overline{x(t - \tau) n(t)} = 0$$

Therefore,

$$r_{yx}(\tau) = \alpha r_{xx}(\tau - \tau_m) \quad (2.4)$$

Since the movement of the disturbances in the flow is random, the signals obtained from the sensors are random signals. Therefore from (2.4), the cross-correlation function $r_{yx}(\tau)$ has a maximum at $\tau = \tau_m$. Thus, if the distance between the two sensing locations, L , is known, the flow velocity can be obtained from the position of the peak, $\tau = \tau_m$, in the cross-correlation function as

$$u = L / \tau_m \quad (2.5)$$

An example of the signals sensed at two locations and their cross-correlation function is shown in Fig. 2-1(b). Since the peak position and not the peak amplitude, in the cross-correlation function is used to estimate the flow rate, the flowmeter can work with large attenuation of the signals [15], and the sensors need not have to be linear and calibrated [8]. However, mismatch in the first and higher order dynamics of the sensors, if any, should be negligible [8]. The lowest frequency component in the signals to be cross-correlated is above 1 Hz; therefore the DC stability of the sensors is not important [8]. In addition, the flowmeter is largely unaffected by wide variations in the fluid properties, because only transit time is measured between two fixed locations.

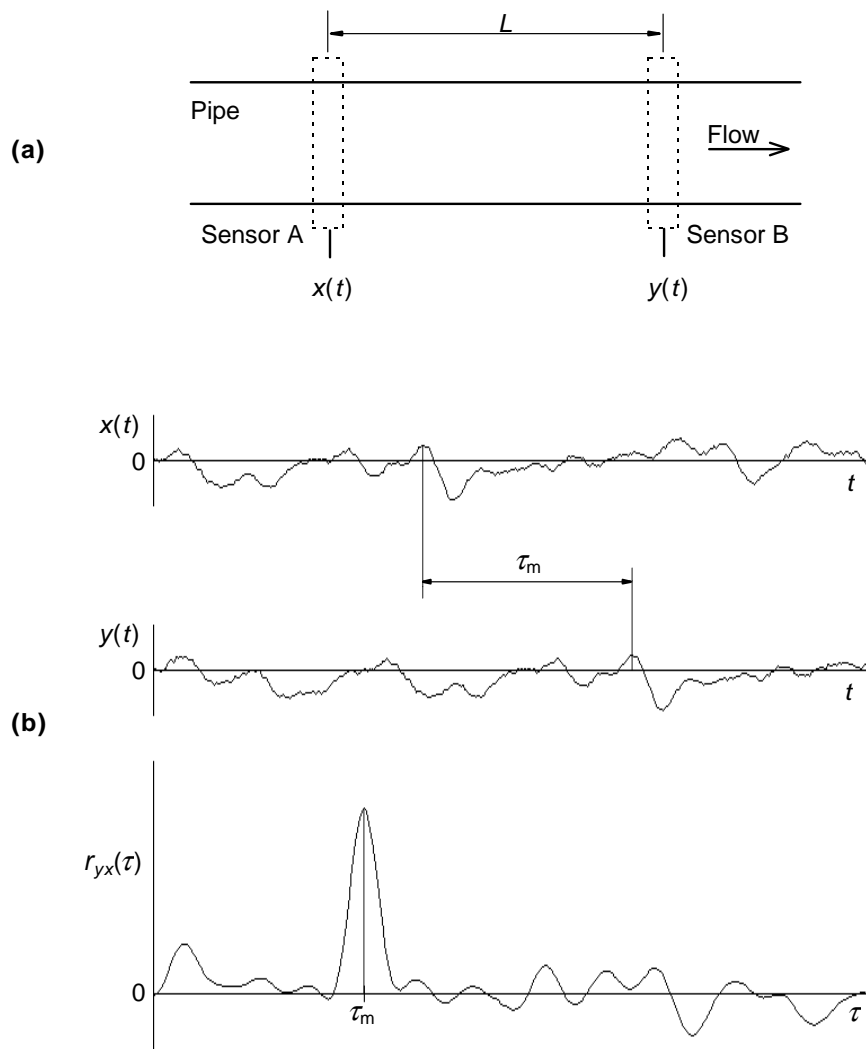


Fig. 2-1. Schematic of flow measurement by cross-correlation. (a) Placement of the sensors along the pipe; (b) examples of the signals $x(t)$ and $y(t)$ sensed by the two sensors, and their cross-correlation function $r_{yx}(\tau)$.

2.2 Flow Resolution and Effect of Sensor Spacing

Since the flow velocity u is inversely proportional to the transit time τ_m of the disturbance pattern in the flow, the resolution in the measurement of τ_m affects the resolution of the measurement of flow velocity u . It helps decide the sensor spacing L and the sampling interval T_s . From (2.5), the flow resolution with respect to τ_m is given by

$$|\Delta u| = \frac{L}{\tau_m^2} |\Delta \tau_m| \quad (2.6)$$

Assuming that the resolution in the measurement of τ_m is the sampling interval T_s , used for evaluating the cross-correlation function, i.e. $\Delta \tau_m = T_s$,

$$\Delta u = \frac{L T_s}{\tau_m^2} \quad (2.7)$$

Using (2.5), the relative flow resolution is given by

$$\frac{\Delta u}{u} = \frac{T_s}{\tau_m} \quad (2.8)$$

The graph of $\Delta u/u$ versus τ_m for a sampling interval of 1 ms is shown in Fig. 2-2. Note that the flow resolution deteriorates significantly as τ_m decreases, because of either high flow velocity or small sensor spacing.

An effect of increasing the sensor spacing is the decrease in the measured correlation due to the break-up of the turbulence pattern as it proceeds along the pipe. This effect is illustrated by the moving-frame cross-correlation function in Fig. 2-3, adapted from [8]. The well-defined and large correlation peak for small sensor spacing enables a very accurate measurement of the peak position. However, the effective center of some transducers (e.g., piezoelectric transducer) is uncertain. This uncertainty can be a significant fraction of a small sensor spacing, leading to errors in the assumed value of the spacing. On the other hand with very large sensor spacing, the peak in the cross-correlation function becomes broad and less distinct, giving rise to considerable errors in estimating the position of the peak. For an ultrasonic cross-correlation flowmeter mounted on a 1" diameter pipe carrying water, Ong (1975, reported in [8]) showed that the optimum sensor spacing would be between 3 and 4 times the pipe diameter. According to Beck and Plaskowski [8], the result given above should be applicable to various pipe diameters.

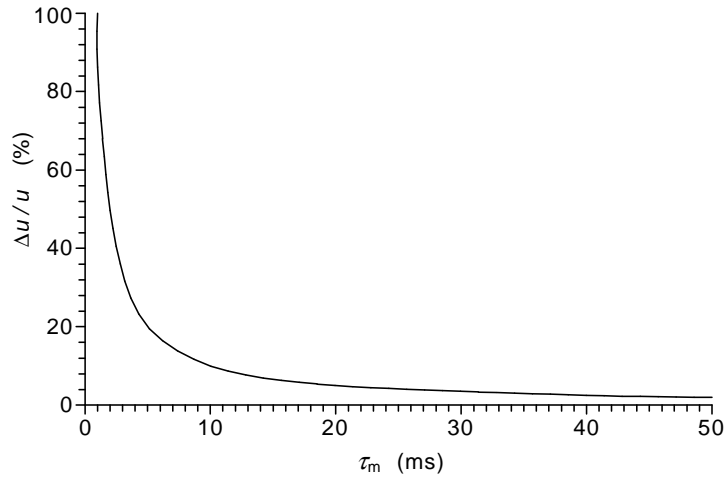


Fig. 2-2. Graph of flow resolution $\Delta u/u$ versus τ_m for sampling interval of 1 ms.

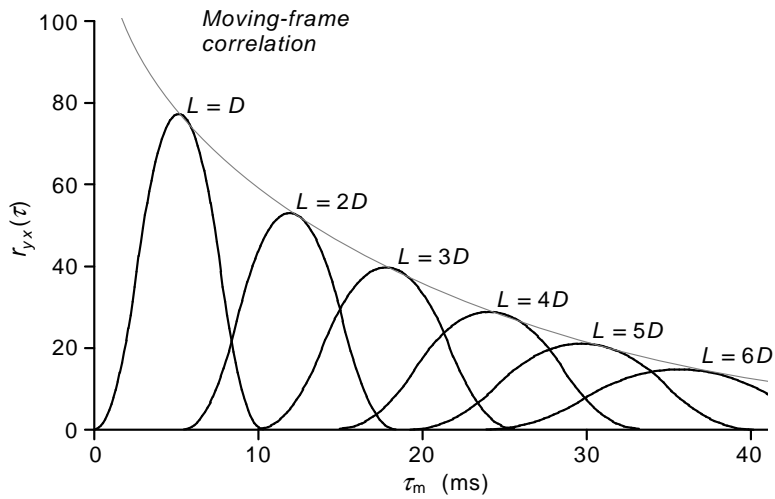


Fig. 2-3. Effect of sensor spacing, L , on the peak in the cross-correlation function $r_{yx}(\tau)$. Flow velocity $u = 4.2$ m/s, and pipe diameter $D = 25$ mm. Adapted from Fig. 6.20 in [8].

2.3 Ultrasonic Sensing Methods

The ultrasonic sensing involves the modulation of an ultrasonic beam by the disturbances in the flowing fluid. If two such beams are spaced axially along the flow, the position of the peak in the cross-correlation function of the received signals is identified as a measure of the flow velocity. The advantages of using external ultrasonic beam are as follows [8]:

1. The sensors can be mounted outside the flow pipe so that they do not invade the flow, thus providing a potentially non-contacting method of measurement. In some cases the transducers can clamp on to an existing pipe.
2. The beam averages the flow information within its cross-section.
3. The performance is independent of temperature, pressure, and viscosity of the fluid.

Cross-correlation flowmeters using ultrasound fall into two general categories, the first using continuous wave ultrasound and the second using pulsed ultrasound. Continuous wave ultrasound systems provide extremely high sensitivity to the conveyed component. The transducer electronics is comparatively simple and the demodulation methods are well-established. However, care has to be taken to avoid errors caused by phase shifts, which occur because of the standing waves, inherent when continuous ultrasound is used in an acoustically reflective pipe situation [9].

The use of pulsed ultrasound avoids the standing wave problem. Pulsed ultrasound systems have been successful for multi-component fluid flow [10], but are less sensitive to the flow-related turbulence [8]. The supporting electronics is expensive. Xu et al. [10] used pulsed ultrasound for the measurement of two-component flow, viz. water with artificially injected air bubbles. The disturbances in the flow were sensed by detecting amplitude modulation of the ultrasonic pulses because of the obstructing air bubbles. In case of flow measurement of single-phase fluid like pure water, as is the objective of our research, natural turbulence is the only disturbance detectable by ultrasound. However, pulsed ultrasound systems being inefficient to detect turbulence, research in single-phase fluid flow measurement using pulsed ultrasonic sensing and cross-correlation technique, to the best of author's knowledge, has not been reported.

The following sections describe the continuous wave sensing techniques and the investigations done on the problems in using it for single-phase flow.

The last section deals with the viability of pulsed ultrasound for single-phase flow measurement.

2.4 Continuous Wave Ultrasonic Sensing Techniques

Sensing the flow disturbances using continuous wave ultrasound is essentially by exploiting modulation of an ultrasonic beam caused by the disturbances. Usually two continuous wave type ultrasonic transducers are mounted diametrically opposite as shown in Fig. 2-4. One transducer transmits the ultrasound into the fluid and the other one placed opposite receives the signal modulated by the fluid disturbances. The ultrasound will be scattered and absorbed by any discontinuous components such as gas bubbles, solid particles, or immiscible droplets, if present in the fluid, and will result in amplitude variation in the received signal. The scattering by the moving discontinuous components will also induce Doppler frequencies. In addition, the ultrasound propagation velocity will change with fluid composition resulting in phase variations, and there will be superimposed phase fluctuations caused by turbulent eddies. The net result is that the received ultrasound is modulated in both amplitude and phase, so that, in principle, amplitude, phase or frequency demodulators can be used to detect the flow disturbances [16]. The conclusion drawn by Beck and Plaskowski [8] based on the investigations of some researchers, indicates that for fluids having a relatively high concentration of the discontinuous component (above about 2 %) there is intense amplitude and phase modulation, so that amplitude, phase, and frequency demodulators work satisfactorily. However, for relatively clean fluids the dominant modulation is due to the turbulent eddies which modulate the phase but not the amplitude. Therefore, phase detection has to be used to obtain higher sensitivity in single-phase flow measurement.

The signal from the receiver is demodulated with the help of a suitable demodulator as shown in Fig. 2-4. The demodulated signal is cross-correlated with the corresponding signal from the transmitter/receiver pair at the other sensing location. The position of the peak in the cross-correlation function indicates the transit time τ_m of the disturbances between the two sensing locations and the flow velocity can be obtained from (2.5).

In the initial stages of our research, the use of continuous wave ultrasound for sensing turbulence was investigated, as the amplitude and frequency demodulation techniques are simple and well-established. The major drawback of continuous wave ultrasound is the interference from the reflected waves. The desired fluid-borne signal is superimposed, as shown in Fig. 2-5, by sources of interference, theoretically and experimentally. The results of investigations are discussed in the following three sections.

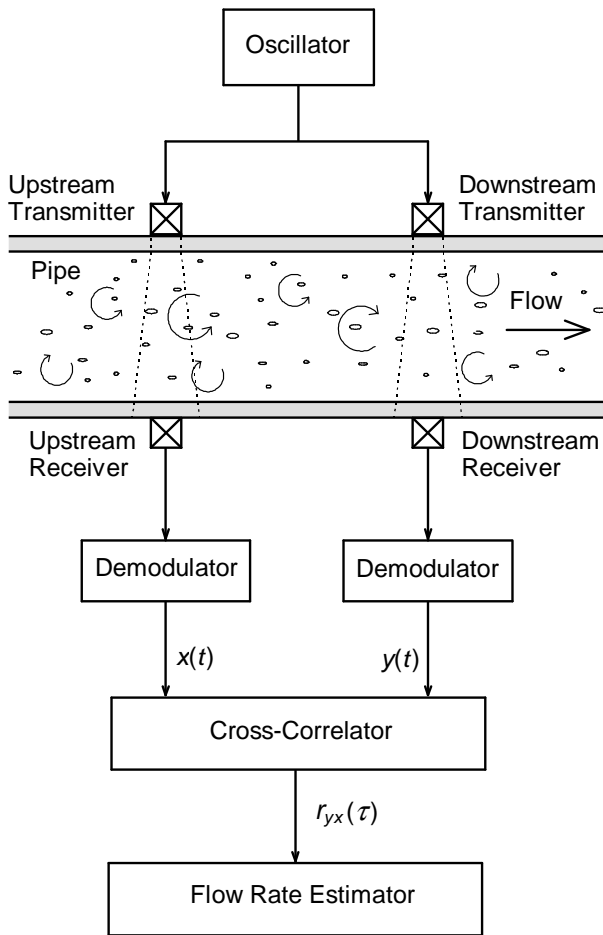


Fig. 2-4. Block diagram of a cross-correlation flowmeter using continuous wave ultrasound.

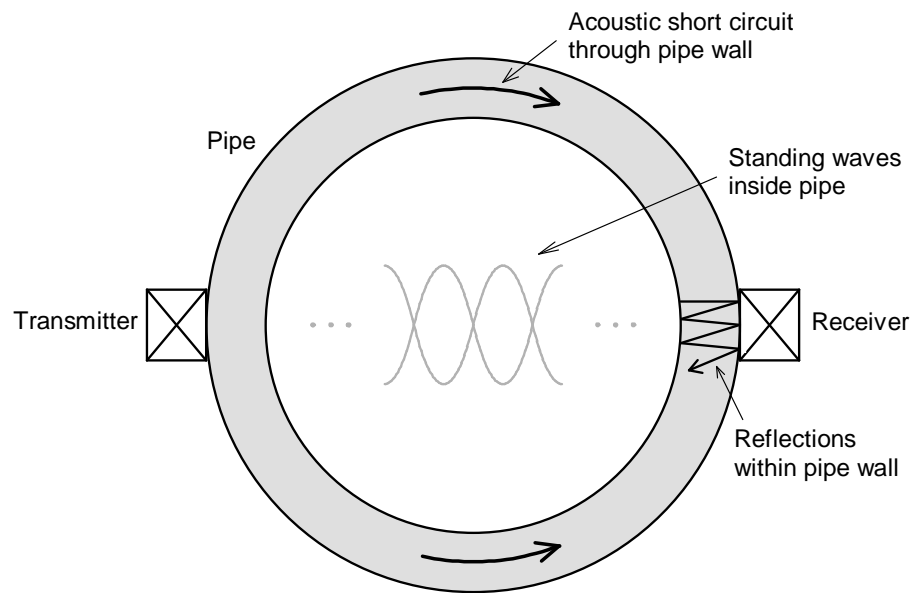


Fig. 2-5. Diagram showing sources of interference in continuous wave ultrasound application: acoustic short circuit through the pipe wall, standing waves inside the pipe, and reflections within the pipe wall.

2.5 Investigation of Standing Waves inside the Pipe

Since pipe walls are efficient reflectors of ultrasound, standing waves are generated in the flow pipe, when continuous wave ultrasound is transmitted across the diameter of the pipe. The reflected waves and the direct wave superimpose to generate stationary pressure zones [17]. The pressure is determined by the amplitudes and relative phases of the interfering waves. At places where the waves interfere destructively, a low pressure area, namely a node, is generated. Where they interfere constructively, a high pressure area, namely an antinode, is generated. The nodes are generated at points $n\lambda/2$ and the antinodes at points $(n+1/2)\lambda/2$ distance away from the transmitter, where λ is the acoustic wavelength of ultrasound in the fluid and n is an integer. Thus a standing wave is formed in the pipe.

2.5.1 Experiment to confirm the presence of standing waves

If the transmitter and receiver transducers are mounted diametrically opposite on a flow pipe, the magnitude of the signal picked up by the receiver will be affected by the standing wave, depending on the total acoustic pathlength across the pipe. This implies that the presence of standing waves can be verified if the magnitude response of the transmitter/receiver pair is corrupted by ripples. In an experiment to detect the presence of standing waves, a continuous wave ultrasonic transmitter/receiver pair was kept face to face in order to ensure the absence of standing waves. The transmitter was given a sinusoidal voltage of fixed amplitude 5 Vp-p from the function generator HP33120A. The receiver output amplitude was measured on the oscilloscope HP54601A. The graph of receiver output versus frequency between 2.150 MHz and 2.450 MHz is shown in Fig. 2-6(a). The graph does not indicate ripples in the magnitude response. The transducers were then mounted diametrically opposite to each other on a PVC pipe filled with water. The inner diameter of the pipe was 83 mm and outer diameter 90 mm. The transmission frequency was varied from 2.150 MHz to 2.450 MHz in steps of 1 kHz. The magnitude response is shown in Fig. 2-6(b) which exhibits the ripples. This verifies the presence of the standing waves.

The frequency of variation in the magnitude response can be used to find the distance between the two reflecting planes. Let f_1 and f_2 be two node frequencies ($f_2 > f_1$), n be the total number of nodes at f_1 , $n+m$ be the total number of nodes at f_2 , d be the distance between the reflecting planes, and c the acoustic velocity in water (1482 m/s). Then

$$d = \frac{nc}{2f_1} = \frac{(n+m)c}{2f_2} \quad (2.9)$$

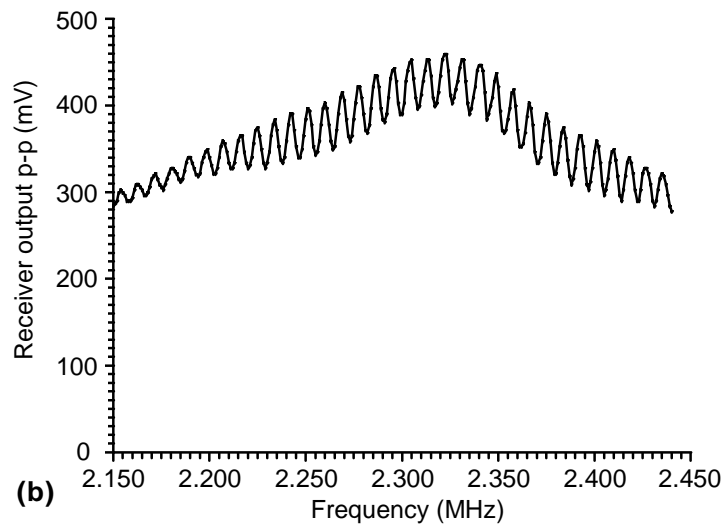
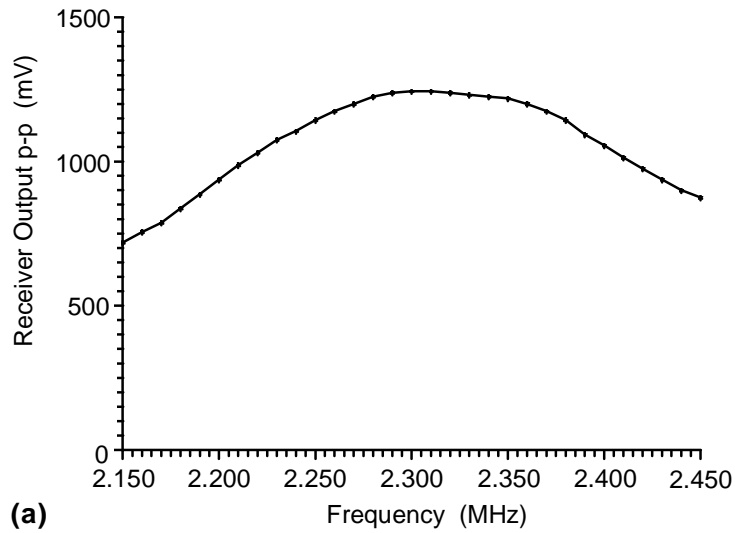


Fig. 2-6. The presence of standing waves observed in the magnitude response of a continuous wave transducer pair when mounted on a PVC pipe filled with water. (a) shows the magnitude response by keeping the transducers face to face so that no standing waves occur. (b) shows ripple in the magnitude response when the transducers are mounted diametrically opposite on the pipe.

and
$$n = \frac{m f_1}{(f_2 - f_1)} \quad (2.10)$$

Therefore,
$$d = \frac{m c}{2 (f_2 - f_1)} \quad (2.11)$$

Substituting two node frequencies in (2.11), the distance between the reflecting surfaces can be found out. For example, taking $m = 10$, $f_1 = 2.255$ MHz, and $f_2 = 2.344$ MHz, we get $d = 83.3$ mm. It implies that the standing waves were generated because of the reflections at the inner pipe walls, as the internal diameter of the pipe was 83 mm.

2.5.2 Effect of variation in standing wave pattern

Since pipe walls are efficient reflectors of ultrasound, standing waves are always generated in the flow pipe and it is necessary to consider the stability of the standing wave pattern and its effect on the accuracy of measurement [8]. Let us consider a pair of ultrasonic transmitter and receiver mounted diametrically opposite on a pipe wall. The reflections from the pipe wall will generate standing waves inside the pipe. The standing wave pattern and positions of the transmitter and receiver are shown in Fig. 2-7(a) on a pressure amplitude versus distance graph. The places of maximum pressure amplitude P_{\max} indicate antinodes and the places of minimum pressure amplitude P_{\min} indicate nodes. As the ultrasound propagation velocity or the oscillator frequency changes, the acoustic pathlength between the transmitter and receiver will vary. The effect of this will be as if the receiver were moving along the standing wave pattern (Fig. 2-7(a)), and the acoustic pressure due to the standing wave modulation will alter in amplitude and phase [8].

The major problem is to set the receivers at the two sensing locations at equal phase angles on the standing wave pattern as shown in Fig. 2-7(a) and maintain the system within the required operating regime once it has initially been set up. The effect of different phase angles at the two receivers is that the phase of the actual cross-correlated signal varies, when turbulent velocity component to be sensed alters the acoustic pathlength. For example, if the difference in the phase angles is 180° as shown in Fig. 2-7(b), and the modulation is by phase (in case of turbulence), the waveform sensed at one location will be an inverted version of the waveform sensed at the other location, for the same turbulence pattern. Thus, the cross-correlation function will invert as shown in Fig. 2-7(e), whereas the ideal cross-correlation function is shown in Fig. 2-7(c). For a 90° phase difference, a severely distorted cross-correlation function will result, as shown in Fig. 2-7(d). These phase errors are significant

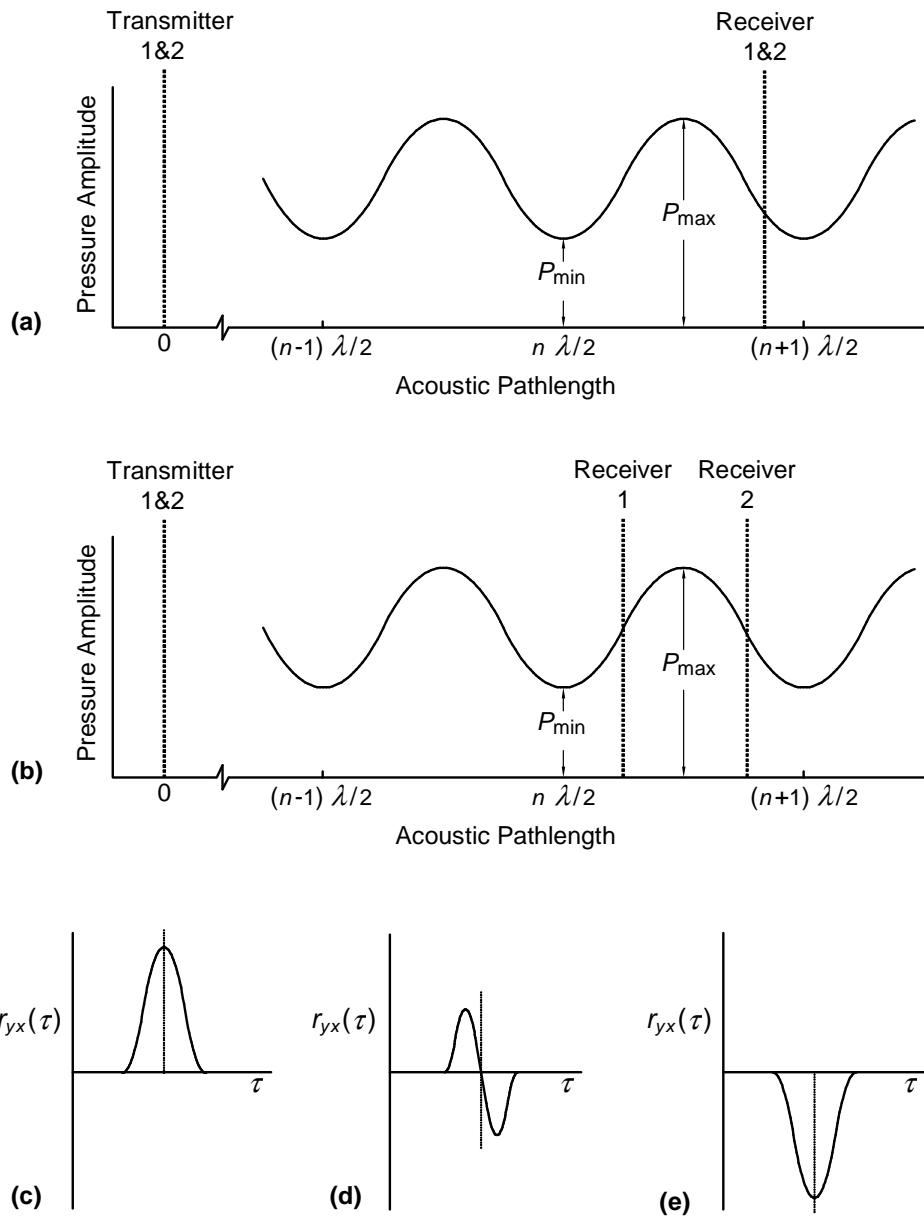


Fig. 2-7. Effect of variation in the standing wave pattern on the cross-correlation function. (a) shows the standing wave pattern with equal pathlength between the transmitter and receiver at the two sensing locations. (b) shows a difference of 180° between the pathlengths at the two sensing locations. The resultant cross-correlation function when the difference in the pathlengths is (c) 0° , (d) 90° , (e) 180° . Partly based on Figs. 3.4, 3.5 in [8].

when the turbulence intensity is small and the modulation is by phase, i.e. vector modulation. For fast fluid flows, the acoustic path changes are of many wavelengths; and for multi-component flow where the modulation of the ultrasound beam is of a scalar nature, there are major amplitude changes; thus phase errors are not significant and a normal cross-correlation function is always obtained [8].

In addition to the variations in oscillator frequency, instability is also due to variations in other parameters, such as temperature, flow velocity, and rheology of the flowing medium, because changes in these alter the acoustic pathlength between the transmitter and receiver affecting the phase of the received signal. Some form of feedback system is therefore necessary to achieve the optimal operating condition. Balchandran and Beck (1980) [9] have reported the use of a closed-loop system for the measurement of multi-component (slurry) flow measurement. They employed a phase-locked loop (PLL) to maintain the acoustic pathlength between the transmitter and receiver at an integral number of half wavelengths. For multi-component flow measurement, the system is locked at P_{\min} condition as shown in Fig. 2-8(c), so that the effect of vector modulation owing to turbulence is minimized and the system is most sensitive to the scalar modulation caused by the conveyed flow component. In case of single-phase flow measurement, Beck and Plaskowski [8] suggest that the phase lock should be at the center of the maximum slope of the standing wave pattern (i.e. midway between P_{\max} and P_{\min}) as shown in either Fig. 2-8(a) or Fig. 2-8(b). This arrangement will make the system most sensitive to vector modulation caused by the turbulent velocity components. However, the application of the PLL for single-phase flow measurement, to the best of author's knowledge, has not been reported.

An attempt to use continuous wave ultrasound for the measurement of single-phase fluid flow was made by Flemons (1977, reported in [8]). The ultrasonic system was clamped onto the outside of thick-walled steel pipes and the problem of an unknown and uncontrollable phase lag distribution across the pipe walls and the fluid was solved by using four synchronous phase demodulators supplied with phase references in each 90° quadrant, and the correct phase to give good cross-correlation functions could be selected automatically. Bazerghi and Serdula, (1977, reported in [8]), evaluated the performance of the flowmeter developed by Flemons and claimed that an accuracy of 3 % was readily obtainable, and with careful installation, an accuracy of better than 2 % should be possible. However, they do not mention how they tackled the problem of acoustic short circuit.

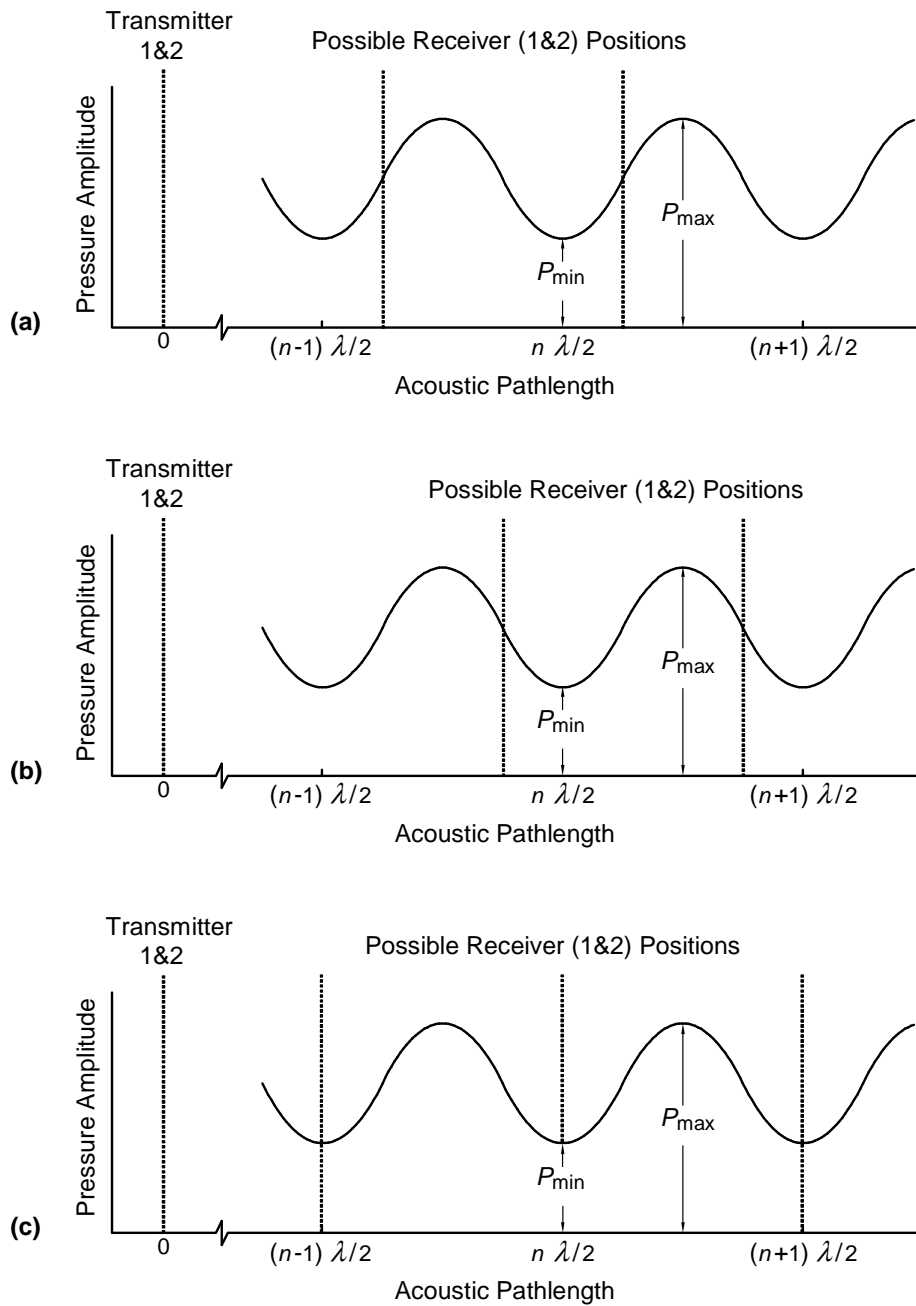


Fig. 2-8. Possible receiver positions obtained by a phase-locked loop. For single-phase flow measurement the receiver positions should be maintained at the maximum slope of the standing wave pattern, as shown in either (a) or (b). For multi-component flow measurement the receiver is maintained at a minimum on the standing wave pattern as shown in (c). Partly based on Fig. 3.4 in [8].

Nuijten et al. (1983, reported in [8]) attempted to prevent the formation of standing waves by directing the ultrasound beams across a diagonal instead of directly across the diameter of the pipe. However, some standing waves will still occur as a result of scattering of the ultrasound. By using diagonal beams, and high frequency transducers (about 4 MHz, above which the attenuation would be excessive) to increase phase modulation, Keech (1982, reported in [8]) could measure the flow of liquid with only a small amount of tracer content, using simple electronics without phase-lock systems. This system is the basis of probably the first ultrasonic cross-correlation flowmeter to be commercially marketed [8]. However, Beck and Plaskowski suggest [8] that phase-lock systems, are still desirable for obtaining the highest sensitivity to small amounts of the tracer or for detecting clean liquid turbulence; the use of high ultrasound frequencies is worthwhile, but the use of diagonal beams may actually reduce the sensitivity by reducing the standing wave ratio and hence the phase deviation (Fig. 2-7(a)).

2.6 Investigation of Reflections within the Pipe Wall

The pipe wall being a good conductor of ultrasound, the signal undergoes multiple reflections within the pipe wall at the receiver, before it dies down. This fact was verified by mounting a pair of pulsed type transmitter/receiver diametrically opposite on a PVC pipe filled with water. The outer diameter of the pipe was 90 mm and the wall thickness was 3.5 mm. The echo of a pulse from within the wall would arrive after 2.94 μ s, assuming the acoustic velocity in PVC is 2380 m/s [18]. The transducers were pulsed type with the resonant frequency of 2.2 MHz. The transmitter was excited by a pulse (shown in Fig. 2-9(a)) from the ultrasonic pulser *Panametrics 5052UA*. As observed from the received output shown in Fig. 2-9 (b), the first pulse is received at about 60 μ s after traveling through water and the pipe walls. From the expanded waveform shown in Fig. 2-9(c), two diminishing pulses can be seen after the direct pulse at intervals of about 3 μ s, representing the echoes of the direct pulse from the inner wall of the pipe at the receiver.

The experiment was repeated for a galvanized iron (GI) pipe and the reflections within the wall were found to be more significant and persistent. The outer diameter and wall thickness of the pipe were 76 mm and 4.5 mm, respectively. The received waveforms for a pair of pulsed type transducers with the resonant frequency of 2.2 MHz are shown in Fig. 2-10(b). It is observed that the reflections persist for longer duration which is about 30 μ s and the echoes merge partially with the previous echoes. The reason for the distortion is better acoustic conductivity and higher acoustic velocity in iron. The echoes were observed

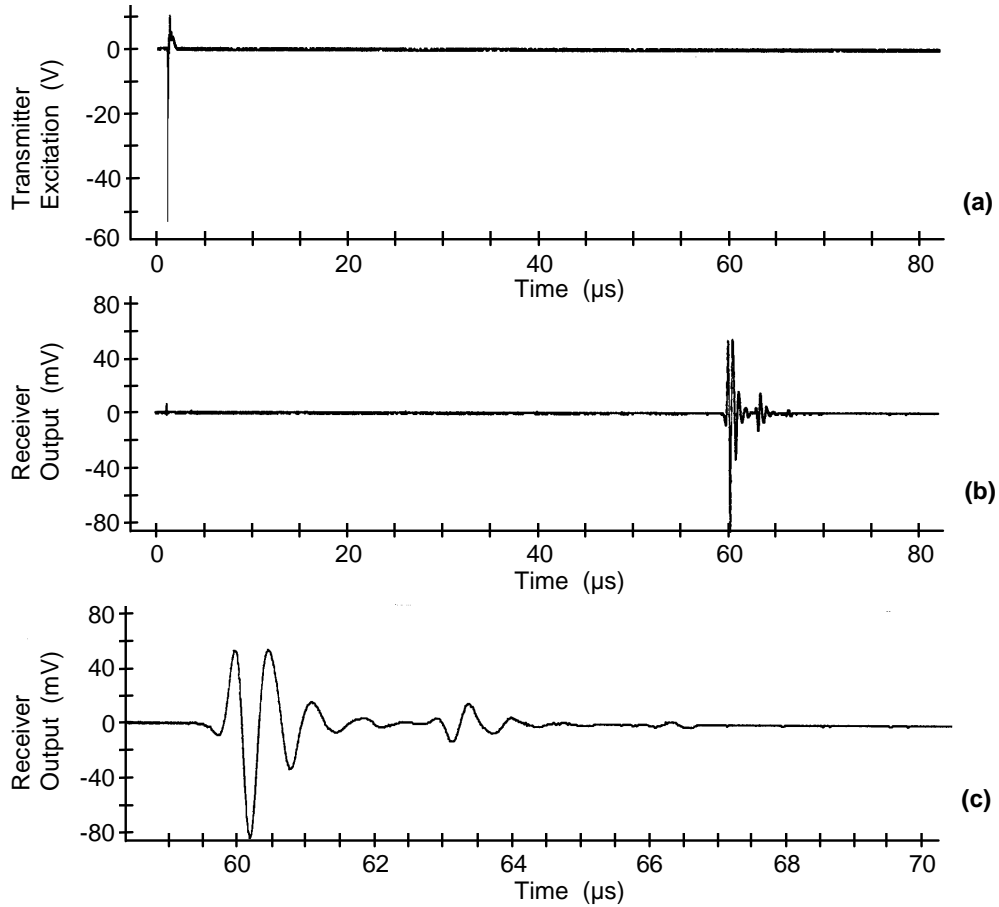


Fig. 2-9. Waveforms showing reflections within a pipe wall for transducers mounted diametrically opposite on a PVC pipe filled with water. Outer diameter of pipe = 90 mm, pipe wall thickness = 3.5 mm. (a) Excitation pulse from the transmitter; (b) received signal: the direct pulse received at 60 μs followed by diminishing pulses; (c) received signal on expanded time scale: the time interval of 3 μs between the pulses, confirming reflections within pipe wall.

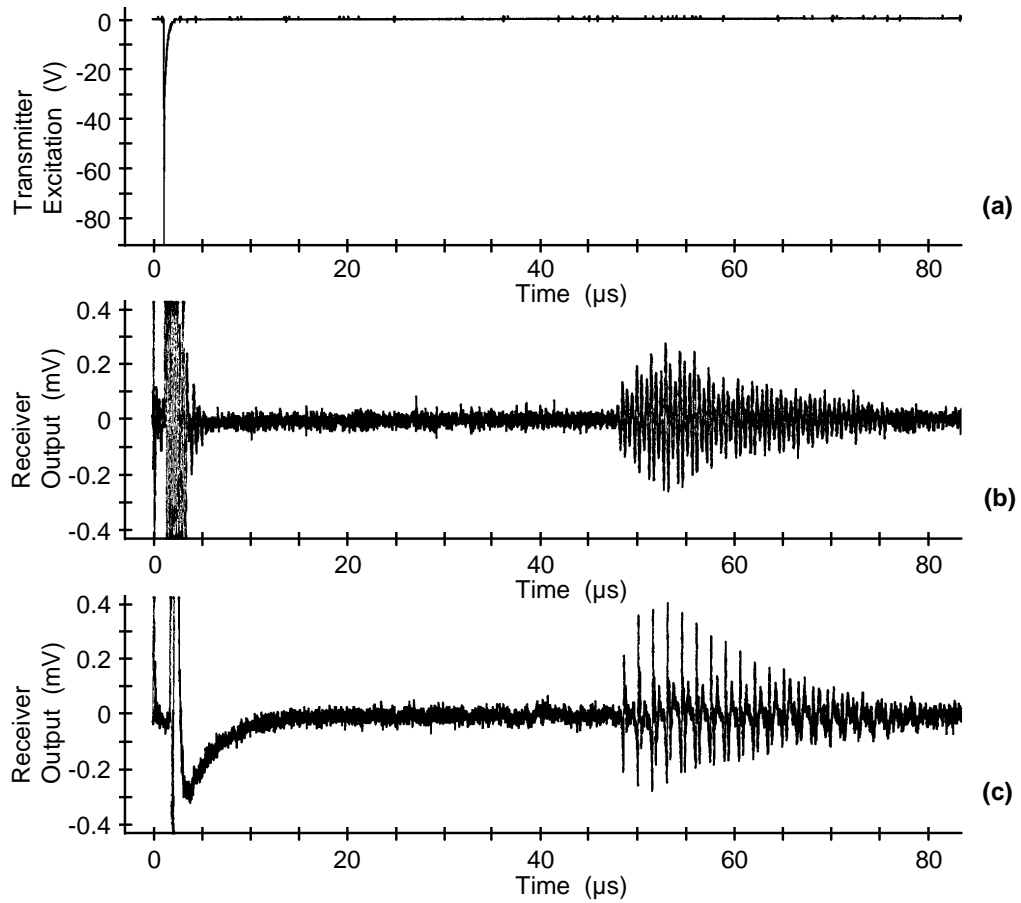


Fig. 2-10. Waveforms showing reflections within pipe wall for a GI pipe of outer diameter 76 mm and wall thickness 4.5 mm. (a) Excitation pulse from the transmitter; (b) received signal for a 2.2 MHz transducer pair; (c) received signal for a 5.0 MHz transducer pair. The transducers were mounted diametrically opposite on the pipe filled with water.

distinctly as shown in Fig. 2-10(c) when a transducer pair of 5.0 MHz resonant frequency was used.

From the results obtained in this experiment, it can be deduced that if continuous wave ultrasound is used for detecting flow disturbances, the standing waves will form within the pipe wall and affect the amplitude of the received signal. The effect of standing waves formed within the pipe wall can be minimized by choosing the ultrasound frequency such that the pipe wall thickness is an odd integral multiple of the half acoustic wavelength in the pipe wall.

2.7 Study of Acoustic Short Circuit through the Pipe Wall

Some ultrasonic flowmeters can be readily clamped onto an existing pipe and facilitate non-intrusive flow measurement. When a clamp-on mounting scheme is employed, the ultrasonic transmitter and receiver are generally mounted diametrically opposite on the outer pipe wall as shown in Fig. 2-11. Therefore some part of ultrasound emitted by the transmitter travels through the pipe wall and reaches the receiver. This phenomenon is called acoustic short circuit [18]. The acoustic short circuit noise carries no information of the disturbances in the fluid, but adds to the signal expected through the fluid and reduces the sensitivity to the disturbances in the flow. Metals being good conductors of ultrasound, the acoustic short circuit noise is significant in case of metal pipes and may swamp the signal through fluid.

2.7.1 Analysis and observation of acoustic short circuit noise

In ultrasonic flowmeters based on cross-correlation technique, the disturbances in the flow are sensed by detecting modulation of ultrasound transmitted across the diameter of the pipe (Fig. 2-4). If the transducers are clamped externally onto the pipe, the signal received by the receiver is superposition of the signal through the fluid and the acoustic short circuit noise through the pipe wall, as shown in Fig. 2-11. As the acoustic short circuit noise gets divided into the two halves of the pipe wall, the resultant acoustic short circuit noise at a point on the circumference of the pipe is the vector sum of the two shear waves traveling along the two halves of the pipe wall.

The acoustic short circuit noise was studied by carrying out experiments on mild steel (MS) pipe of 76 mm outer diameter and 4.5 mm wall thickness. The acoustic short circuit waves are shear waves through the pipe wall. The shear

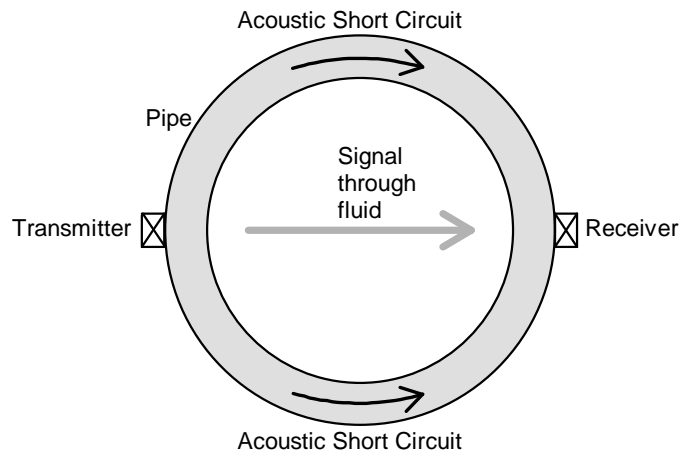


Fig. 2-11. Diagram showing acoustic short circuit path through the pipe wall.

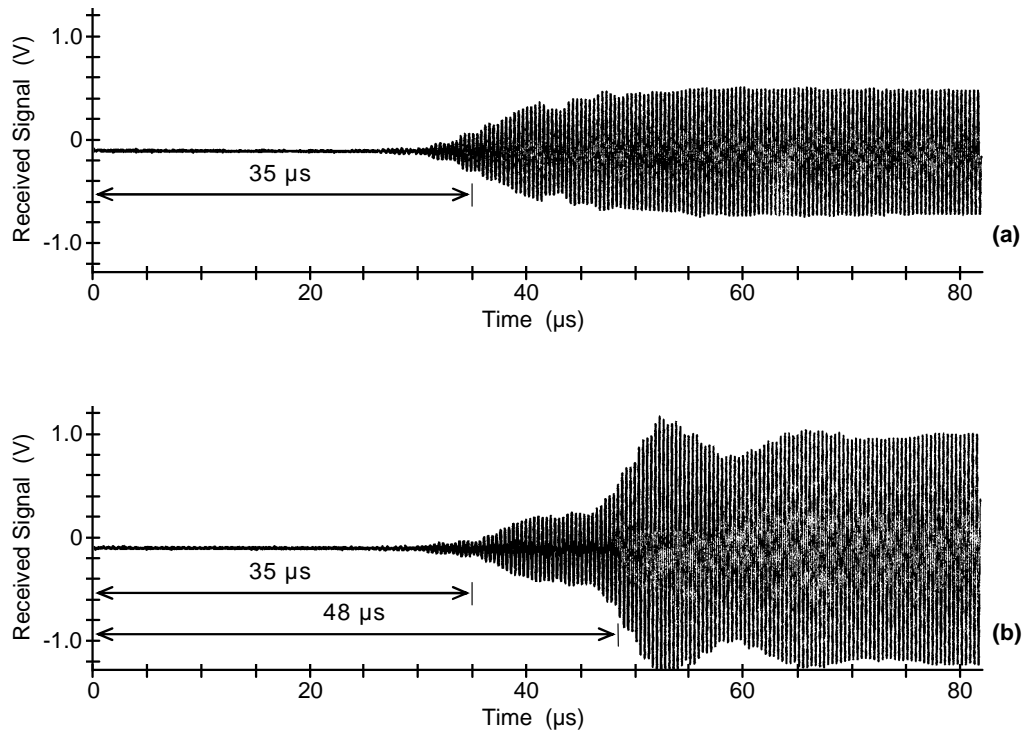


Fig. 2-12. Waveforms showing acoustic short circuit noise and fluid-borne signal in two cases: (a) empty pipe (only acoustic short circuit noise is observed); (b) pipe filled with water (acoustic short circuit superimposed on the fluid-borne signal is observed). The origin is at the start of the gating signal.

velocity c_s in MS is 3240 m/s [18]. The time required for the acoustic short circuit waves to reach the receiver is

$$t_{SC} = \pi D_m / 2 c_s \quad (2.12)$$

where D_m is the mean diameter of the pipe. From the pipe dimensions given above $D_m = 71.5$ mm. Therefore, $t_{SC} = 34.6$ μ s. The wave passing through water is a longitudinal wave with velocity $c = 1482$ m/s and it passes through the pipe walls longitudinally with velocity $c_L = 5930$ m/s [18]. The time required for the water-borne signal to reach the receiver is

$$t_W = (D_i / c) + 2(h / c_L) \quad (2.13)$$

where D_i = internal pipe diameter and h = pipe wall thickness. Therefore, $t_W = 48.0$ μ s. Thus, the acoustic short circuit noise reaches the receiver before the signal through water.

In the experiments, gated continuous wave ultrasound was used for testing, in order to study the superposition of the signal through fluid and acoustic short circuit noise, and to measure their transit times. A pair of continuous wave ultrasonic transmitter and receiver was mounted diametrically on the pipe wall. The transmitter was excited by a gated sinusoid. With the empty pipe only acoustic short circuit noise was received as shown in Fig. 2-12(a). When the pipe was filled with water, the received signal was the acoustic short circuit noise plus the signal through water as shown in Fig. 2-12(b). As seen from the waveforms, the acoustic short circuit noise reaches the receiver before the water-borne signal. It was also observed that a slight displacement of the receiver along the circumference of the pipe as shown in Fig. 2-13 affected the magnitude of the acoustic short circuit noise. A theoretical analysis of the observations is given in the following subsections.

2.7.2 Diametrically opposite mounting

In order to study the nature of the acoustic short circuit noise at the receiver, consider the short circuit path mapped on a paper as shown in Fig. 2-14(a). The ends denote the transmitter position and the midpoint denotes the receiver position. From the diagram it can be observed that when the receiver is diametrically opposite the transmitter, i.e. equidistant from both sides, the acoustic short circuit waves traveling through the two halves are always in phase at the receiver. Thus, they are added constructively irrespective of the transmission frequency and the acoustic short circuit is maximum. It implies that the diametrically opposite mounting of the transmitter and receiver should be avoided.

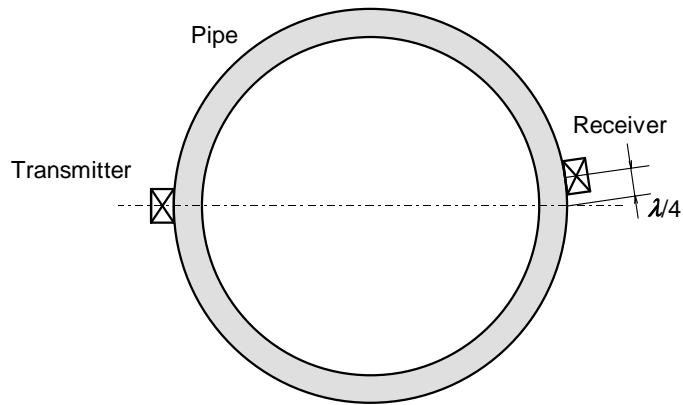


Fig. 2-13. Position of the receiver (displaced by $\lambda/4$ along the circumference of the pipe), in order to minimize acoustic short circuit noise.

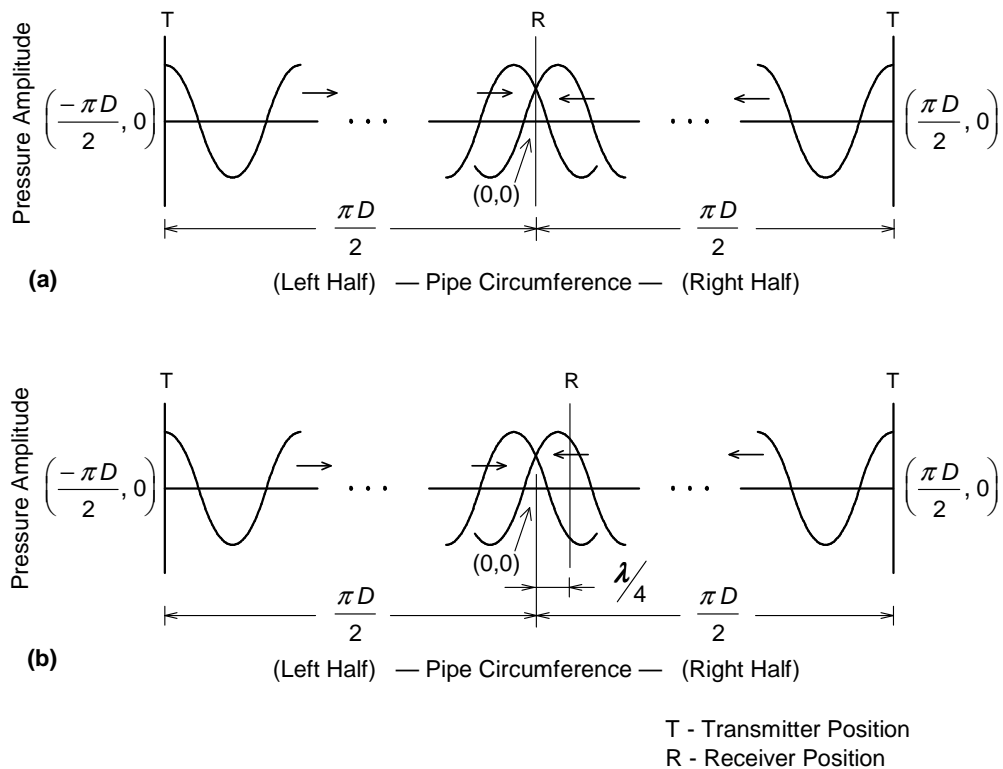


Fig. 2-14. Acoustic short circuit path in two cases: (a) Receiver diametrically opposite to the transmitter; (b) Receiver displaced by $\lambda/4$ along the acoustic short circuit path.

2.7.3 Receiver displaced by $\lambda/4$

It is helpful to consider the case where the receiver is displaced by a distance of $\lambda/4$ from the diametrically opposite position as shown in Fig. 2-13. λ is the acoustic wavelength of the ultrasonic shear wave in the pipe wall,

$$\lambda = c_s / f$$

where c_s is shear velocity of ultrasound in the pipe wall and f is frequency of ultrasound. From Fig. 2-14(b) it is seen that the distance of $\lambda/4$ corresponds to the phase difference of $\pi/2$, and the two short circuit waves will have the phase difference of π at the receiver. Thus, the resultant short circuit noise is the vector addition of the two short circuit waves that are out of phase, and the short circuit noise is zero. This phenomenon repeats at points that are at a distance of $\pm(n\lambda \pm \lambda/4)$ from the diametrically opposite point of the transmitter (Fig. 2-15), where n is an integer. However, the effect diminishes as n increases, because of the increasing difference in the magnitudes of the two short circuit waves. Moreover at around a displacement of $\lambda/4$, the increase in the magnitude of the short circuit noise caused by variation in the transmission frequency is minimum.

2.7.4 Analysis for full contact of receiver

The explanation given above assumes a line contact between the transducer and the pipe wall. However, in order to increase the sensitivity, couplants and wedges are used for obtaining maximum contact. An analysis of the acoustic short circuit noise in case of full contact between the transducer and the pipe wall is given below.

Let us consider that the receiver is placed at the point of the minimum short circuit noise, as described in the previous section, i.e. at a distance of $\lambda/4$ from the diametrically opposite point of the transmitter, where λ is the wavelength of ultrasonic shear wave through the pipe wall. For an ultrasonic wave of 2 MHz frequency, $\lambda/4 = 0.4$ mm in MS pipe; whereas the contact area of the transducer is substantially large, about 20 mm in diameter.

Considering the origin at the center of the receiver contact area, the short circuit waves traveling in the two halves of the pipe wall are shown in Fig. 2-16.

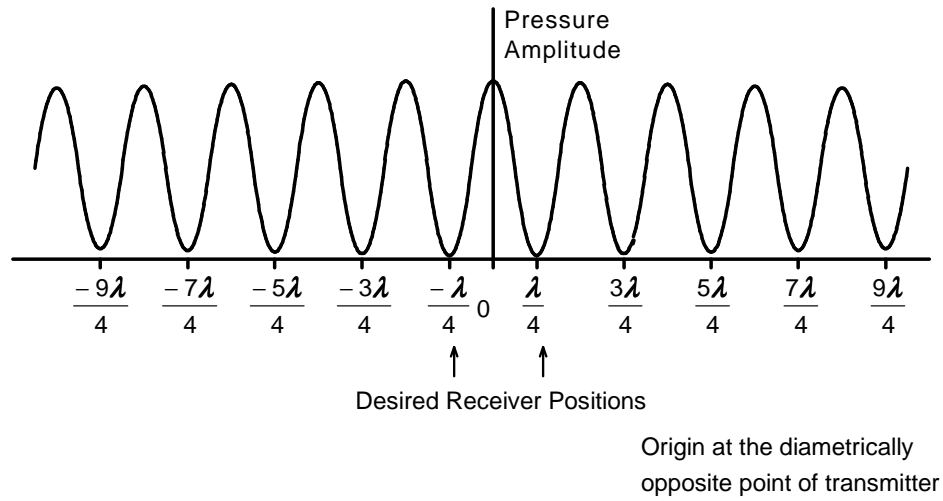


Fig. 2-15. The graph of pressure amplitude of acoustic short circuit versus displacement of the receiver.

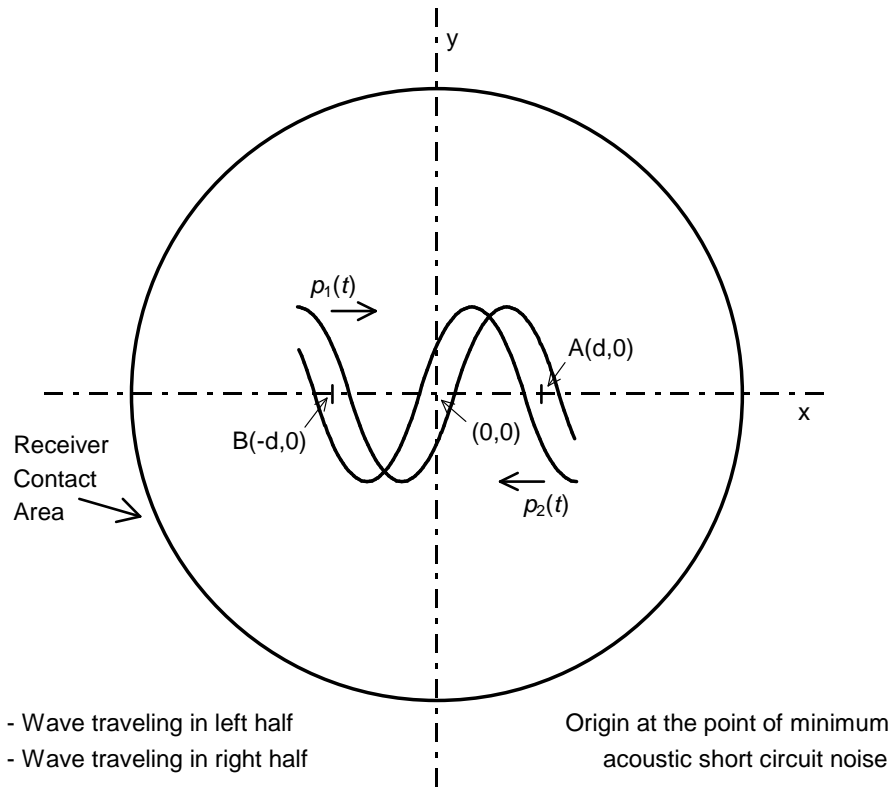


Fig. 2-16. Acoustic short circuit waveforms for the receiver in full contact with the pipe.

Let the wave in the left half be

$$p_1(t) = P_m \cos(\omega t) \quad (2.14)$$

As explained in Section 2.7.4, the wave in the right half will be out of phase, i.e.

$$p_2(t) = P_m \cos(\omega t + \pi) = -P_m \cos(\omega t) \quad (2.15)$$

Consider the two points A($d,0$) and B($-d,0$) at a distance of d from the origin which is the center of the receiver contact area (Fig. 2-16). The pressure amplitude at A is

$$\begin{aligned} p_A(t) &= p_{1A}(t) + p_{2A}(t) \\ &= P_m \cos\left(\omega t + \frac{2\pi d}{\lambda}\right) - P_m \cos\left(\omega t - \frac{2\pi d}{\lambda}\right) \end{aligned} \quad (2.16)$$

The pressure amplitude at B is

$$\begin{aligned} p_B(t) &= p_{1B}(t) + p_{2B}(t) \\ &= P_m \cos\left(\omega t - \frac{2\pi d}{\lambda}\right) - P_m \cos\left(\omega t + \frac{2\pi d}{\lambda}\right) \end{aligned} \quad (2.17)$$

From (2.16) and (2.17),

$$p_B(t) = -p_A(t) \quad (2.18)$$

Hence the two points equidistant from y-axis experience the pressure waves which are out of phase. Consequently, the electrical charge developed in the crystal at the two points will have equal magnitudes but opposite polarities, and will be canceled. Thus, the acoustic short circuit noise is minimum, if the receiver is displaced from the diametrically opposite point of the transmitter by a distance of $\lambda/4$ along the circumference of the pipe.

From the theoretical and experimental study of the acoustic short circuit noise given in this Section (2.7), it can be concluded that the acoustic short circuit noise is maximum, irrespective of the transmission frequency, when the transmitter and receiver are placed exactly diametrically opposite. Therefore, diametrically opposite mounting of the transducers should be avoided. For a given frequency the magnitude of short circuit noise is almost zero, if one of the transducers is displaced from the diametrically opposite point by a distance of $\pm(n\lambda \pm \lambda/4)$ along the circumference.

2.8 Conclusions

For sensing turbulence in single-phase flow through pipes, phase demodulation of continuous wave ultrasound, transmitted across the pipe diameter, has to be used. However, the use of continuous wave ultrasound generates standing waves inside the pipe, and a change in the standing wave pattern owing to variations in oscillator frequency, temperature, or rheology of the flowing medium can affect the accuracy of the measurement. The reflections within the pipe wall, also affect the strength of the fluid-borne signal. In addition, the acoustic short circuit through the pipe wall tends to swamp the fluid-borne signal.

Usually the most significant problem, viz. standing waves inside the pipe, is minimized with the help of a feedback control [9]. However, minimizing all the three problems simultaneously is difficult. This is probably the main reason why researchers later changed over from continuous wave ultrasound to pulsed ultrasound. In 1988, Xu et al. [10] used pulsed ultrasound for two-component flow measurement in a vertical pipe carrying water with artificially injected air bubbles. The amplitude modulation of ultrasonic pulses, as a result of scattering by air bubbles, was detected at two locations and used for flow velocity calculation using cross-correlation. However, application of pulsed ultrasound for single-phase flow measurement by cross-correlation, to the best of author's knowledge, has not been reported, though single-phase flow is most common in industrial applications, e.g. clean water flow. The major difficulty in applying pulsed ultrasound for single-phase flow has been that, the only disturbance detectable by ultrasound in single-phase flow is the natural turbulence, and pulsed ultrasound is minimally sensitive to turbulent eddies.

From the literature survey and the investigations reported in this chapter, we deduced that the continuous wave ultrasound would be unsuitable for single-phase flow measurement, and examined the viability of pulsed ultrasound for sensing turbulence. Preliminary experiments, using pulsed ultrasound on clean water flow in PVC pipe, showed no amplitude modulation of the pulses. However, minute variations in the transit time of the pulses were observed. Consequently, a new technique was devised to facilitate sensing variations in the transit time of the ultrasonic pulses caused by the turbulence. The technique is explained in Chapter 3.

Chapter 3

A NEW TECHNIQUE FOR SENSING TURBULENCE BY PULSED ULTRASOUND

A steady turbulent flow can be regarded as a mean flow velocity vector, with additional fluctuating velocities that average out to zero over sufficiently long period [19]. The fluctuating velocities mainly result from the irregular motions of the eddies. The turbulent velocity component normal to the flow axis can be sensed by measuring the change in the time of flight of an ultrasonic pulse transmitted along the pipe diameter. The variation in the time of flight of an ultrasonic pulse, in the presence of the turbulent velocity component, is extremely small compared with the total time of flight of the pulse across the pipe, and therefore difficult to measure reliably, e.g. the transit time of an ultrasonic pulse across a pipe of 90 mm diameter carrying water (acoustic velocity = 1482 m/s) is about 60 μ s and the variation in transit time caused by a turbulent velocity component of 0.1 m/s is approximately 4 ns. Besides, the uncertainty in detecting the exact instant of pulse arrival is considerably large, since the received pulse lacks a dominant leading edge because of initial build-up [20]. Therefore, it is practically impossible to detect the variations by measuring the transit time even with highly accurate devices. A new technique has been developed to overcome these difficulties. This chapter provides a description of the technique, its circuit implementation, tests by sensing water currents artificially generated in a tank, and application for detecting turbulence non-invasively in a PVC pipe carrying water.

3.1 The Technique

The block diagram of the system used to sense the turbulent velocity component perpendicular to the flow axis in a pipe is shown in Fig. 3-1. Two ultrasonic transducers, T1 and T2, both of which act as transmitter and receiver, are mounted diametrically opposite each other on the pipe wall. The two transducers facing each other transmit ultrasonic pulses at the same instant and in opposite directions. Each pulse, after passing through the fluid in the pipe, is received by the opposite transducer now acting as a receiver. The received signals $q_1(t)$ and $q_2(t)$ from the two transducers are fed to a differential amplifier. Under ideal conditions and in the absence of the turbulent velocity component, the two pulses arrive at the same instant and the differential amplifier output is zero.

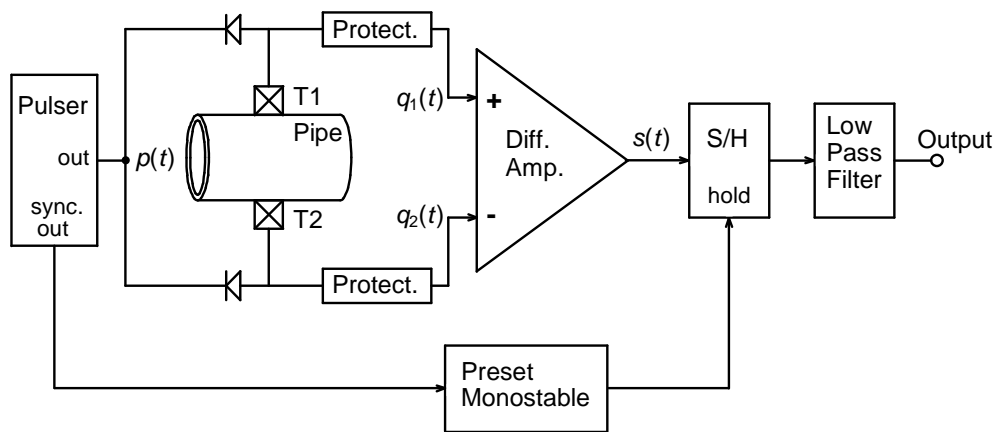


Fig. 3-1. Block diagram of the system used to sense turbulence using pulsed ultrasound.

When the flow is turbulent, the turbulent velocity component in the direction of the axis of placement of the transducers alters the velocity of the pulses. Therefore, the instants of arrival of the pulses are different and the output of the differential amplifier is non-zero. The turbulent velocity component alters the time of flight of the two pulses by the same magnitude but in opposite directions. The turbulent velocity component, although varying along distance, its profile can be considered to be constant during the time of flight. The differential amplifier output $s(t)$ is a function of the turbulent velocity component, during the pulse travel. The output of the differential amplifier is sampled at its peak, in order to maximize the sensitivity to the turbulent velocity component. The peak of the differential amplifier output occurs at a time corresponding to the transit time of the ultrasonic pulses at no flow. Therefore, the sampling instant for maximum sensitivity is not affected by the magnitude of the turbulent velocity component and the sampling instant can be derived from the instant of pulse transmission with the help of a preset delay set equal to the transit time of the ultrasonic pulses across the pipe at no flow. The sampled signal value is a function of the turbulent velocity component encountered by the pulses during their travel.

A train of pulses can be used for periodically sampling the effect of turbulent velocity component, provided that the pulse repetition frequency substantially exceeds twice the bandwidth of the flow turbulence signal, in order to obtain a proper reconstruction of the flow turbulence. A sample-and-hold amplifier followed by a low pass filter is employed for this purpose.

3.2 Circuit Implementation of the Technique

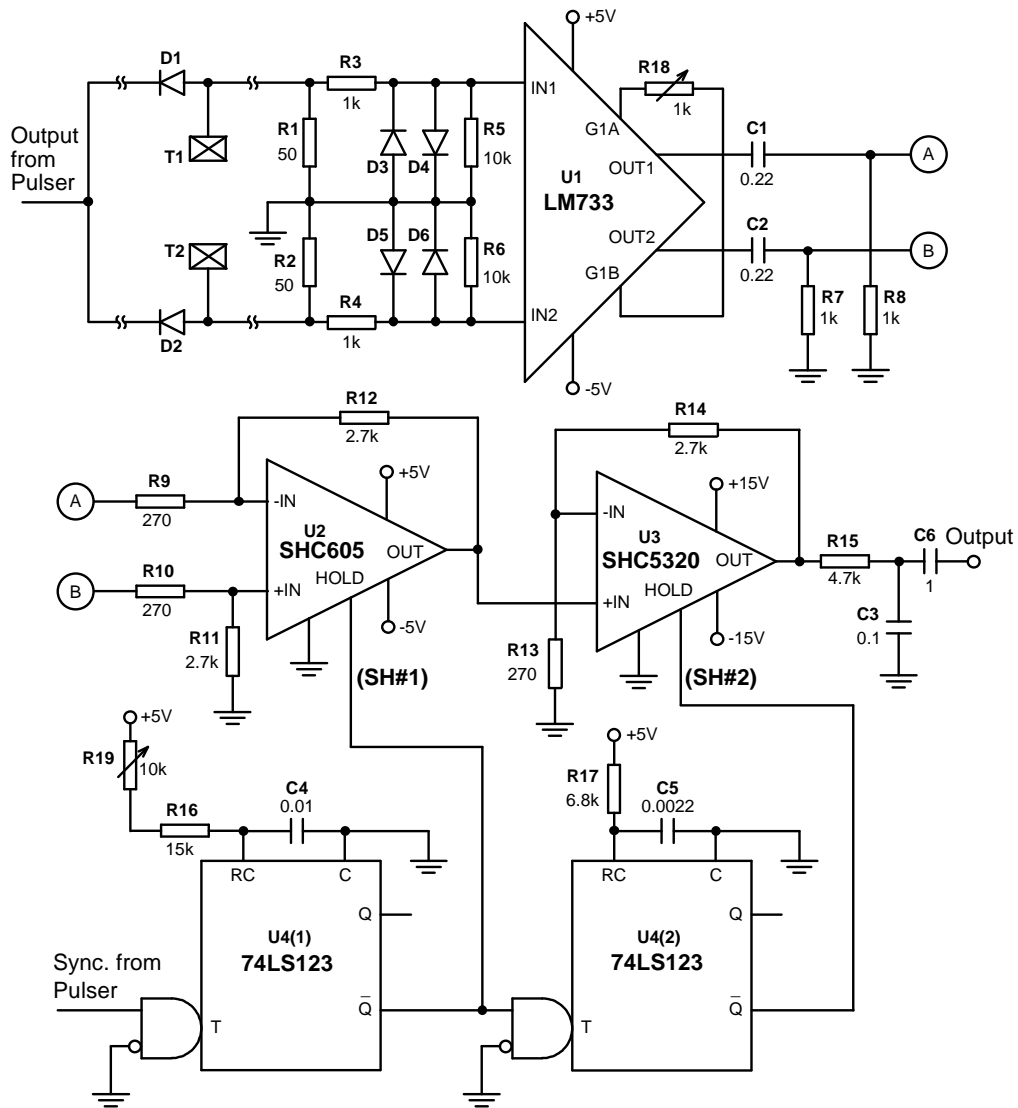
For a circuit implementation of the technique shown as a block diagram in Fig. 3-1, the bandwidth of the signals should be calculated. The ultrasonic transducers used in the experiment have the resonant frequency of 2 MHz and 6 dB bandwidth of 60 %, hence the frequency response contains significant frequency components up to 3.2 MHz. Considering that the bandwidth of the differential amplifier is required to be greater than 5 times the maximum frequency component in the signals, the differential amplifier should have a bandwidth greater than 16 MHz. The important specifications of a sample-and-hold circuit are the acquisition time, aperture delay, aperture uncertainty, and droop rate [21]. In this application, the sample-and-hold is required to hold its output without appreciable decay until the next sampling instant which succeeds the reception of the next set of ultrasonic pulses. The pulse repetition rate of transmission of ultrasonic pulses, based on the criterion stated in the previous section, is usually about 1 k pulses/s. Hence for a 16-bit data acquisition system with full scale input voltage of 20 Vp-p, the droop rate

should not exceed 0.3 mV/ms. The acquisition time should be insignificant (less than 1 %) compared with the pulse repetition period, so that the distortion in the sampled waveform during acquisition is eliminated by the smoothing filter. Hence the required acquisition time should be less than 10 μ s. The aperture delay can be compensated for by altering the sampling instant accordingly. The maximum slew rate of the input signal determines the desired aperture uncertainty. The maximum slew rate of a 20 Vp-p sinusoid of frequency 2 MHz is 125 V/ μ s, and the aperture uncertainty for 16-bit data acquisition is required to be less than 2.44 ps [21].

The technique represented by the block diagram in Fig. 3-1, was implemented using the circuit diagram shown in Fig. 3-2, with the components selected in accordance with the required specifications. The differential amplifier is LM733 which has a bandwidth of 40 MHz for a gain of 400, and CMRR of 60 dB at 5 MHz. A sample-and-hold amplifier with the desired specifications, viz. aperture uncertainty less than 2.44 ps and droop rate less than 0.3 mV/ms, was not available. In order to achieve low dynamic sampling error and low droop rate, two sample-and-hold amplifiers have been used. The first stage consists of SHC605, high-speed operational track-and-hold amplifier, which has an aperture delay of 1.7 ns, aperture uncertainty of 2.4 ps rms, and full power bandwidth of 32 MHz. However, its hold time is considerably small, viz. 2 μ s maximum; therefore the second stage of sample-and-hold should have acquisition time less than 2 μ s. In addition, it should satisfy the requirement of droop rate. The SHC5320, high speed sample/hold amplifier, was found suitable, as its maximum acquisition time is 1.5 μ s to 0.01 %, and typical droop rate is 0.08 μ V/ μ s with internal hold capacitor. The logic signals for the sample-and-hold amplifiers have been generated with the help of TTL monostable multivibrator 74LS123. The following subsections explain the operation of each block of the circuit.

3.2.1 Transmitter-receiver circuit

An ultrasonic pulser is employed to excite the transducers when they are used as transmitters. The pulser applies a short negative high voltage pulse to the transducers through the diodes (D1, D2) (Fig. 3-2). The diodes isolate the signals received by the transducers when the same transducers work as receivers. The received signals after 50 Ω termination (R1, R2) are passed through the diode protection circuit which protects the differential amplifier LM733 from the high voltage spike generated by the pulser. The LM733 is a differential input, differential output, wideband video amplifier [22]. The characteristics of LM733 are given in Appendix A. As shown in Fig. 3-2, the gain of the differential amplifier is adjustable from 10 to 400 with the help of a preset resistance R18.



All resistors are in Ω .
 All capacitors are in μF .
 All diodes are 1N4148.

Fig. 3-2. Circuit diagram of the system used to sense turbulence using pulsed ultrasound.

3.2.2 Sample-and-hold

As mentioned earlier, the sample-and-hold amplifier has been realized using two stages, SH#1 and SH#2. The differential output from LM733 goes to the track-and-hold amplifier SHC605 which is configured for a differential gain of 10. The SHC605 is basically a high-speed operational amplifier which can hold its output on command. The SHC605 can be used with non-inverting, inverting, or differential gains. The differential internal hold capacitors in SHC605 provide a first-order correction for many errors including distortion, pedestal, and droop [23]. The second stage of the sample-and-hold has SHC5320 in non-inverting configuration with a gain of 10. The important specifications of SHC605 and SHC5320 are given in Appendix A. The output of SH#2 is followed by a first order low pass filter of cut-off frequency 340 Hz in order to smoothen the sampled waveform. The capacitor C6 removes the offset at the output of SH#2. The ac component of the signal is a function of the turbulent velocity component perpendicular to the flow direction.

3.2.3 Timing block

The sampling instant corresponds to the zero crossing instant of either of the received pulses at zero flow in order to maximize sensitivity to the measured turbulent velocity component. Since the turbulent velocity components alter the time of flight of the two ultrasonic pulses traveling in opposite directions, by almost the same magnitude but in the opposite directions, the sampling instant for maximum sensitivity does not depend on the magnitude of turbulent velocity component and may be derived from fixed delays. The sample/hold signals for the two sample-and-hold amplifiers are generated with the help of the two monostable multivibrators in 74LS123. The hold signal to the sample-and-hold amplifier SH#1 is generated by the first monostable. The trigger of the first monostable is obtained from the synchronization output of the pulser and the pulse width is preset to obtain the hold signal at the zero crossing of a received pulse at no flow. The pulse width of the second monostable which controls the sample-and-hold SH#2, is kept larger than its acquisition time (1.5 μ s) and smaller than the hold time of SH#1 (2 μ s).

3.3 Sensing Water Currents in a Tank

The operation of the circuit has been tested by sensing water currents generated artificially in a tank. In this experiment, the circuit shown in Fig. 3-2 was assembled using the following components:

U1 : Two stage amplifier with AD524 Instrumentation amplifier and LM318 Op-Amp, with the first stage gain set for 100 and the second stage gain set for 18, i.e. overall nominal gain = 1800.

U2, U3 : LF398 Sample-and-Hold Amplifier,

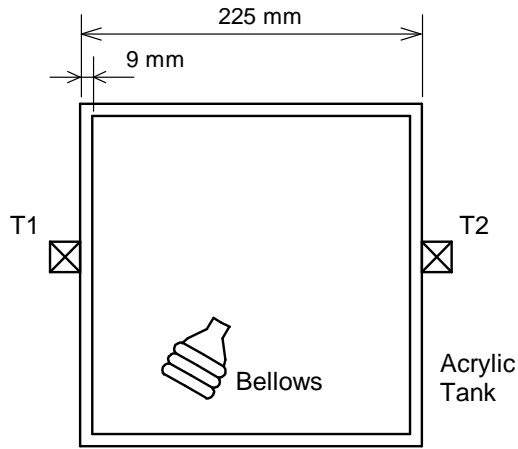
U4 : 74LS123 Monostable Multivibrator.

The results given in this and the following section are obtained using these components.

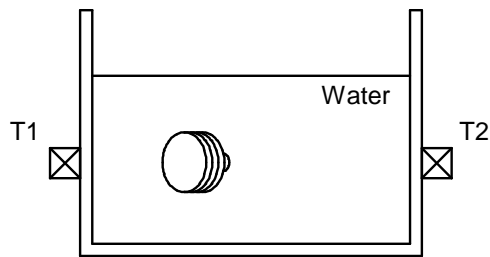
Two pulsed-type ultrasonic transducers T1 and T2 were mounted facing each other, from outside the opposite walls of a rectangular water tank, as shown in Fig. 3-3. The tank was made of acrylic sheets of 9 mm thickness. The distance between the transducers was 225 mm. Bellows were used to generate a water current with a velocity component in the direction of propagation of ultrasound. The specifications of the ultrasonic transducers are:

Center frequency: 2.25 MHz
6 dB bandwidth: between 40 % and 70 %
Active element diameter: 25 mm

A pulser excites both the transducers simultaneously at a pulse repetition rate of 1 k pulses/s. The ultrasonic pulses generated by the transducers travel through water in opposite directions and are received by the transducers which now act as receivers. The difference in the received signals is amplified using the differential amplifier stage that has a gain of 5 measured at 2 MHz. The received signals when water in the tank is undisturbed, are shown in Fig. 3-4 (a) and (b), and the differential amplifier output is shown in Fig. 3-4(c). The signals were recorded with 8-bit resolution at a sampling rate of 100 M sample/s for a record length of 16 k samples ($\approx 160 \mu\text{s}$) per waveform, using the signal analyzer *Analogic model DATA6000*. The expanded waveforms are shown in Fig. 3-5. It can be observed that the ultrasonic pulses (Fig. 3-5(a), (b)) have reached at the same time, and have identical shapes and equal magnitudes; hence the differential amplifier output (Fig. 3-5(c)) is negligible (50 mVp-p) after an amplification of 5. Fig. 3-6 shows the output of the differential amplifier in three cases: no disturbance (Fig. 3-6(a)), water current in one direction (Fig. 3-6(b)), and water current in the opposite direction (Fig. 3-6(c)). It is observed that the waveform gets inverted if the direction of water current is reversed. By varying the intensity of water currents it is also noted that the peak amplitude increases for larger flow currents.



(a) Top View



(b) Front View

Fig. 3-3. Diagram of the set-up for sensing water currents in a tank. (a) Top view, showing transducer positions and the bellows to generate water currents in the tank. (b) Front view of the set-up.

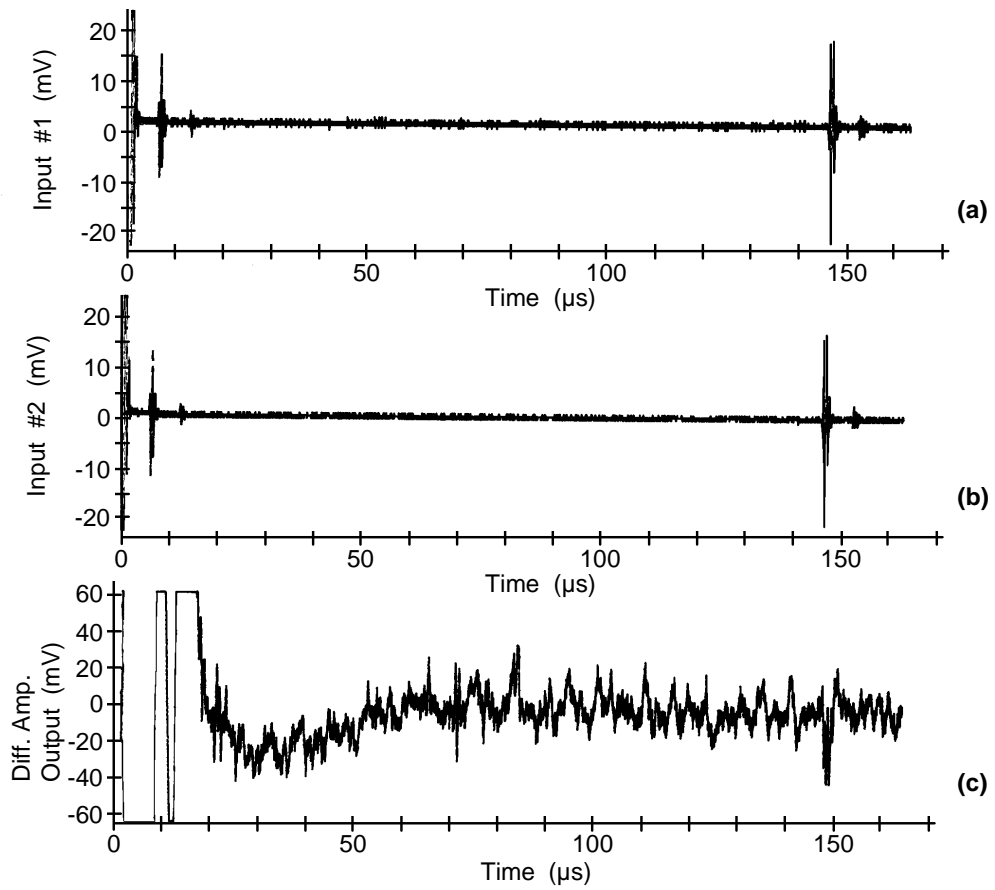


Fig. 3-4. Input and output waveforms of the differential amplifier for still water. (a) and (b) inputs to the differential amplifier from the two transducers; (c) output of the differential amplifier. The gain of the differential amplifier is 5 at 2 MHz. The origin is at the instant of pulse transmission. The pulses have reached the receivers at about 148 μs . The portion of the waveforms around 148 μs is shown on expanded time scale in Fig. 3-5.

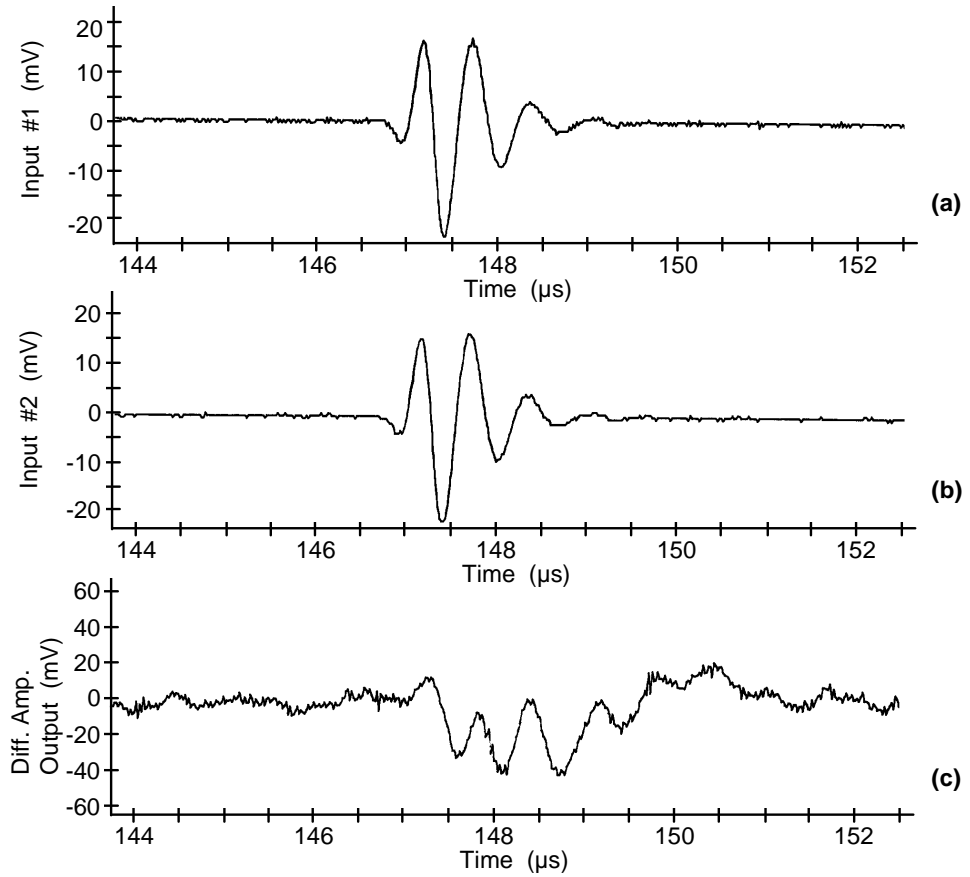


Fig. 3-5. Expanded waveforms of Fig. 3-4. (a) and (b) inputs to the differential amplifier from the two transducers; (c) output of the differential amplifier. The gain of the differential amplifier is 5 at 2 MHz. Note that the two inputs are identical and the differential amplifier output is insignificant.

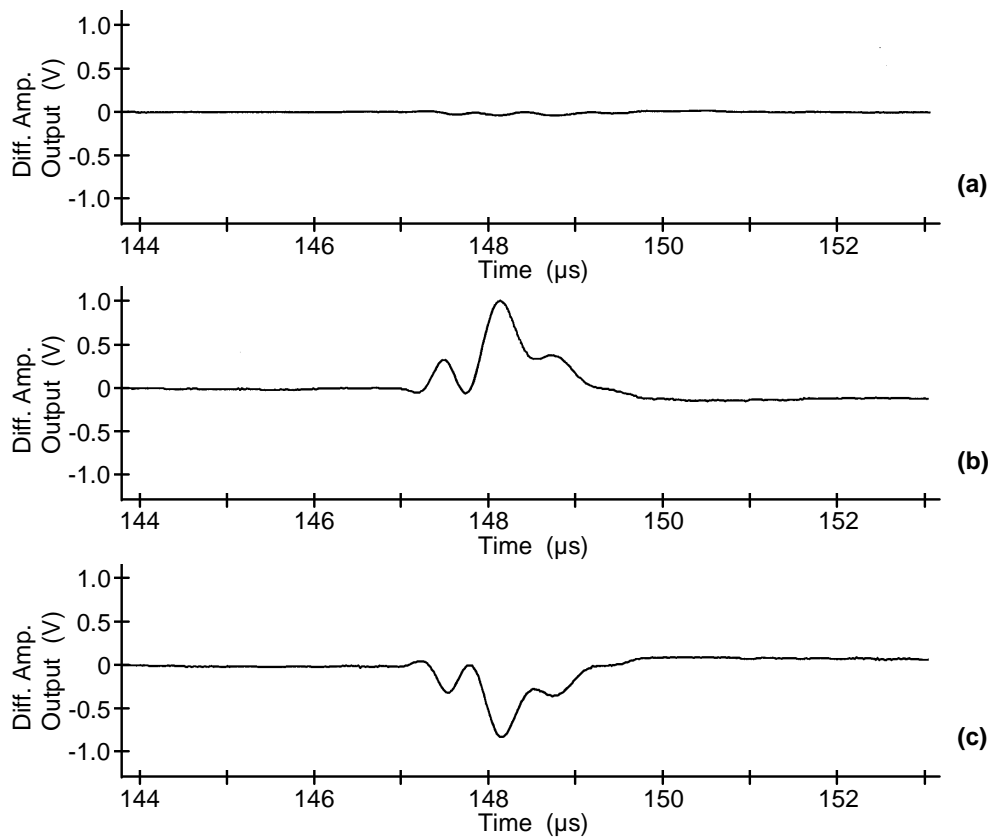


Fig. 3-6. Differential amplifier output in three cases: (a) still water; (b) water current in one direction; (c) water current in the opposite direction.

The peak amplitude is a function of the velocity component of water current in the direction of pulse propagation. The velocity component is obtained as a function of time by sampling the peak amplitude with the help of a sample-and-hold circuit. Typical waveforms for S/H operation are shown in Fig. 3-7. Two stages of sample-and-hold, SH#1 and SH#2, are required in order to obtain low dynamic sampling error and low droop rate. The Sample/Hold signal to SH#1 is obtained from the monostable multivibrator. The S/H#1 input, S/H control signal, and the output are shown in Fig. 3-7 (a), (b), (c), respectively, and the time expanded waveforms are shown in Fig. 3-8. The SH#1 goes into sampling mode when the ultrasonic pulses are transmitted (Fig. 3-7(b)), and the pulse width of the monostable is so adjusted that SH#1 holds its output at the peak of the signal as shown in Fig. 3.8(c). The second stage of sample-and-hold, SH#2, holds the signal sampled by SH#1, without appreciable decay, till the next set of pulses is received. The monostable multivibrator controlling the sample-and-hold signal of SH#2 is triggered by the hold signal of SH#1, and its pulse width is adjusted larger than the acquisition time of SH#2 and shorter than the hold time of SH#1. Fig. 3-9(b) shows the sample/hold control signal to SH#2. Fig. 3-9(a) and (c) show the input and output of SH#2, respectively. These waveforms expanded on time scale are shown in Fig. 3-10.

3.4 Sensing Turbulence in Pipe

The set-up described in the previous section was employed to sense the turbulence in a PVC pipe carrying water. The transducers were mounted diametrically opposite as shown in Fig. 3-1, on a PVC pipe fixed in the water circulation system (described in Section 5-2). The outer diameter of the pipe was 90 mm and the transducers were pulsed type with the specifications as given below.

Center frequency:	2.25 MHz
6 dB bandwidth:	between 40 % and 70 %
Active element diameter:	25 mm

The turbulence waveforms were recorded for 1.5 s with various flow rates. These waveforms are shown in Fig. 3-11 for approximate flow rates of (a) 100 L/min, (b) 300 L/min, (c) 500 L/min, and (d) 650 L/min. The corresponding spectra of the turbulence signals are given in Fig. 3-12. These are the graphs of magnitude coefficient (peak value of a frequency component) versus frequency obtained with the help of the signal analyzer *Analogic model DATA6000*. It can be observed that the amplitude and bandwidth of turbulence signal increase with higher flow rates.

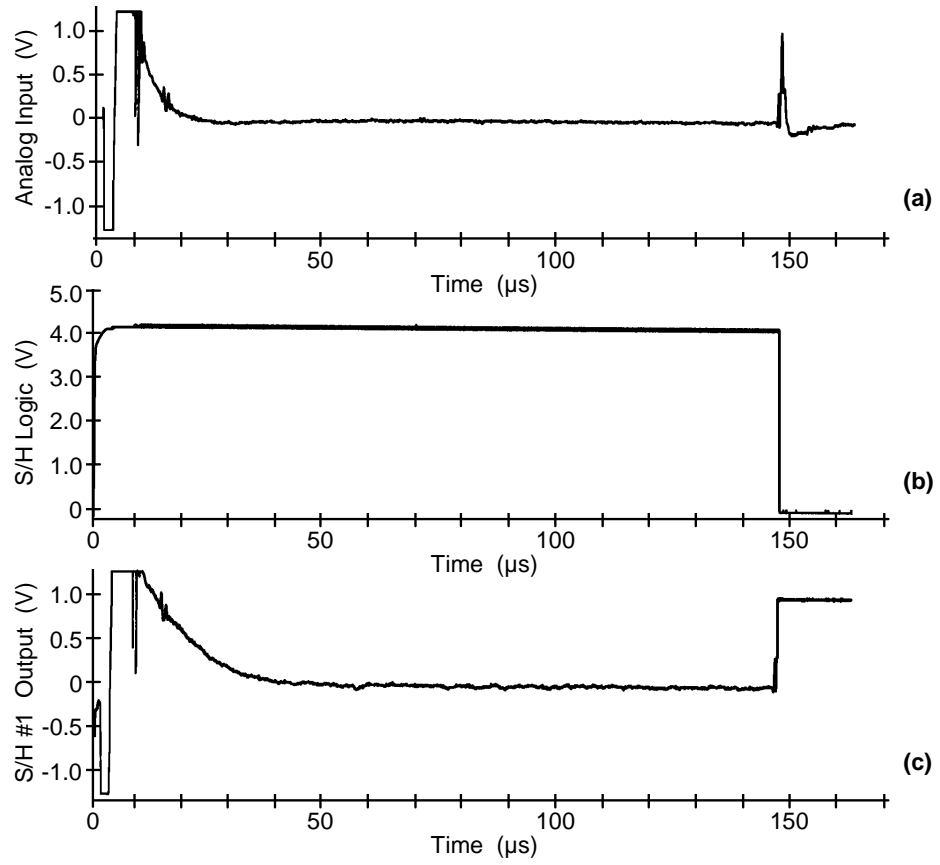


Fig. 3-7. Waveforms for S/H#1. (a) Analog input signal from the differential amplifier; (b) S/H logic signal from monostable multivibrator #1; (c) output of S/H#1. The origin is at the instant of pulse transmission. The waveforms expanded on the time scale are shown in Fig. 3-8.

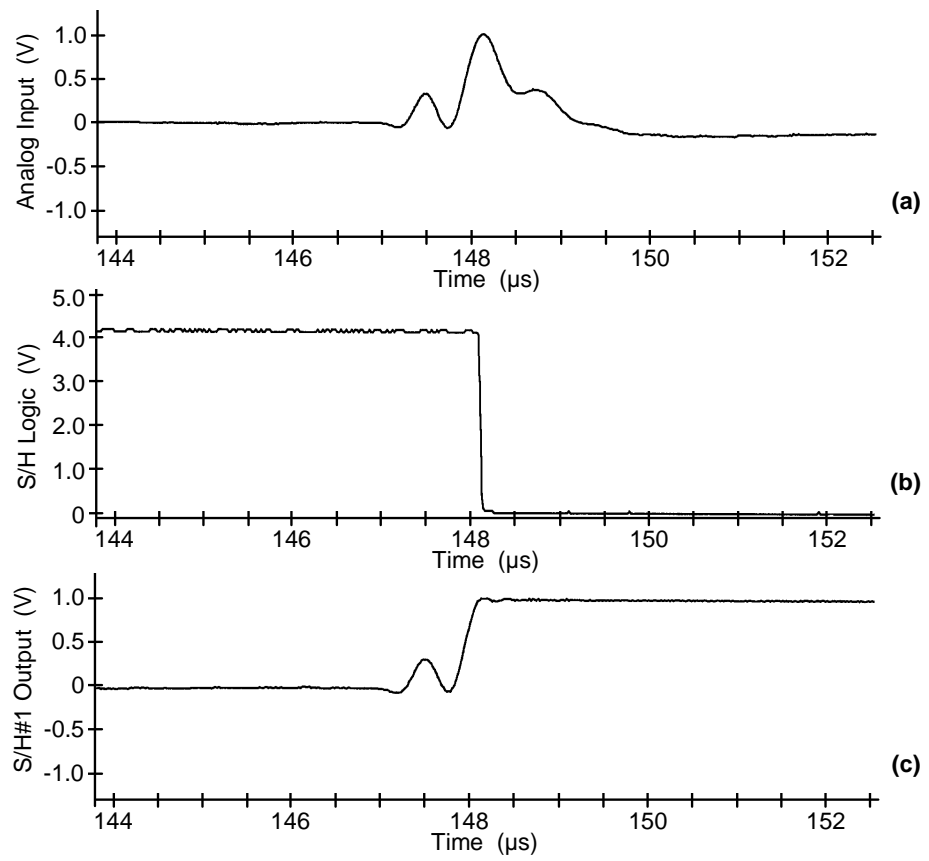


Fig. 3-8. Expanded waveforms for S/H#1. (a) Analog input signal from the differential amplifier; (b) S/H logic signal from monostable multivibrator #1; (c) output of S/H#1.

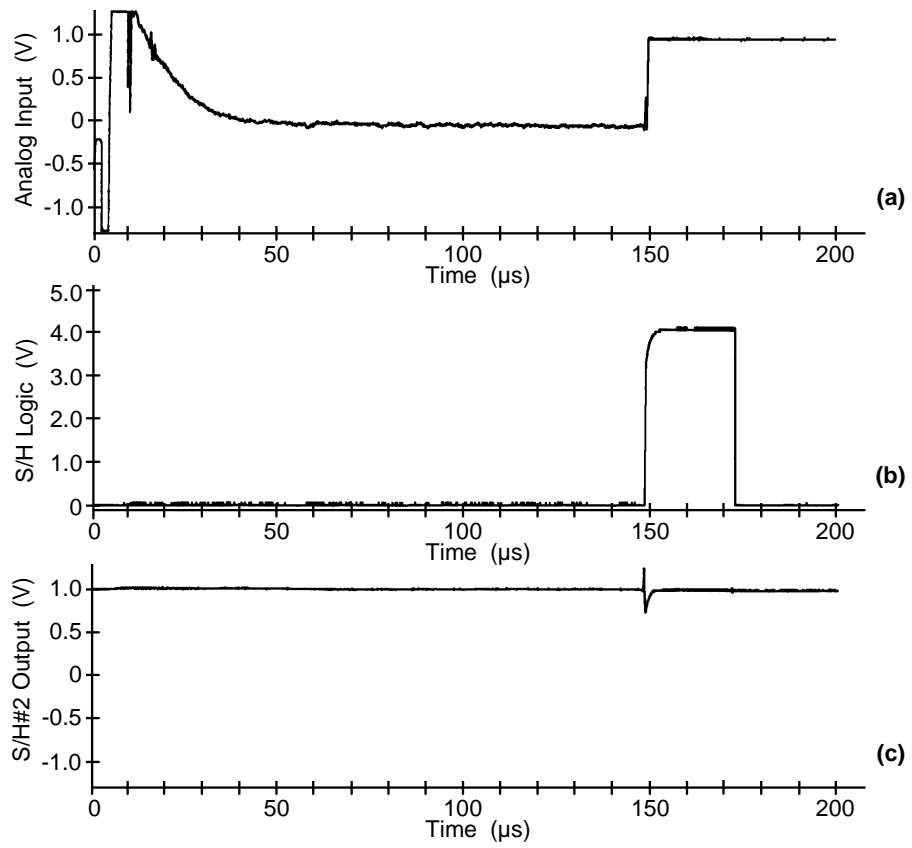


Fig. 3-9. Waveforms for S/H#2. (a) Analog input signal from SH#1; (b) S/H logic signal from monostable multivibrator #2; (c) output of S/H#2. The origin is at the instant of pulse transmission. The waveforms expanded on the time scale are shown in Fig. 3-10.

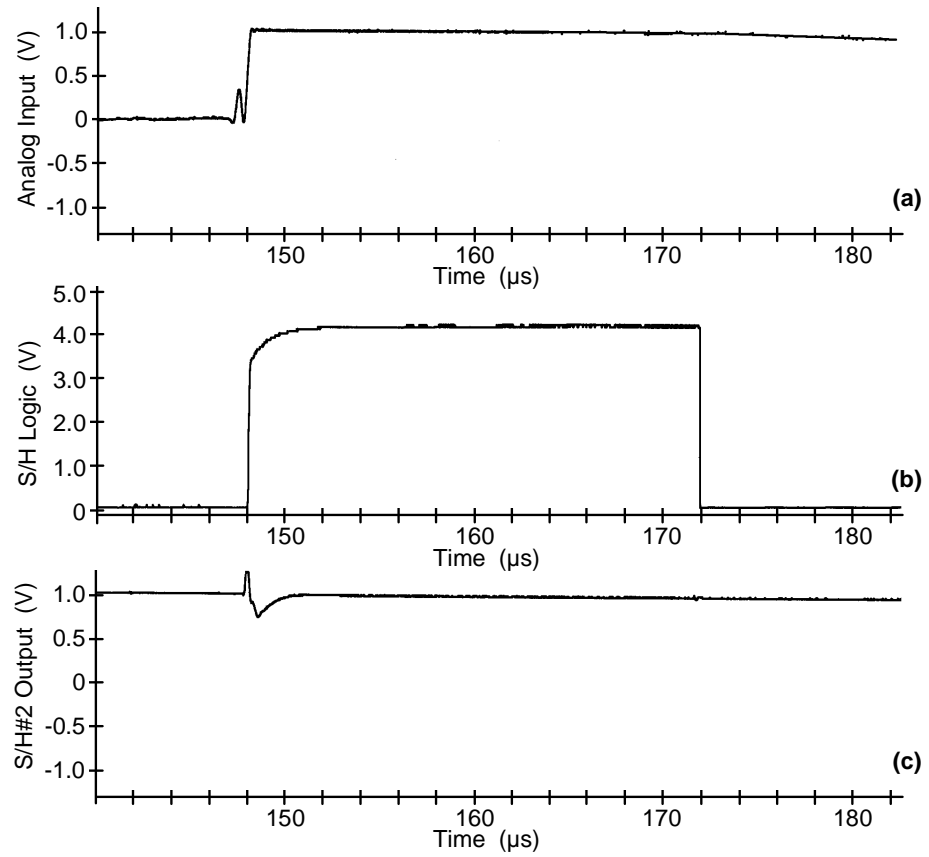


Fig. 3-10. Expanded waveforms for S/H#2. (a) Analog input signal from SH#1; (b) S/H logic signal from monostable multivibrator #2; (c) output of S/H#2.

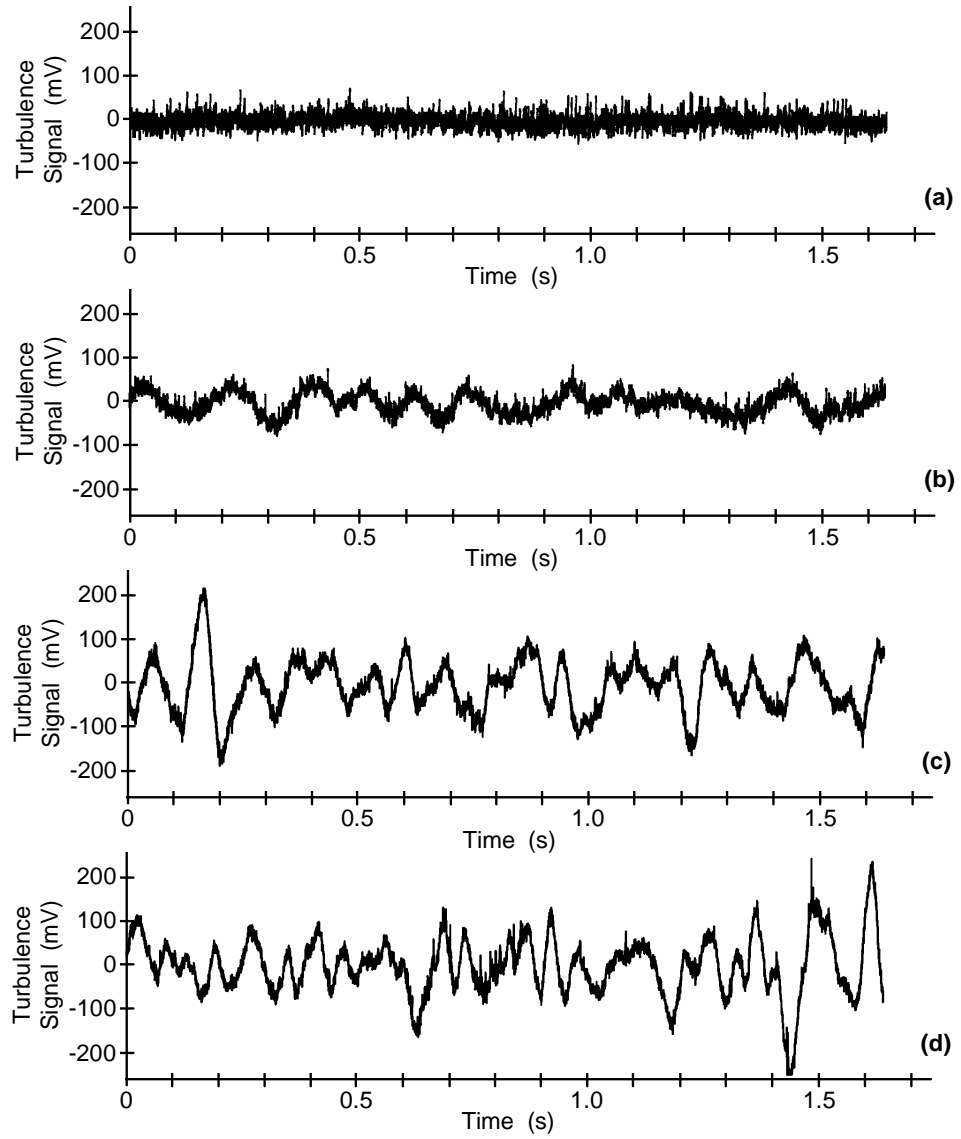


Fig. 3-11. Turbulence signal in a flow pipe sensed by the system at flow rates of approximately (a) 100 L/min, (b) 300 L/min, (c) 500 L/min, (d) 650 L/min.

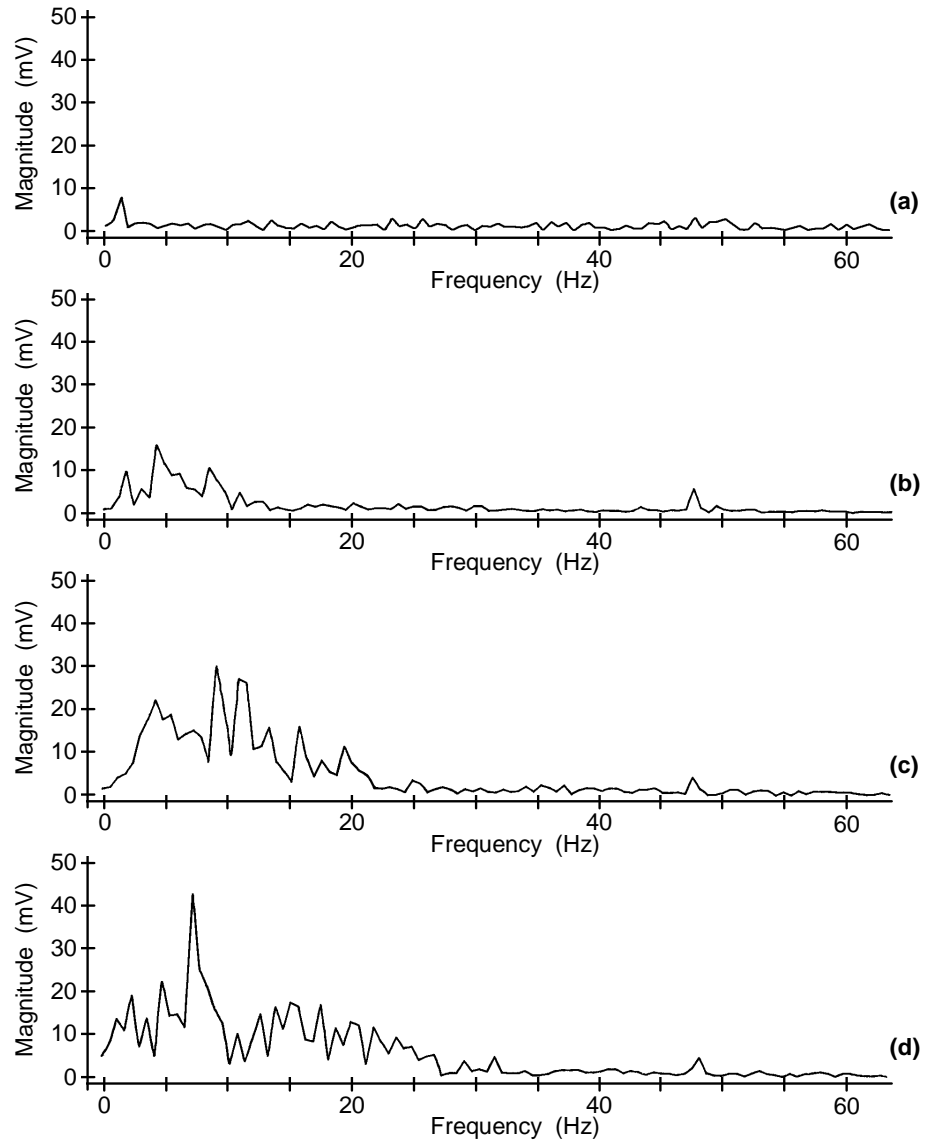


Fig. 3-12. The magnitude spectra of the turbulence signals shown in Fig. 3-11. Flow rates are approximately (a) 100 L/min, (b) 300 L/min, (c) 500 L/min, (d) 650 L/min.

The turbulence waveforms thus sensed at two suitable locations on the pipe may be cross-correlated and used to measure flow rate as described in the following section.

3.5 Flow Measurement by Cross-Correlation

The block diagram of a flowmeter using cross-correlation of the turbulence signals sensed by the technique explained above is shown in Fig. 3-13. Two pairs of ultrasonic transducers T_{A1} - T_{A2} and T_{B1} - T_{B2} are mounted at suitable locations on a pipe. The pulser excites the transducers simultaneously. The circuit explained in Section 3.2 receives the signals obtained from the upstream transducer pair and generates the turbulence signal $x(t)$. An identical circuit generates the downstream turbulence signal $y(t)$ from the signals obtained at the other pair of transducers. The cross-correlator computes the cross-correlation function of $x(t)$ and $y(t)$, and determines the flow rate from the peak in the cross-correlation function. A theoretical treatment of this technique and results of a numerical simulation are given in the next chapter. A description of the experimental set-up for using this technique for flow measurement, and the results are given in Chapter 5.

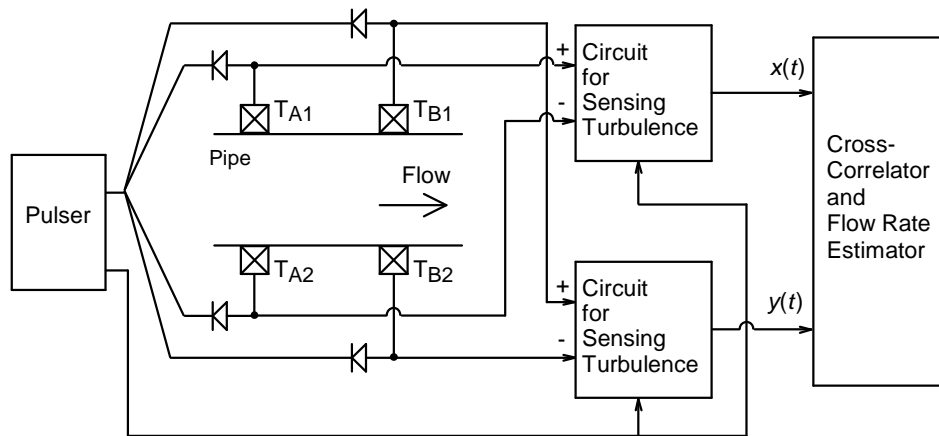


Fig. 3-13. Block diagram of the cross-correlation flowmeter based on ultrasonic sensing of turbulence.

Chapter 4

MODELING AND NUMERICAL SIMULATION

The technique developed for sensing turbulence using pulsed ultrasound, and its application for sensing water current in a tank and turbulence in a pipe carrying water have been described in the previous chapter. The technique facilitates sensing turbulent velocity component perpendicular to the flow axis in a pipe, by detecting the difference in the transit times of two ultrasonic pulses simultaneously transmitted in opposite directions across the pipe diameter. The pulses after traveling through the fluid are received by the same pair of transducers. The turbulent velocity component alters the velocity of the pulses and the times of flights of the pulses change.

As discussed earlier, the difference in the time of flight of an ultrasonic pulse, caused by the turbulent velocity component, is extremely small and practically difficult to detect by measuring the time of flight of the pulse. The proposed technique, as explained in Chapter 3, detects the difference in the times of flights of the two pulses by subtracting the received pulses with the help of a differential amplifier. The differential amplifier output is sampled at its peak in order to maximize the sensitivity to the turbulent velocity component. The sampled amplitude is a function of the turbulent velocity component.

In Section 4.1, the relationship between the difference in the times of flights of the two pulses and the turbulent velocity component is derived. The relationship between the sampled differential amplifier output and the difference in times of flights is derived in Section 4.2. A model representing ultrasonic pulse transmission and reception, associated with the new technique of sensing turbulent velocity component, is given in Section 4.3. A numerical simulation based on the theoretical model has been carried out. The simulation and the results are given in Section 4.4. The turbulence pattern alters between the two sensing locations as it moves along the pipe. The dispersion in turbulence pattern has been simulated by adding random noise in the downstream signal for studying its effect on the cross-correlation function. Effect of using finite number of bits in digitization of the sensed signals has also been studied.

4.1 Relationship between Turbulence and Change in Time of Flight

The turbulent eddies generate flow velocity components in the direction perpendicular to the flow axis. These components alter the time of flight (TOF) of an ultrasonic pulse transmitted perpendicular to the flow axis.

Consider a pair of transducers T1 and T2, mounted on a pipe of diameter D , as shown in Fig. 4-1. Consider the ultrasonic pulses transmitted by the two transducers simultaneously in opposite directions. Let the velocity component of the flow at point $P(r)$, along the path of ultrasound propagation, be $v(r)$; and the acoustic velocity in water be c . The effective velocity of the pulse traveling in the direction of the turbulent velocity component at point P is $c+v(r)$. Here we assume that the profile of $v(r)$ does not change during the time of flight of the pulse. The resultant TOF is the line integral of the TOF (along the pipe diameter) owing to the local velocity component $v(r)$.

The TOF in the absence of the turbulence is the same for the pulse transmitted in either direction and is given as

$$t_0 = \frac{D}{c} \quad (4.1)$$

When the turbulence is present, the TOF of the pulse sent in the direction of $v(r)$ is

$$\begin{aligned} t_1 &= \int_{-D/2}^{D/2} \frac{1}{c+v(r)} dr \approx \frac{D}{c} - \frac{1}{c^2} \int_{-D/2}^{D/2} v(r) dr \\ &= t_0 - \Delta t \end{aligned} \quad (4.2)$$

Similarly TOF of the pulse sent in the direction opposite to $v(r)$ is

$$\begin{aligned} t_2 &= \int_{-D/2}^{D/2} \frac{1}{c-v(r)} dr \approx \frac{D}{c} + \frac{1}{c^2} \int_{-D/2}^{D/2} v(r) dr \\ &= t_0 + \Delta t \end{aligned} \quad (4.3)$$

From (4.2) and (4.3), the difference in TOF of the pulses in the two directions is given by

$$t_2 - t_1 = 2 \Delta t \approx \frac{2}{c^2} \int_{-D/2}^{D/2} v(r) dr \quad (4.4)$$

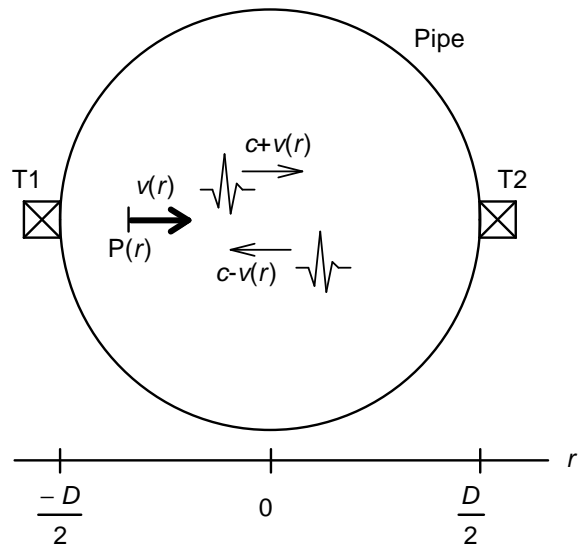


Fig. 4-1. Effect of turbulent velocity component $v(r)$ on the velocity of the two ultrasonic pulses traveling in opposite directions.

4.2 Relationship between Sampled Differential Voltage and Change in Time of Flight

The sampled version of the output of the differential amplifier is of interest. The excitation pulse and the received pulse are shown in Fig. 4-2 (a) and (b). Let us take the zero crossing immediately following the peak of the received pulse as $t=0$. Considering that the two transducers are excited by pulse $p(t)$, in the presence of turbulence, the time of flight of the received pulses will be altered by Δt , one of them delayed and the other advanced. The two received pulses $q_1(t)$ and $q_2(t)$ can be approximated about $t=0$, by two sinusoids $q_{1a}(t)$ and $q_{2a}(t)$ with amplitude A_m , and frequency ω , as shown in Fig. 4-2(d).

$$q_{1a}(t) = -A_m \sin(\omega t - \theta) \quad (4.5)$$

$$q_{2a}(t) = -A_m \sin(\omega t + \theta) \quad (4.6)$$

where θ is the phase change due to the turbulent velocity component

$$\theta = \omega \Delta t \quad (4.7)$$

From (4.4),

$$\Delta t \approx \frac{1}{c^2} \int_{-D/2}^{D/2} v(r) dr \quad (4.8)$$

The differential signal

$$\begin{aligned} s(t) &= q_{1a}(t) - q_{2a}(t) \\ &= 2 A_m \cos(\omega t) \sin \theta \end{aligned} \quad (4.9)$$

and is shown in Fig. 4-2(e). The sensitivity of the sampled value to the phase change is maximum at $t=0$, therefore the signal is sampled at $t=0$. In addition, the signal has zero slope at $t=0$ and it offers high immunity to slight variations in the sampling instant. The received signals are fed to a differential amplifier with a gain of A , and the differential amplifier output at $t=0$ is

$$s(0) = 2 A A_m \sin(\omega \Delta t) \quad (4.10)$$

Thus, (4.4) and (4.10) together relate the sampled value of the differential voltage to the turbulent velocity component along the path of the ultrasound.

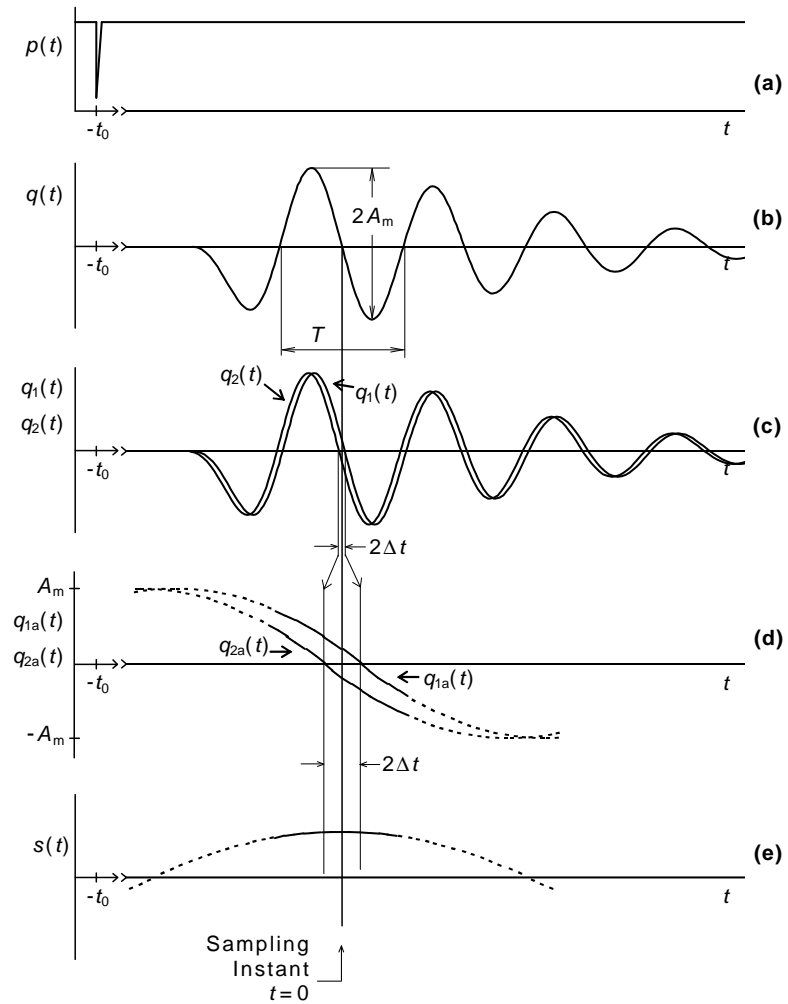


Fig. 4-2. Received pulses and differential amplifier output. (a) Excitation pulse $p(t)$; (b) a received pulse $q(t)$ in the absence of turbulence; (c) received pulses $q_1(t)$ and $q_2(t)$ in the presence of turbulence (Δt is the change in time of flight of a pulse caused by the turbulent velocity component); (d) the received pulses approximated about $t=0$ by sinusoids $q_{1a}(t)$ and $q_{2a}(t)$ shown on expanded time scale; (e) differential amplifier output $s(t)$. The sampling instant is at $t=0$.

4.3 A Theoretical Model of Pulse Transmission and Reception

Consider two ultrasonic transducers T1 and T2 mounted facing each other and diametrically opposite on a pipe as shown in Fig. 4-1, and used in the set-up shown in Fig. 3-1. Let D be the distance between the transducers, c be the acoustic velocity in the fluid flowing through the pipe, and v be the velocity component of turbulence in the direction of pulse propagation. The transducers transmit ultrasonic pulses simultaneously, and the pulses after propagation in the opposite directions are received after the delays as given in (4.2) and (4.3). The difference in the two received signals is sampled at an appropriate instant as explained in Section 4.2. The sampled magnitude is a function of the turbulence velocity component. A model of the transmission and reception of ultrasonic pulses is developed with the following simplifying assumption:

The impulse responses of a transducer as a transmitter $h_a(t)$ and as a receiver $h_b(t)$ are related as

$$h_b(t) = -k h_a(t) \quad (4.11)$$

where k is a constant and is the same for both the transducers.

With this assumption, we can model the two transducer set-up of Fig. 3-1 as a block diagram shown in Fig. 4-3 [24]. The pulser is modeled as an impulse generator. The transducers T1 and T2 as transmitters are modeled by the impulse responses $h_{1a}(t)$ and $h_{2a}(t)$ respectively, and the transmitted pulses arrive at the receivers after the delays of t_2 and t_1 , respectively. T1 and T2 as receivers are modeled by the impulse responses $h_{1b}(t)$ and $h_{2b}(t)$, respectively. Therefore the outputs of the two receivers are

$$q_1(t) = h_{2a}(t) * \delta(t-t_1) * h_{1b}(t) \quad (4.12a)$$

$$q_2(t) = h_{1a}(t) * \delta(t-t_2) * h_{2b}(t) \quad (4.12b)$$

The differential amplifier output is

$$\begin{aligned} s(t) &= A [q_1(t) - q_2(t)] \\ &= A [h_{2a}(t) * \delta(t-t_1) * h_{1b}(t) - h_{1a}(t) * \delta(t-t_2) * h_{2b}(t)] \end{aligned} \quad (4.13)$$

From (4.1)–(4.3) for zero turbulent velocity component, we get

$$t_1 = t_2 = t_0 = \frac{D}{c} \quad (4.14)$$

and the differential amplifier output at zero turbulent velocity component is

$$s_0(t) = A [h_{2a}(t) * h_{1b}(t) - h_{1a}(t) * h_{2b}(t)] * \delta(t-t_0)$$

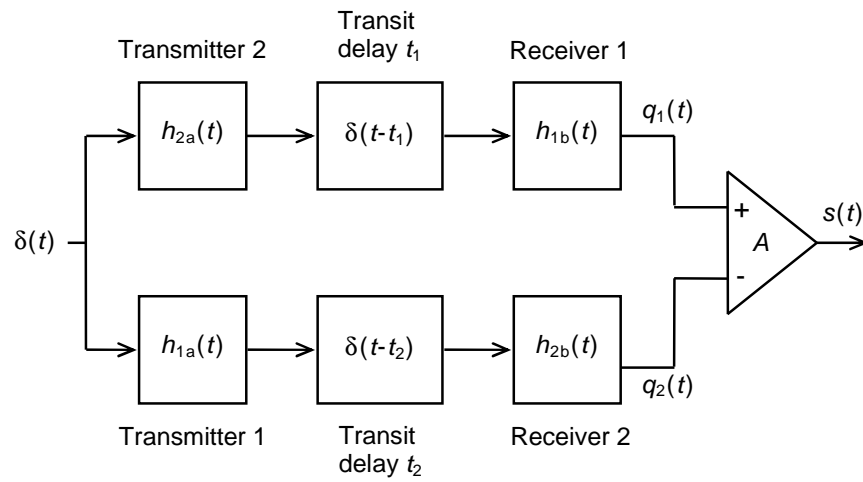


Fig. 4-3. Model of ultrasonic pulse transmission and reception.

Since in the absence of water currents, the experimentally recorded differential amplifier signal is zero as shown earlier in Fig. 3-6(a), we get

$$h_{2a}(t) * h_{1b}(t) = h_{1a}(t) * h_{2b}(t)$$

which is also obtained by applying the assumption about the transducer's impulse responses in its two roles as given in (4.11). With the assumption of (4.11) applied to (4.13), we get

$$s(t) = -A k h_{1a}(t) * h_{2a}(t) * [\delta(t-t_1) - \delta(t-t_2)] \quad (4.15)$$

As explained in Section 4.2, the differential amplifier output is sampled at $t = t_0$ in order to obtain maximum sensitivity, and the sampled value is a function of the turbulent velocity component. Therefore the sampled value is

$$x = s(t) \Big|_{t=t_0} \quad (4.16)$$

For a sequence of excitation pulses, the successive values of x after lowpass filtering give the turbulence signal $x(t)$.

4.4 Numerical Simulation of the Turbulence Sensing Technique and Cross-Correlation

The numerical simulation has been carried out with the ultrasonic transducer modeled as a second order underdamped system, with the impulse response given by

$$h(t) = \frac{1}{\sqrt{1-\zeta^2}} e^{-\zeta\omega_0 t} \sin(\omega_0 t \sqrt{1-\zeta^2}) \quad (4.17)$$

where ω_0 = undamped natural frequency of oscillation,
 ζ = damping ratio,

and is shown in Fig. 4-4 for $\zeta = 0.15$ which corresponds to 6 dB bandwidth of 48 % of the resonant frequency [25], [26]. The range of bandwidth of the transducers is generally from 20 % to 100 % depending on the damping.

The received waveforms $q_1(t)$ and $q_2(t)$ are calculated for $\zeta = 0.15$ and are shown in Fig. 4-5(b) for no turbulence. The velocity component of turbulence along the path of ultrasound propagation causes a change in the time of flight Δt as given in (4.1) and (4.3). For turbulent flow, Δt can be modeled as a random variable. For each excitation pulse, the value of Δt is obtained from a pseudo random number generator. The output of the generator is lowpass filtered in order to simulate the effect of the integration of the velocity profile and the band limited nature of the turbulence signal.

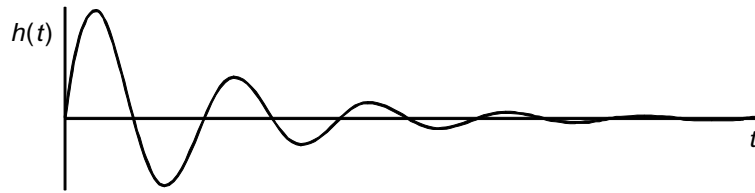


Fig. 4-4. Simulated impulse response $h(t)$ of the transducer.

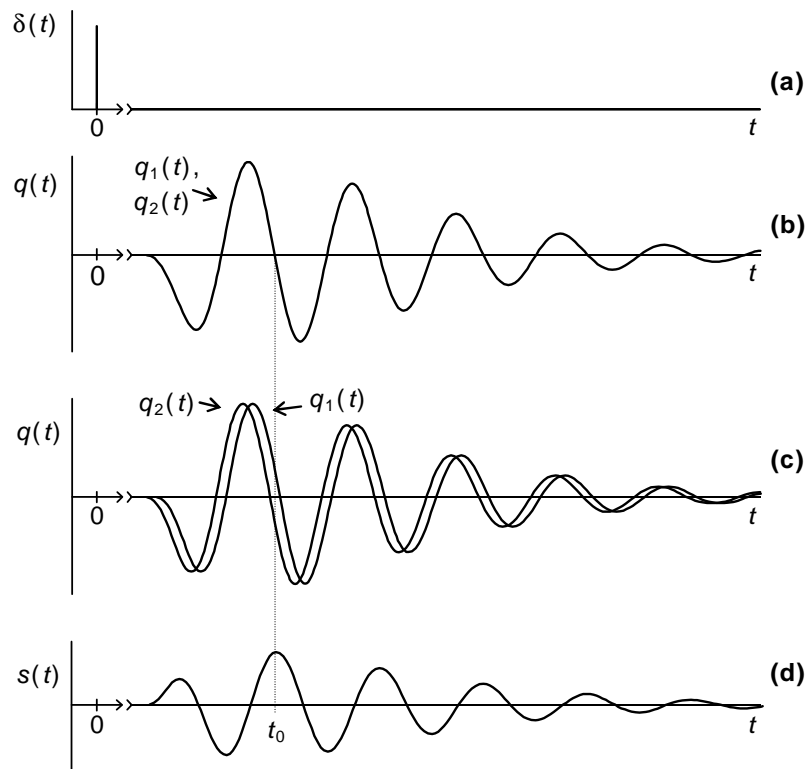


Fig. 4-5. Results of simulation of the model given in Fig. 4-3. (a) Excitation impulse $\delta(t)$; (b) receiver outputs $q_1(t)$ and $q_2(t)$ in the absence of turbulence; (c) receiver outputs and (d) differential amplifier output $s(t)$ in the presence of a turbulent velocity component. t_0 indicates the sampling instant.

The receiver outputs $q_1(t)$ and $q_2(t)$, and the differential amplifier output $s(t)$, in the presence of turbulent velocity component are shown in Fig. 4-5 (c) and (d), respectively. The differential amplifier output is sampled at $t = t_0$ as shown in Fig. 4-5(d) to give x , the value of the turbulence signal, for the particular excitation pulse. Successive values for a sequence of excitation pulses are used to obtain $x(n)$, the discretized version of the turbulence signal.

A set-up for flow measurement using cross-correlation of turbulence signals is shown in Fig. 3-13, of Section 3.5. The discretized version of turbulence signal, $x(n)$, sensed at the upstream location is obtained by the numerical simulation method given above. Assuming that the turbulence pattern remains unchanged between the two sensing locations, the signal $y(n)$ sensed at the downstream location on the pipe is obtained by delaying $x(n)$ by samples corresponding to the transit time of the turbulence pattern between the two sensing locations. The cross-correlation function $r_{yx}(j)$ is calculated as

$$r_{yx}(j) = \sum_n x(n-j) y(n) \quad (4.18)$$

Examples of $x(n)$ and $y(n)$ with a delay of 100 samples are shown in Fig. 4-6 (a) and (b), respectively, and their cross-correlation function shown in Fig. 4-6(c) contains a distinct peak at $j = 100$.

4.5 Simulation of Dispersion in Turbulence Pattern

In real flows, the random movements of molecules of the fluid in the pipe alter the turbulence pattern as it moves between the two sensing locations. Let $x(n)$ and $y(n)$ be the output signals of the upstream sensor A and downstream sensor B, respectively. As the disturbance pattern moves from A to B, the downstream signal is a delayed attenuated version of the upstream signal corrupted by additive noise. Therefore, we can represent the downstream signal as

$$y(n) = \alpha x(n - j_m) + \beta z(n) \quad (4.19)$$

where α is the attenuation in the original disturbance pattern, j_m corresponds to the transit time of the disturbance pattern between the sensing locations, and $z(n)$ is additive noise. Assuming that the mean squared value of the turbulence remains the same, we have

$$\beta^2 = 1 - \alpha^2 \quad (4.20)$$

Assuming that the dispersion in the turbulence pattern is random and independent of the flow profile, the signal $y(n)$ from the downstream sensor can be obtained using (4.19), as shown in Fig. 4-7. Examples of the cross-correlation function $r_{yx}(j)$ for noise-to-signal ratios of 0, 1, 2, 3, 4 are shown in Fig. 4-8 (a), (b), (c), (d), (e), respectively. Note that the peak in the cross-correlation function

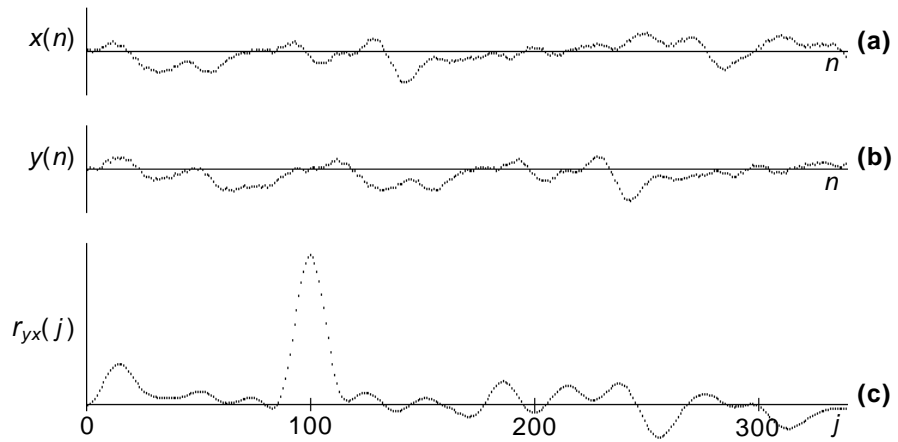


Fig. 4-6. Results of cross-correlator simulation. (a) Turbulence signal $x(n)$ obtained at upstream sensor; (b) turbulence signal $y(n)$ obtained at downstream sensor, simulated as a delay of 100 samples in $x(n)$; (c) cross-correlator output $r_{yx}(j)$, calculated using 1024 samples of $x(n)$ and $y(n)$.

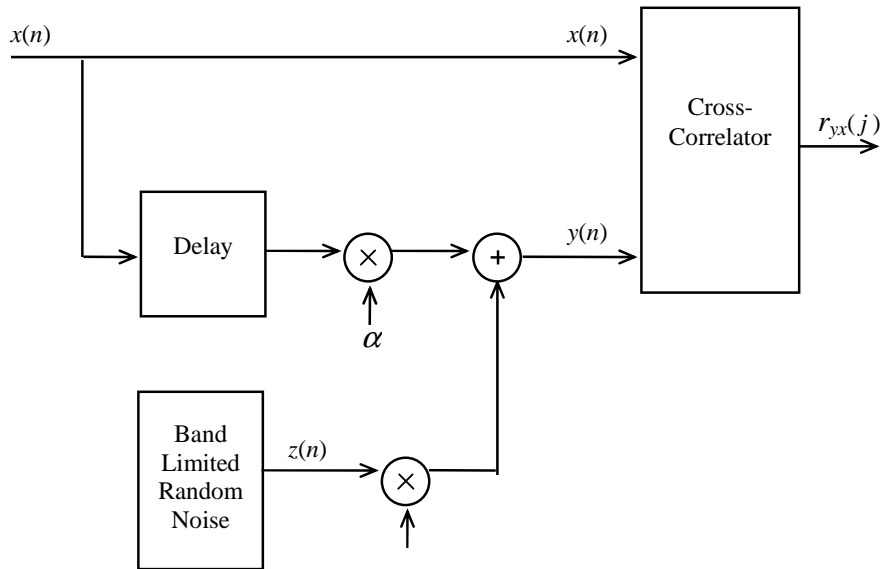


Fig. 4-7. Simulation of dispersion in turbulence to study its effect on the cross-correlation function.

becomes less distinct with more dispersion in the turbulence pattern. This result gives some insight into choosing the distance between the two sensing locations. A larger sensor spacing results in decreased correlation between the cross-correlated signals, and the peak in the cross-correlation function becomes small and may have flat top, causing errors in the estimation of the position of the peak. On the other hand, a small sensor spacing gives a distinct peak in the cross-correlation function. However, for a very small sensor spacing, the error in the measurement of the sensor spacing may be large, as the effective center of the transducers is uncertain and the uncertainty can be a significant fraction of the sensor spacing.

4.6 Simulation of Effect of Quantization

For building an instrument set-up based on the turbulence sensing technique, the signals will be digitized, i.e. sampled and quantized for discrete-time cross-correlation calculation. The flow rate is estimated from the location of the peak in the cross-correlation function. In the numerical simulation, the results presented so far, the quantization has been represented using floating point numbers. In actual implementation of the technique, the turbulence signals will be quantized using a finite number of bits ' n ', and it is of interest to study the effect of number of quantization bits on the sharpness of the peak in the cross-correlation function.

The quantization error due to finite number of bits in the ADC can be generally modeled as additive random white noise [12] with an rms value given as

$$\sigma_q = \frac{2V_m/2^n}{\sqrt{12}} \quad (4.21)$$

where the analog input range is $\pm V_m$. If we assume that the full range of the ADC is being used for quantizing the turbulence signal, and the turbulence signal has uniform amplitude distribution, the rms value of the signal is given by

$$\sigma_s = \frac{2V_m}{\sqrt{12}} \quad (4.22)$$

If the turbulence signal is modeled to have Gaussian amplitude distribution, and the input range is adjusted for near-zero probability of saturation, the rms value of the signal is given by

$$\sigma_s = \frac{V_m}{4} \quad (4.23)$$

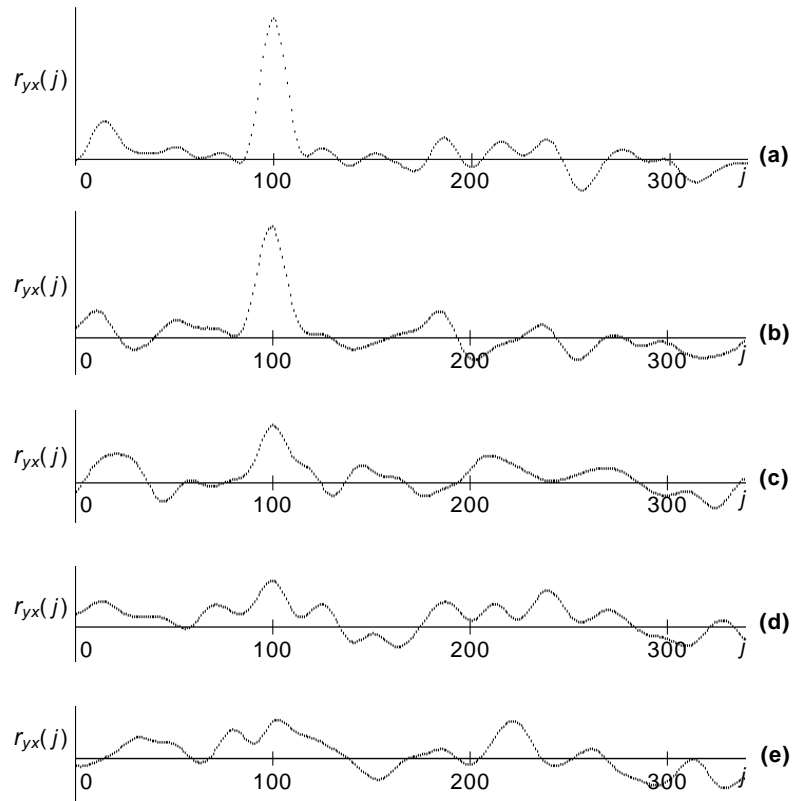


Fig. 4-8. Output of the cross-correlator with random noise added in the turbulence signal obtained at the downstream sensor. The noise-to-signal ratios are: (a) 0, (b) 1, (c) 2, (d) 3, and (e) 4.

Thus the signal-to-quantization noise ratios ρ_u and ρ_g for the turbulence models of uniform and Gaussian amplitude distributions respectively, are given as

$$\rho_u = \frac{2V_m}{\sqrt{12}} / \frac{2V_m/2^n}{\sqrt{12}} = 2^n \quad (4.24)$$

$$\rho_g = \frac{V_m}{4} / \frac{2V_m/2^n}{\sqrt{12}} = \frac{\sqrt{3}}{4} 2^n \quad (4.25)$$

The simulation for studying the effect of the number of quantization bits was carried out by using the turbulence signals, $x(n)$ and $y(n)$ of 1024 sample length, generated as explained in Section 4.4, and adding quantization error noise with relative rms value corresponding to $n = \infty, 8, 4, 2, 1$, as given by (4.24). The respective cross-correlation functions were calculated and are shown in Fig. 4-9. For 8-bit quantization the cross-correlation function is almost identical to that obtained without quantization. The sharpness of the peak in the cross-correlation function decreases as n decreases, and for $n = 1$ the peak is barely distinct. Therefore, 8-bit quantization would be adequate for sampling the turbulence signals.

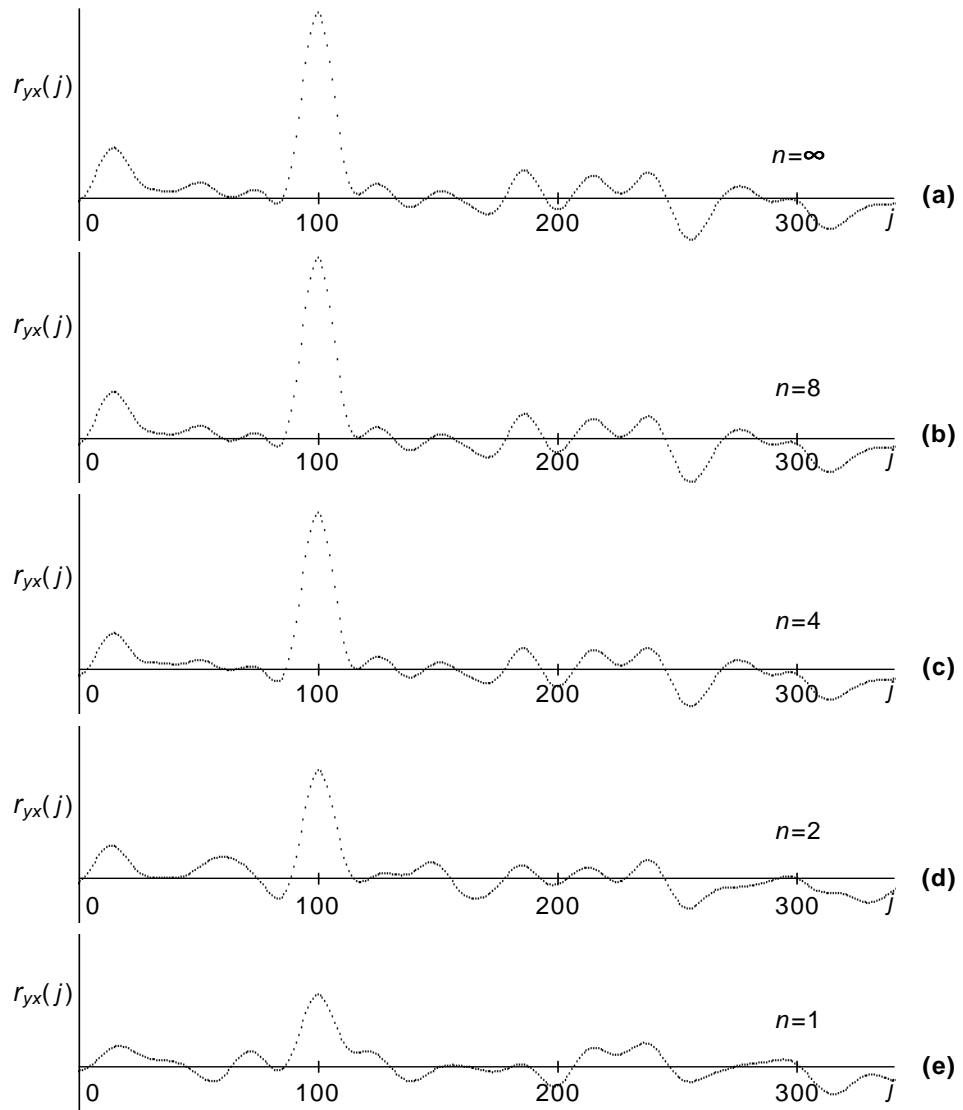


Fig. 4-9. Effect of quantization noise on the cross-correlator output, for various bits of quantization, n .

Chapter 5

FLOW MEASUREMENT SET-UP AND EXPERIMENTAL RESULTS

The technique developed for sensing turbulent velocity components using pulsed ultrasound has been explained in Chapter 3. A theoretical model of the pulse transmission-reception process and the results of a numerical simulation of a cross-correlation flowmeter based on the model have been discussed in Chapter 4. An instrumentation system based on the technique has been developed for the measurement of water flow in a water circulation set-up. This chapter includes the description of the experimental set-up, results of the flow measurement as compared with a venturimeter, and a discussion on the results.

5.1 Experimental Set-up

The block diagram of the system used for sensing turbulence in a pipe and the circuit diagram of the system have been shown earlier in Fig. 3-1 and Fig. 3-2, respectively. The hardware for sensing turbulence was built in duplicate to sense turbulence in the pipe at two locations. The transducers were clamped as shown in Fig. 5-1, on a PVC pipe of 90 mm outer diameter and 3.5 mm wall thickness, placed in the water circulation system. The block diagram of the experimental set-up for flow measurement is shown in Fig. 5-2. The specifications of the transducers used are:

Center frequency:	2.2 MHz
6 dB bandwidth:	between 20 % and 60 %
Active element diameter:	20 mm.

The criteria for selection of the pulse repetition frequency (PRF) are that the pulse repetition period should be longer than the transit time of the pulse across the pipe, and that the corresponding PRF should exceed twice the bandwidth of the flow turbulence signal, in order to give an accurate reconstruction of the flow turbulence. Taking the acoustic velocity in water equal to 1482 m/s, the transit time of the pulse across the pipe of 90 mm diameter is about 60 μ s, indicating that PRF should be below 16.6 k pulses/s. The bandwidth of the turbulence signal as observed in the experiments described in Section 3.4 is below 50 Hz, and it requires that PRF should be higher than 100 pulses/s. Hence a pulse repetition frequency in the range of 0.5–5 k pulses/s can be considered as appropriate.

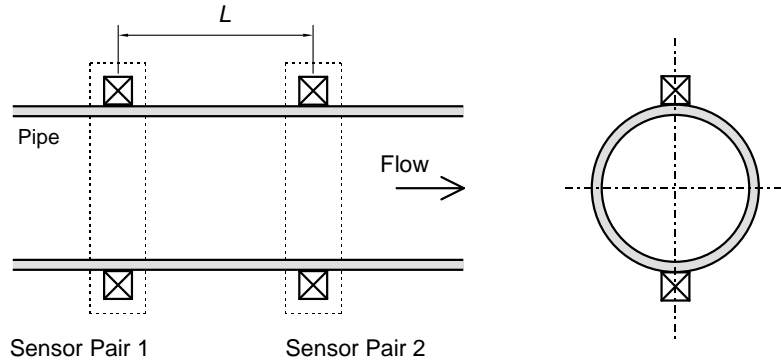


Fig. 5-1. Placement of ultrasonic transducers in the cross-correlation flowmeter.

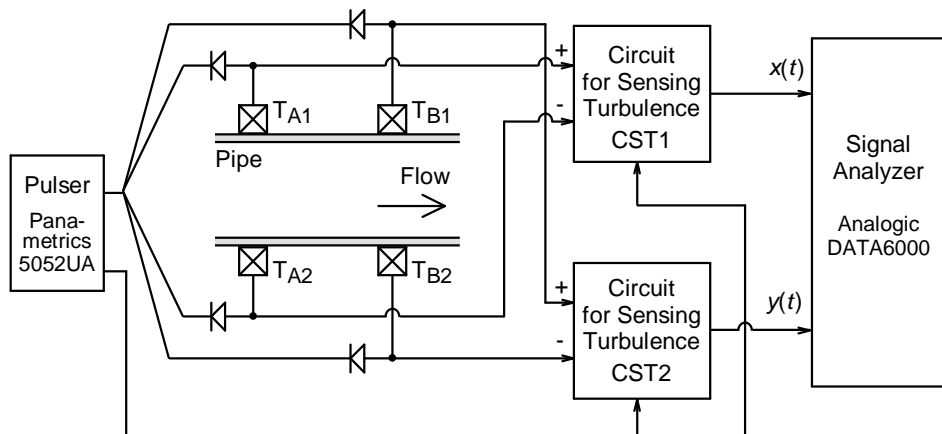


Fig. 5-2. Block diagram of the experimental set-up used to measure flow by cross-correlation technique.

The transducers at both the locations were excited simultaneously by the ultrasonic pulser *Panametrics 5052UA*. The pulse repetition frequency was kept at 1 k pulses/s. The turbulence signals obtained at the two locations were acquired by the signal analyzer *Analogic DATA6000* (Appendix B) with 8-bit amplitude resolution, at a sampling rate of 1 k samples/s for 1 s, and the cross-correlation function was computed with the help of the built-in cross-correlation function in the signal analyzer. The signal analyzer also found the location of the peak in the cross-correlation function.

The position of the peak in the cross-correlation function is taken as an estimate of the transit time τ_m of the turbulence pattern between the sensing locations. The flow velocity u is found from the relation

$$u = L / \tau_m \quad (5.1)$$

Since L , the spacing between the sensing locations is fixed and can be measured accurately, it is the measurement of τ_m that determines the precision of the flow measurement. Thus, obtaining sharp and consistent peak is of utmost importance in cross-correlation flowmeters. In the experimental set-up, for a constant flow a unique and consistent peak was observed in the cross-correlation function. The location of the peak was found automatically by the peak location function of the signal analyzer.

The schematic of the water circulation system, as a line diagram, is shown in Fig. 5-3. A pumpset of 1.5 kW power circulates water from a tank of 1000 liter capacity. The testing line consists of an 80 mm (3") venturimeter in series with the PVC pipe on which the ultrasonic transducers are mounted externally. The bypass adjusts the flow through the testing line. All valves are ball-type which have minimum leakage when off and minimum resistance when turned on. The rubber pipe at the outlet of the pumpset prevents the vibrations of the pump from being transmitted to the transducers. For transit time ultrasonic flowmeters, Liptak [1] has suggested that the straight pipe length upstream the flowmeter should be greater than 10 times the pipe diameter and downstream greater than 5 times the pipe diameter, in order to reduce the influence of bends and obstructions on the flow profile at the flowmeter. Assuming that the requirements for a cross-correlation flowmeter would be the same, sufficient straight pipe length is maintained. The transducers are mounted on a straight PVC pipe of outer diameter 90 mm and the straight pipe length upstream the flowmeter is 1 m and downstream is 0.6 m.

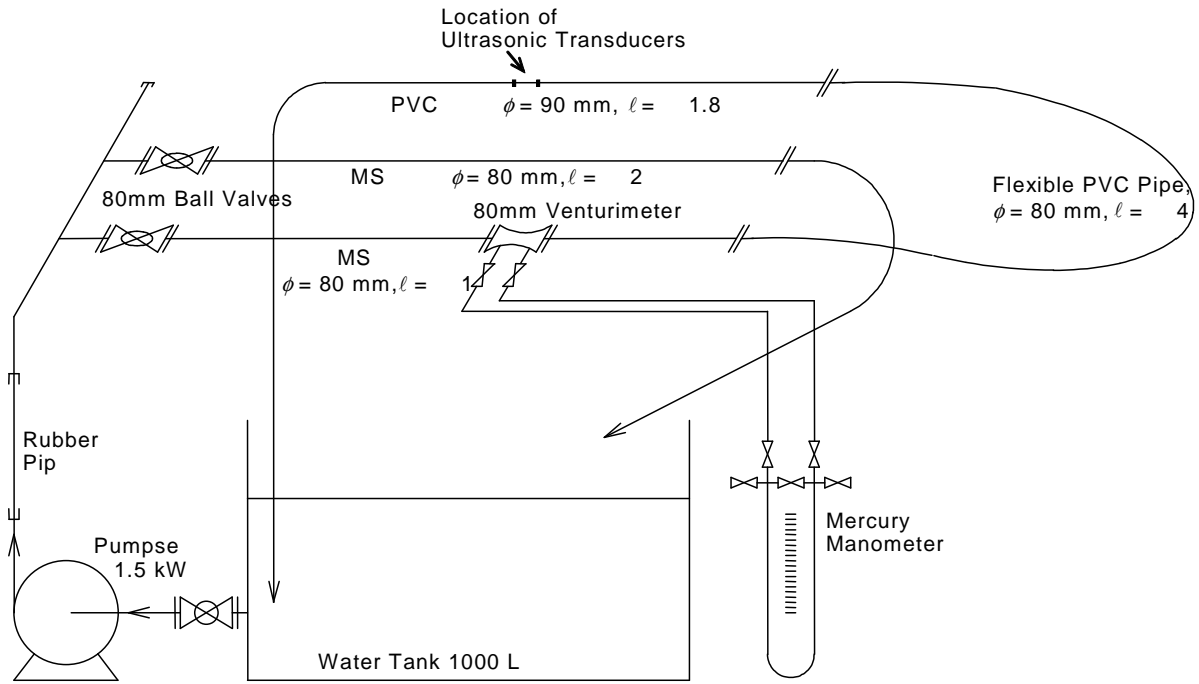


Fig. 53. Schematic of water circulation system

A flow rate up to 660 L/min can be obtained in this water circulation system. It corresponds to a linear flow velocity of 2 m/s for a 90 mm pipe (83 mm inner diameter), assuming a uniform flow profile. Since the flow measurement technique relies upon the presence of turbulence, it is useable only if the flow is turbulent. Flow is generally turbulent when the Reynolds number (Re) is above 4000 [28], [29].

$$Re = uD/\nu \quad (5.2)$$

where u is the mean linear flow velocity, D is the pipe diameter and ν is the kinematic viscosity of the fluid. For water at 25°C, $\nu = 8.97 \times 10^{-7} \text{ m}^2/\text{s}$ [28]. Table 5-1 shows the lower limit of water flow for which the flow is turbulent for various pipe diameters.

A standard volumetric flowmeter of high accuracy and fast response for comparison of the results was not available. A venturimeter and a measurement tank were tried. In the measurement tank method, the flow is diverted to the tank and the time required to fill a definite volume between two levels is used to calculate the volumetric flow. The measurement tank averages the volumetric flow over a long duration and hence the measurement is not affected by the fluctuations in the flow. However, this method is very slow and the ripples in the water level are considerably high and affect the precision of measurement. The venturimeter has been used in the experiments as it is comparatively much faster and it has good repeatability. A mercury manometer has been used to indicate the pressure difference at the venturimeter tapings. The level difference in the manometer has been measured by visual averaging of the vibrations in the level caused by the fluctuations in the flow.

Table 5-1. The lower limit of flow for which water flow through a pipe is turbulent, i.e. the Reynolds number (Re) is 4000. The mean linear velocity u and volumetric flow Q are calculated from (5.2).

PVC pipe size	inch	1	1¼	1½	2	2½	3	3½	4
	mm	25	32	40	50	63	75	90	100
Internal Diameter	mm	21.4	28.4	36.4	44.4	57.4	69.4	83.0	93.0
Flow Rate	Linear u (m/s)	0.17	0.13	0.099	0.081	0.063	0.052	0.043	0.039
	Volumetric Q (L/min)	3.62	4.80	6.15	7.51	9.71	11.73	14.03	15.72

The volumetric flow measured by the cross-correlation flowmeter was calculated assuming uniform flow profile and was compared with the flow obtained by the venturimeter in the water circulation system. The experiments were carried out for various combinations of flow rates and sensor spacings, and the results are given in the following section.

5.2 Measurement Results

The transducers were mounted on a PVC pipe having outer diameter of 90 mm and thickness of 3.5 mm. The pulse repetition frequency used was 1 k pulses/s, and the two turbulence signals were digitized with 8-bit amplitude resolution, at a sampling rate of 1 k samples/s. Record length of 1000 samples was used for computing the cross-correlation function, and the location of the peak in the cross-correlation function was used for calculation of the volumetric flow assuming a uniform flow profile. The average flow rate measured by cross-correlation (\bar{Q}_C) and by the venturimeter (Q_V) were recorded for various sensor spacings over a flow range of 300–600 L/min.

For a particular sensor spacing and setting of the flow controlling valves, the flow rate was measured using the venturimeter. A number of cross-correlation functions were sequentially recorded using the set-up and used for finding τ_m and Q_C . From these values, the average and standard deviation of the two quantities were calculated.

For a sensor spacing of 187 mm, $\bar{\tau}_m$, σ_{τ_m} , \bar{Q}_C , and σ_{Q_C} are given in Table 5-2. The graphs of average flow measured by cross-correlation flowmeter (\bar{Q}_C) versus flow measured by venturimeter (Q_V) for the sensor spacings of 35 mm, 50 mm, 101 mm, 187 mm, and 254 mm are shown in Figs. 5-4(a)–(e), respectively. Another set of graphs in Figs. 5.5(a)–(e) shows the standard deviation of τ_m and corresponding standard deviation of Q_C plotted against \bar{Q}_C for the sensor spacings mentioned above.

5.3 Discussion

From the graphs shown in Figs. 5-4(a)–(e), it is observed that for small sensor spacing (35 mm) the deviation of the plotted points, from the linear best fit line is large; it reduces progressively as the sensor spacing is increased from 35 mm to 187 mm. However, further increase in the sensor spacing to 254 mm again results in more deviation from the best fit line. A table of standard deviation (σ) and maximum deviation (δ) from the linear best fit line, for various sensor spacings (L) is given in Table 5-3.

Table 5-2. Measurement results showing volumetric flow Q_V measured by the venturimeter and mean volumetric flow \bar{Q}_C (measured by cross-correlation flowmeter assuming uniform flow profile) and its standard deviation σ_{Q_C} . Sensor spacing $L = 187$ mm. n = number of observations. $\bar{\tau}_m$ and σ_{τ_m} are the mean and standard deviation of the peak position in the cross-correlation function.

Q_V (L/min)	n	$\bar{\tau}_m$ (ms)	σ_{τ_m} (ms)	\bar{Q}_C (L/min)	σ_{Q_C} (L/min)
270	14	200	3	303.5	4.3
295	12	184	2	329.8	4.0
300	15	180	4	337.3	6.6
315	17	170	4	358.1	7.4
320	19	170	4	358.3	8.4
338	20	160	2	380.5	6.0
340	22	160	3	379.3	6.9
365	18	147	3	413.3	8.8
380	16	145	2	419.5	6.7
390	17	140	2	432.5	7.1
393	18	139	3	435.5	8.8
400	17	138	3	439.9	9.5
425	19	128	3	474.4	11.7
435	14	125	3	485.4	11.8
450	12	120	1	505.3	5.6
460	22	118	3	513.5	11.4
470	16	116	2	525.8	8.7
478	18	114	2	532.7	9.2
482	18	115	3	530.0	12.6
485	20	112	2	540.6	10.8
500	18	110	2	554.1	10.7
505	17	108	2	561.0	8.8
520	17	105	2	579.9	8.7
530	18	105	2	580.1	8.8
530	15	104	2	583.9	10.1
537	15	103	2	589.9	9.1
560	17	98	1	617.7	9.1
565	13	97	1	624.5	8.4

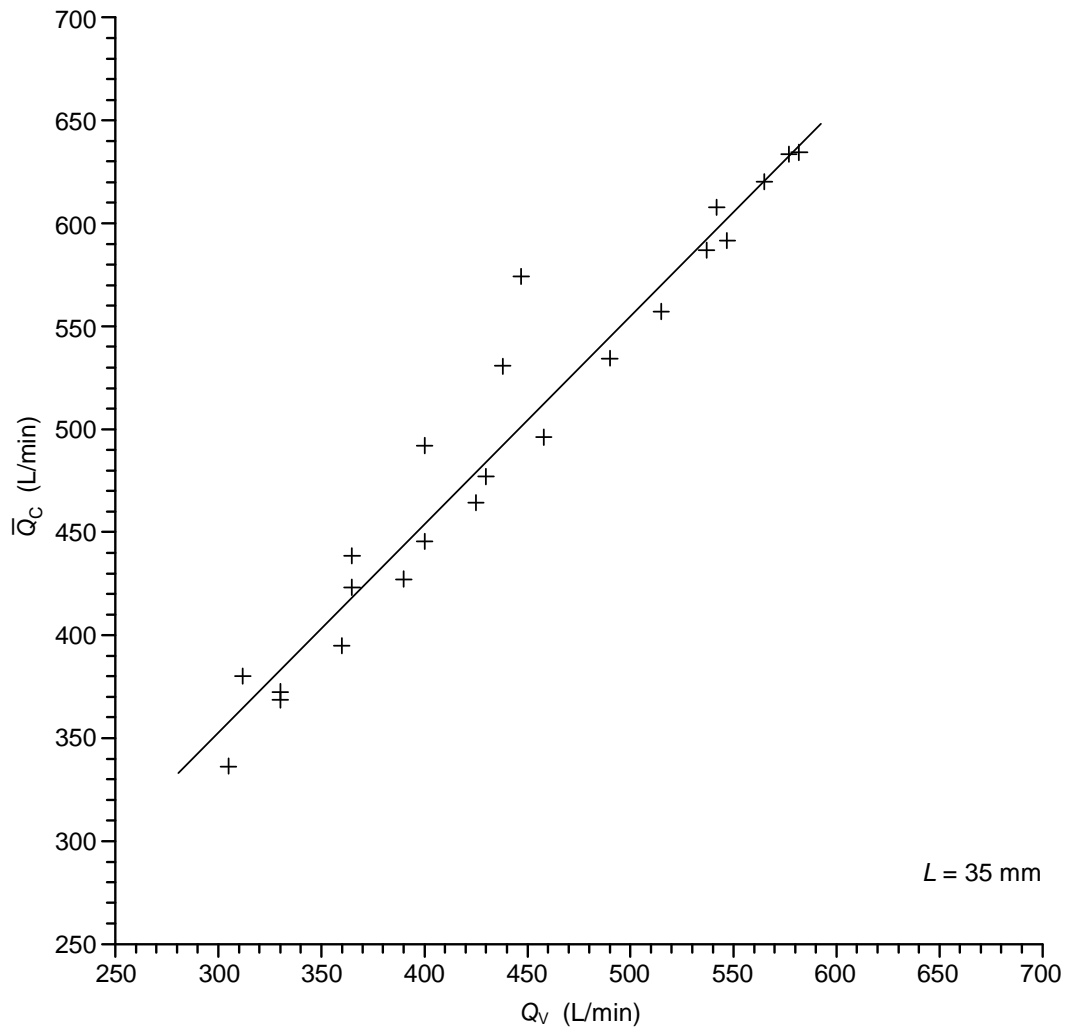


Fig. 5-4(a). Graph of average flow measured by cross-correlation flowmeter (\bar{Q}_C) versus flow measured by venturimeter (Q_V) for sensor spacing of 35 mm. Equation of the best fit line is $y = 1.02x + 48.53$. Standard deviation from the best fit line, $\sigma = 23$ L/min. Maximum deviation from the best fit line, $\delta = 72$ L/min.

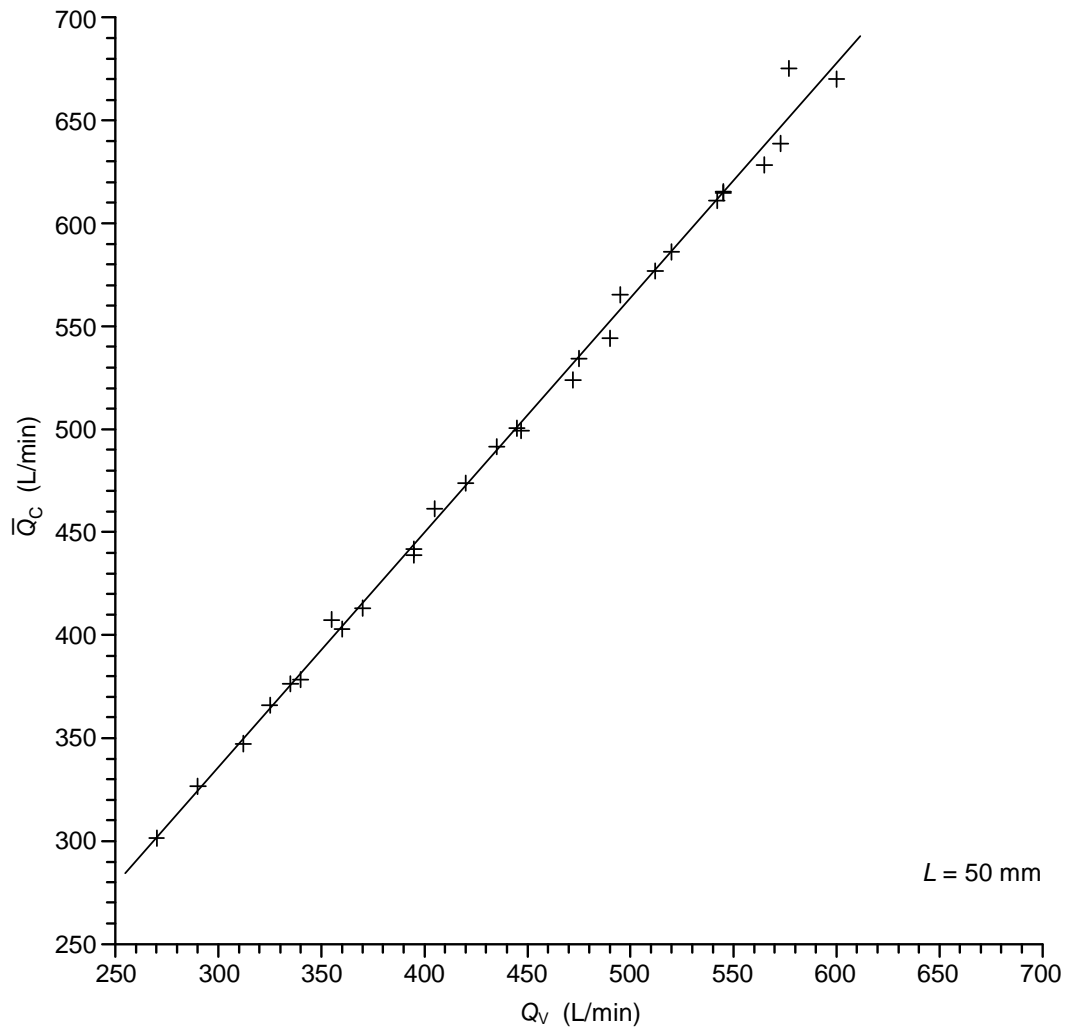


Fig. 5-4(b). Graph of average flow measured by cross-correlation flowmeter (\bar{Q}_C) versus flow measured by venturimeter (Q_V) for sensor spacing of 50 mm. Equation of the best fit line is $y = 1.14x - 4.56$. Standard deviation from the best fit line, $\sigma = 6 \text{ L/min}$. Maximum deviation from the best fit line, $\delta = 25 \text{ L/min}$.

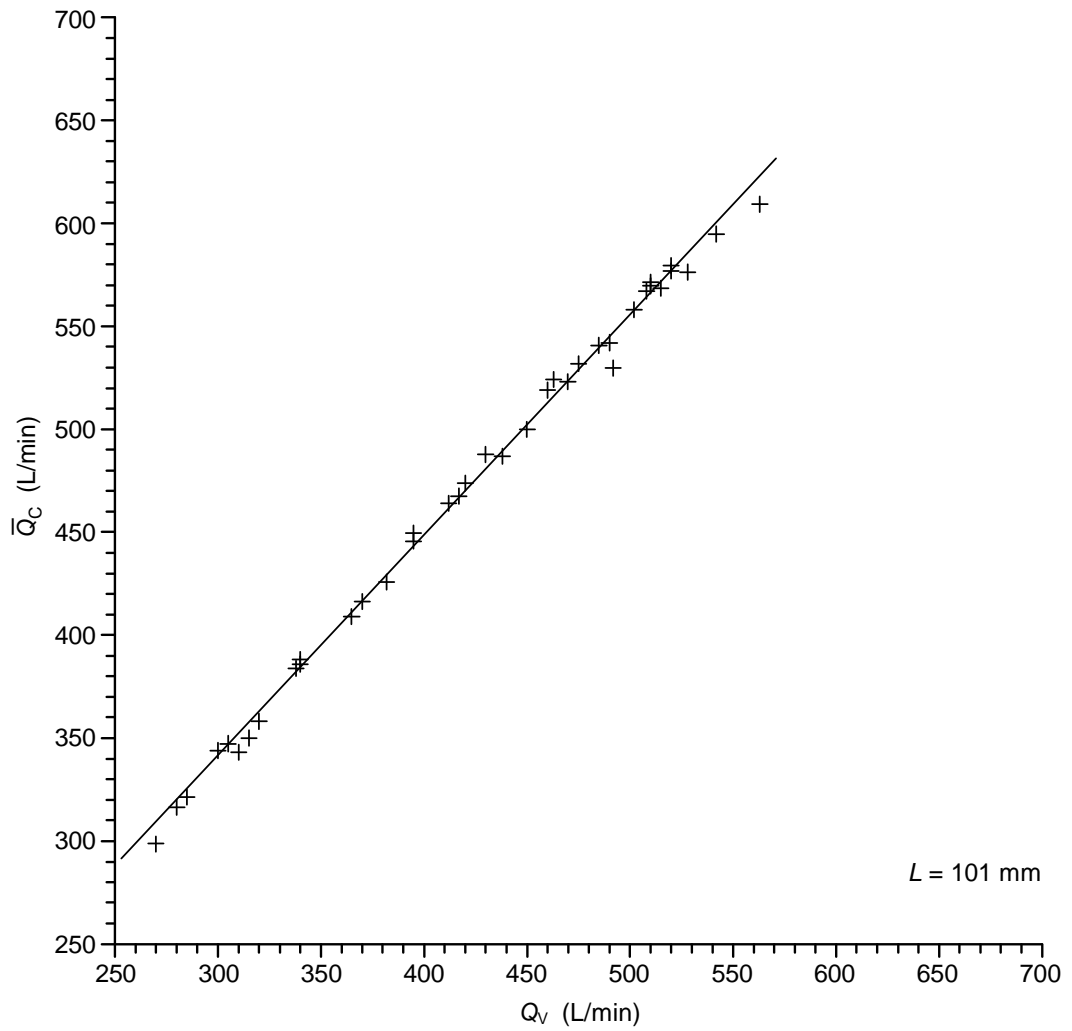


Fig. 5-4(c). Graph of average flow measured by cross-correlation flowmeter (\bar{Q}_C) versus flow measured by venturimeter (Q_V) for sensor spacing of 101 mm. Equation of the best fit line is $y = 1.07x + 18.42$. Standard deviation from the best fit line, $\sigma = 6 \text{ L/min}$. Maximum deviation from the best fit line, $\delta = 9 \text{ L/min}$.

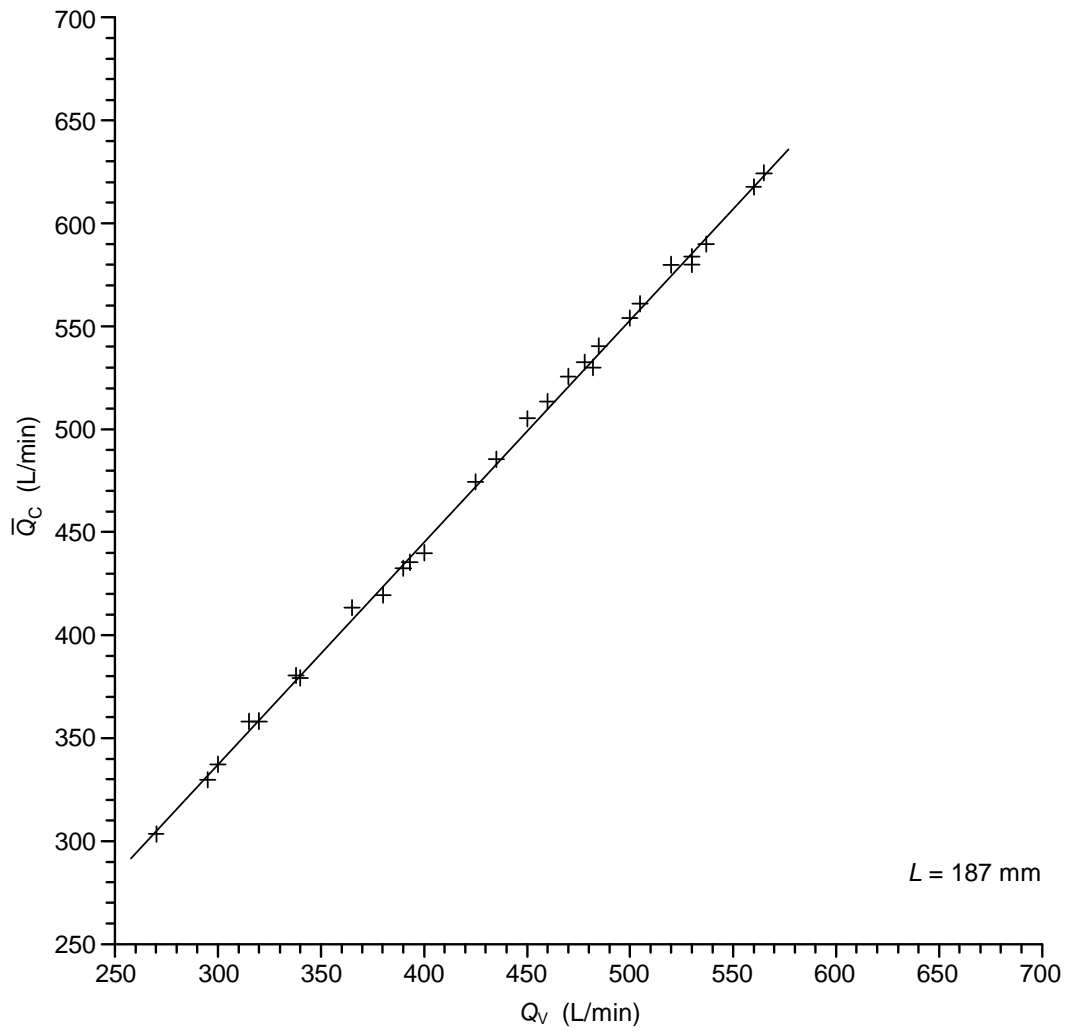


Fig. 5-4(d). Graph of average flow measured by cross-correlation flowmeter (\bar{Q}_C) versus flow measured by venturimeter (Q_V) for sensor spacing of 187 mm. Equation of the best fit line is $y = 1.08x + 13.07$. Standard deviation from the best fit line, $\sigma = 3 \text{ L/min}$. Maximum deviation from the best fit line, $\delta = 5 \text{ L/min}$.

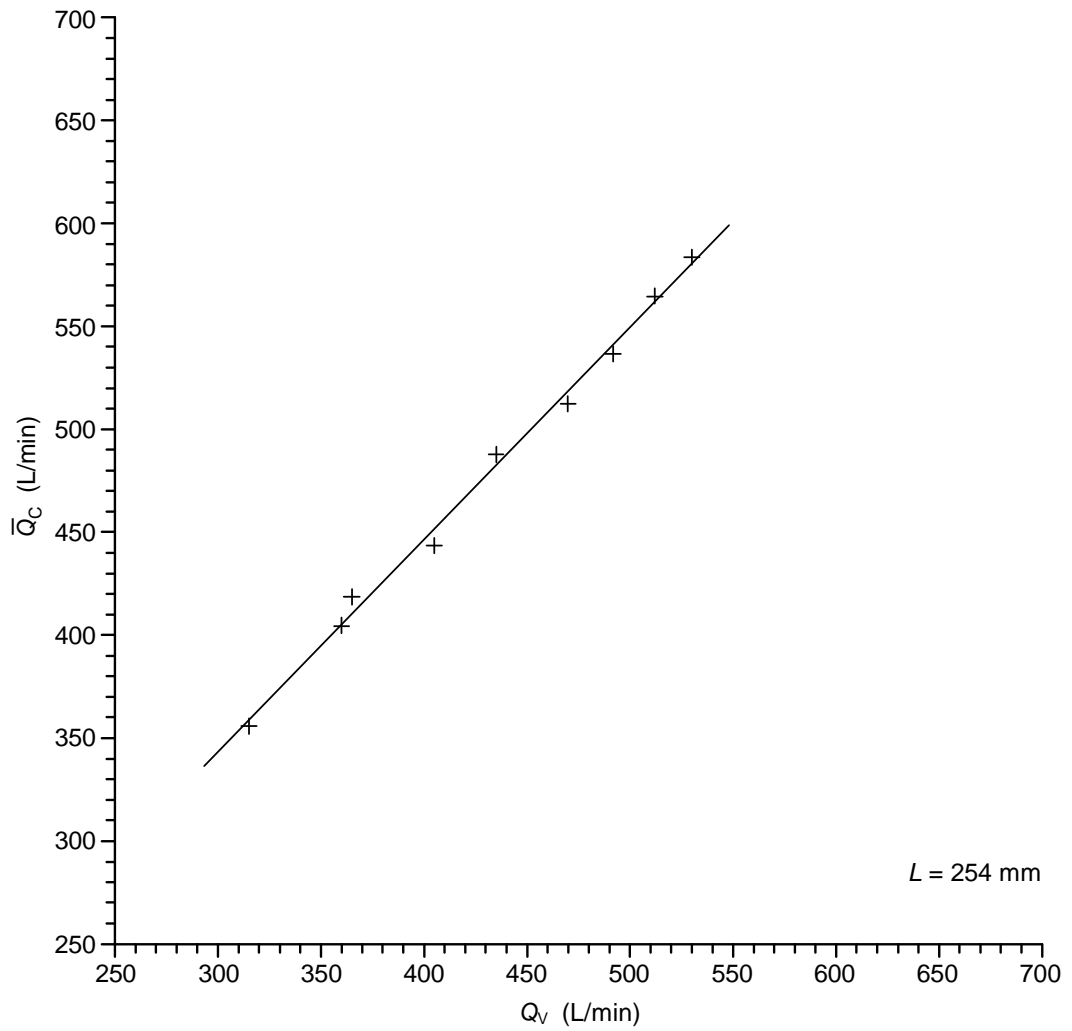


Fig. 5-4(e). Graph of average flow measured by cross-correlation flowmeter (\bar{Q}_C) versus flow measured by venturimeter (Q_V) for sensor spacing of 254 mm. Equation of the best fit line is $y = 1.03x + 33.04$. Standard deviation from the best fit line, $\sigma = 6 \text{ L/min}$. Maximum deviation from the best fit line, $\delta = 9 \text{ L/min}$.

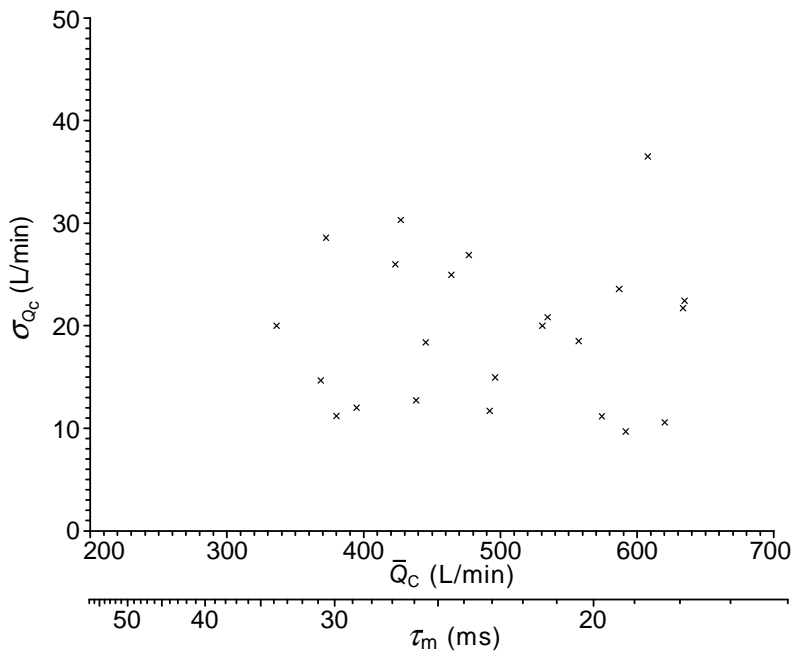
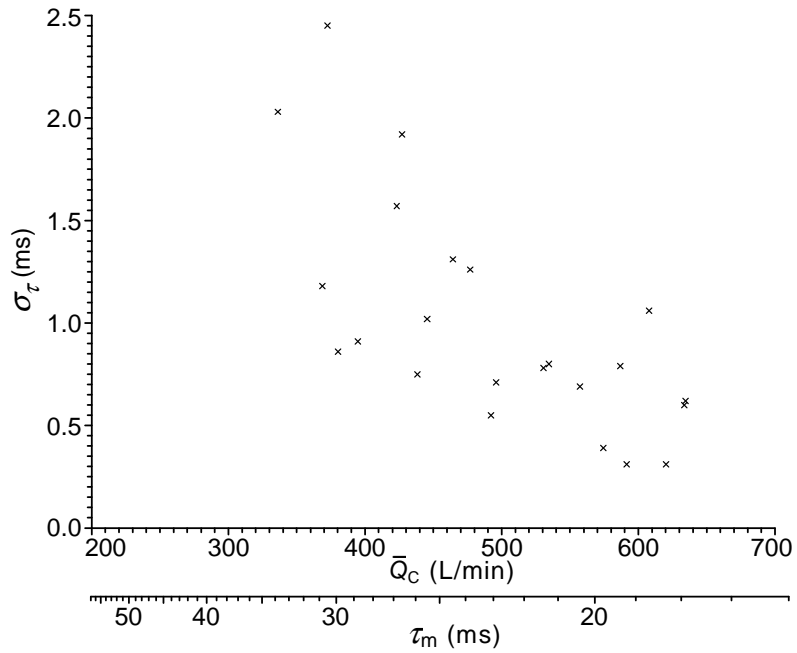


Fig. 5-5(a). Graphs of standard deviation of the turbulence transit time (σ_τ) and standard deviation of the flow measured by cross-correlation (σ_{Q_C}), versus mean flow measured by cross-correlation (\bar{Q}_C) for the sensor spacing (L) of 35 mm.

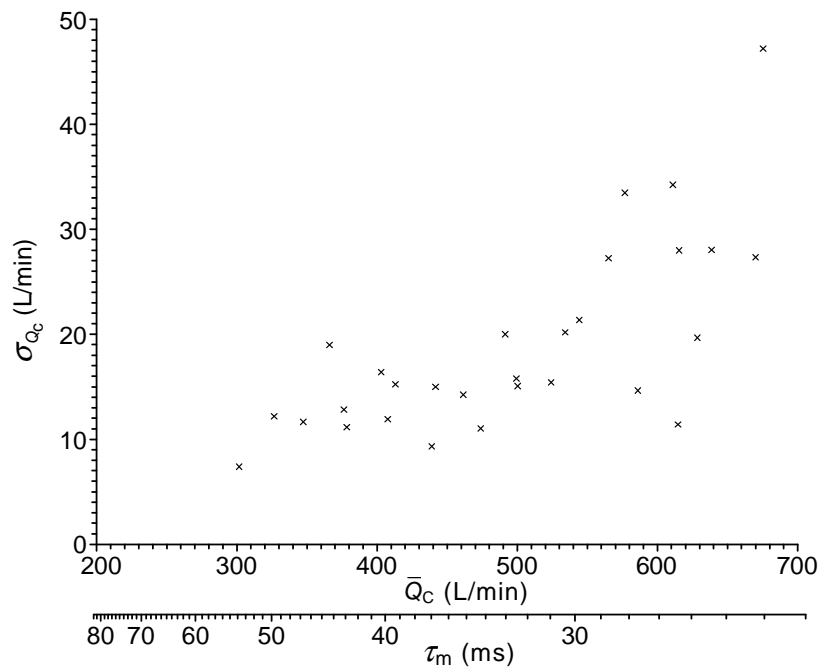
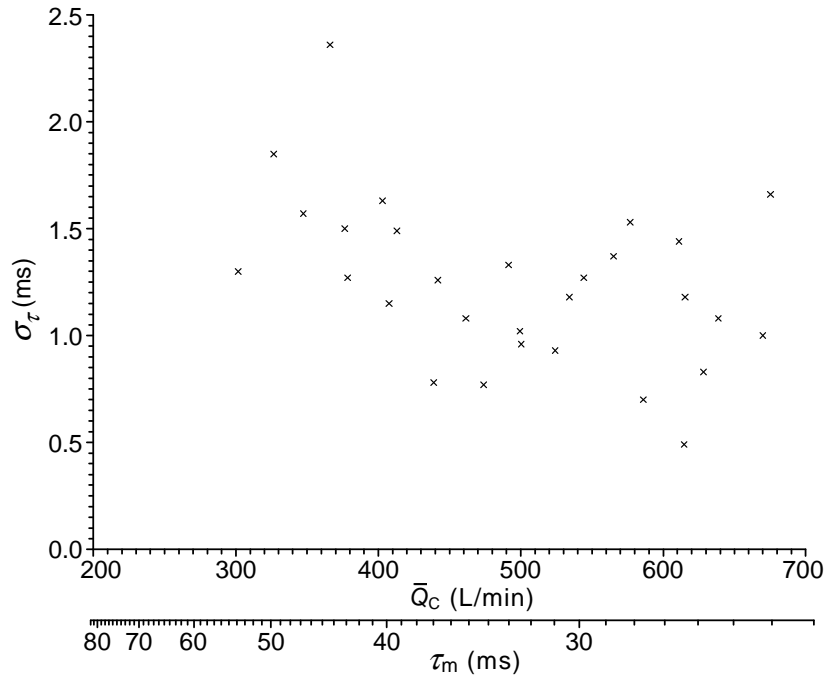


Fig. 5-5(b). Graphs of standard deviation of the turbulence transit time (σ_{τ}) and standard deviation of the flow measured by cross-correlation (σ_{Q_C}), versus mean flow measured by cross-correlation (\bar{Q}_C) for the sensor spacing (L) of 50 mm.

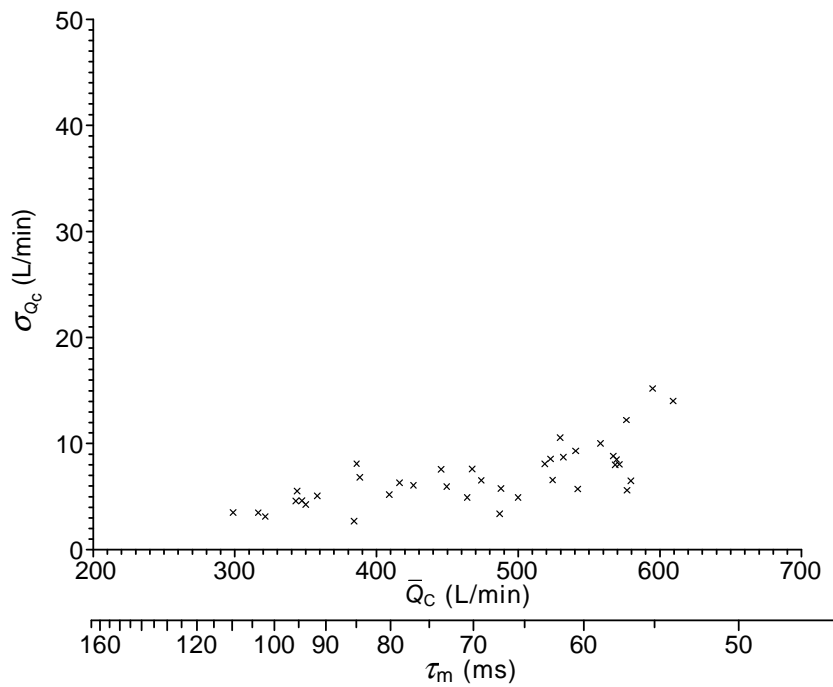
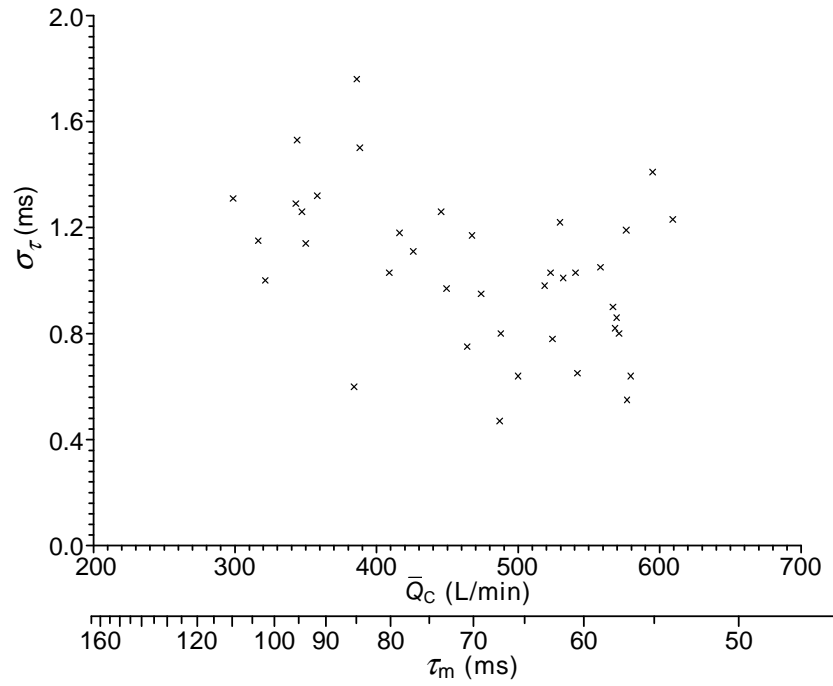


Fig. 5-5(c). Graphs of standard deviation of the turbulence transit time (σ_τ) and standard deviation of the flow measured by cross-correlation (σ_{Q_C}), versus mean flow measured by cross-correlation (\bar{Q}_C) for the sensor spacing (L) of 101 mm.

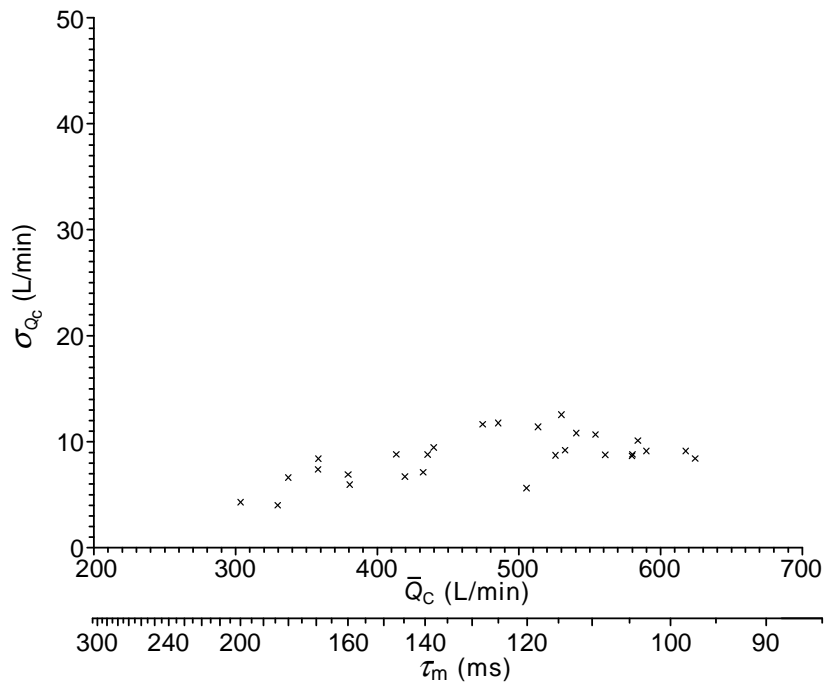
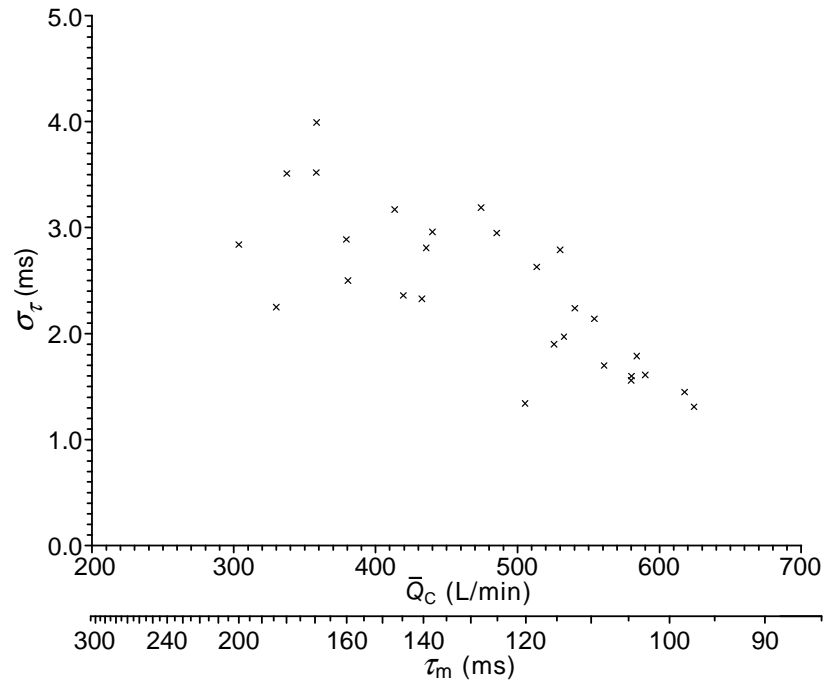


Fig. 5-5(d). Graphs of standard deviation of the turbulence transit time (σ_τ) and standard deviation of the flow measured by cross-correlation (σ_{Q_C}), versus mean flow measured by cross-correlation (\bar{Q}_C) for the sensor spacing (L) of 187 mm.

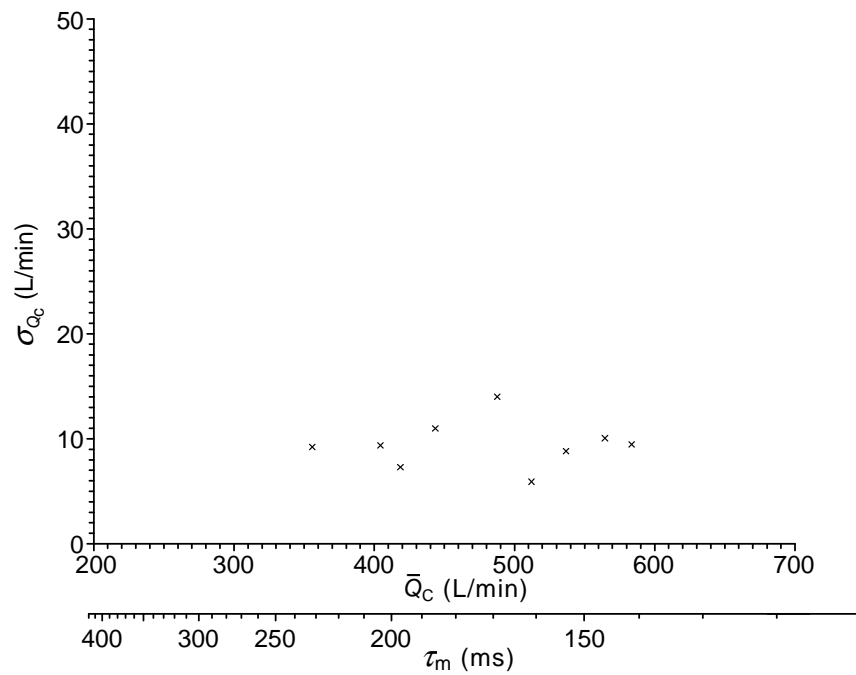
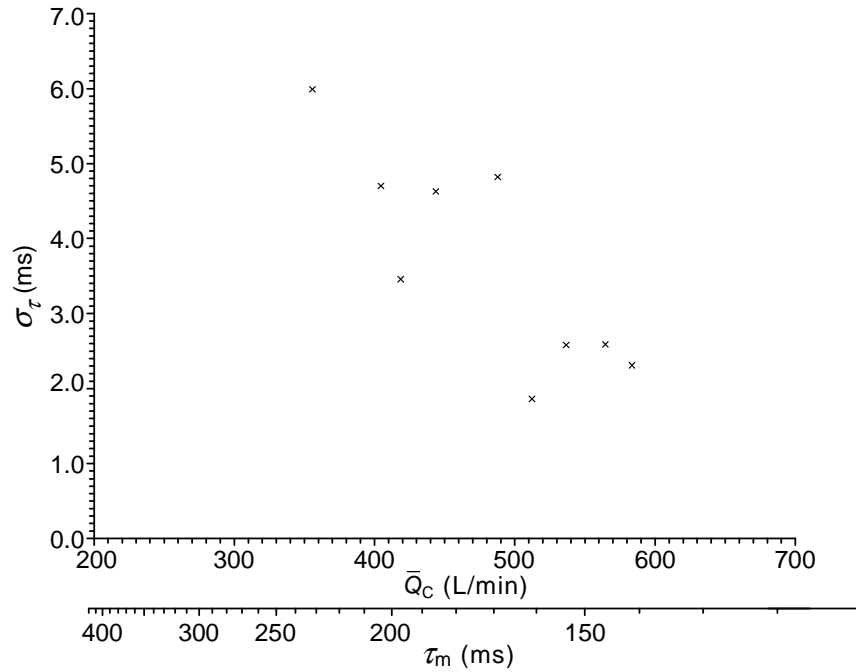


Fig. 5-5(e). Graphs of standard deviation of the turbulence transit time (σ_τ) and standard deviation of the flow measured by cross-correlation (σ_{Q_C}), versus mean flow measured by cross-correlation (\bar{Q}_C) for the sensor spacing (L) of 254 mm.

As seen from equation (2.6) in Section 2.2, at fixed sampling rate (1 kHz), for small transit time (τ_m) of the flow disturbances, the resolution in the measured flow is poor. The smaller the sensor spacing, smaller is τ_m . Hence the resolution is poor for sensor spacing of 35 mm and the flowmeter readings deviate more from the best fit line in Fig. 5-4(a). In addition, the higher the flow, smaller is τ_m , hence poor resolution. This explains larger deviation from the best fit line at higher flow velocities evident in Fig. 5-4(b) with the given sampling rate and sensor spacing.

The effect of increase in the sensor spacing is the decrease in the correlation as the turbulence pattern breaks up while it proceeds along the pipe. Therefore, the peak in the cross-correlation function becomes broad and less distinct and may introduce considerable errors in estimating the position of the peak. Hence, the flowmeter readings deviate more when the sensor spacing is increased from 187 mm (Fig. 5-4(d)) to 254 mm (Fig. 5-4(e)).

The best fit line equations given in Fig. 5-4 show that the meter factor of the cross-correlation flowmeter (defined as the ratio of the true flow rate to the measured flow rate [30], [8]) is less than 1. The eddies in the flow near the pipe axis are large, disperse less, and have higher velocity, whereas the eddies near the pipe wall are small and disperse fast. Therefore, the eddies near the pipe axis contribute more to the cross-correlation function and the cross-correlation flowmeter reads higher.

Table 5-3. Standard deviation (σ) and maximum deviation (δ) from the linear best fit line, in the flow measured by cross-correlation technique for various sensor spacings (L).

L (mm)	σ (L/min)	δ (L/min)
35	23	72
50	6	25
101	6	9
187	3	5
254	6	9

From the graphs of σ_τ and σ_{Q_c} versus \bar{Q}_c given in Figs. 5.5(a)–(e), it is observed that in general σ_τ decreases at higher flow rates, but σ_{Q_c} increases. This can be explained referring to equation (2.6) in Section 2.2, which shows that the error in flow rate is proportional to the error in τ_m but inversely proportional to τ_m^2 .

Table 5-4 shows the mean value of the standard deviation in the measurement of the transit time τ , and flow rate Q over the flow range of 300–600 L/min for various sensor spacings. The value of $\bar{\sigma}_\tau$ and $\bar{\sigma}_Q$ can be considered as a measure of precision of the set-up. The value of $\bar{\sigma}_\tau$ ranges over 1.0–3.7 ms and the value of $\bar{\sigma}_Q$ ranges over 7–19 L/min. The table also shows the mean value of the relative errors, i.e. $\overline{\sigma_\tau/\bar{\tau}}$ and $\overline{\sigma_Q/\bar{Q}}$. The relative error in the flow measurement ranges over 1.45–4.07%. From the values of relative error in the measurement and the corresponding sensor spacing, it is seen that the most suitable sensor spacing will be about 100 mm. For this sensor spacing, the range of the relative error is 0.7–2.6 %.

Table 5-4. Mean values of standard deviation of transit time τ and standard deviation of flow rate Q , mean values of relative errors $\sigma_\tau/\bar{\tau}$ and σ_Q/\bar{Q} , for various sensor spacings over the flow range of 300–600 L/min.

Sensor spacing L (mm)	35	50	101	187	254
mean (σ_τ) (ms)	0.99	1.24	1.03	2.40	3.66
mean (σ_Q) (L/min)	19.46	18.83	6.95	8.58	9.46
mean $\left(\frac{\sigma_\tau}{\bar{\tau}}\right) \times 100$ (%)	4.02	3.69	1.45	1.81	2.02
mean $\left(\frac{\sigma_Q}{\bar{Q}}\right) \times 100$ (%)	4.07	3.70	1.45	1.81	2.02

In the water circulation system, fluctuations in the flow have been observed, as noted from the mercury column of the manometer that measured the pressure difference at the venturi tube. Over the entire flow range, fluctuations of up to 20 L/min, in the frequency range of 1–5 Hz have been found. These fluctuations in the flow are likely to have affected the precision of the results at low flow rates and large sensor spacings where the resolution is sufficiently good. Therefore, we anticipate better precision in reality than 1.45 % that has been reported in Table 5-4.

The experimental results given in Section 5-2 are obtained on the largest pipe (90 mm) mounted in the water circulation system. The cross-correlation flowmeter should exhibit better precision on pipes of lower diameters, because for the same flow range the Reynolds number will be higher, causing the bandwidth of the turbulence signal to increase, and the peak in the cross-correlation function will be sharper. For a given transducer diameter, as the pipe diameter is decreased, the spatial averaging along the diameter increases resulting in the decrease in the bandwidth of the turbulence signal sensed by the transducer.

The range of the cross-correlation flowmeter can be calculated as follows: Let the sampling rate = 1 k samples/s, number of samples used in the calculation of cross-correlation function = 1000. The position of peak in the cross-correlation function should be earlier than 333 ms, so that at least two third samples contribute to the cross-correlation function near the peak. Similarly, the peak has to be after 100 ms so that the resolution is greater than 1 %. Consider that the lowest possible sensor spacing is 35 mm when the transducers at the two locations are touching each other, and the highest useable sensor spacing is 250 mm, beyond which the peak in the cross-correlation function is not detectable precisely. Thus, the minimum velocity that can be measured by the system is about 0.1 m/s, and maximum velocity is 2.5 m/s, provided the Reynolds number is greater than 4000. Table 5-5 shows the maximum and minimum flow velocity and volumetric flow the system can measure for pipes of various diameters. For pipes with inner diameter less than 36 mm, the lower limit of flow is decided by the Reynolds number.

Table 5-5. The range of linear flow (u) and volumetric flow (Q) that can be measured by the cross-correlation flowmeter described in Section 5.1, for pipes of various diameters. Uniform flow profile has been assumed while calculating the volumetric flow.

Inner Diameter of Pipe (mm)	Minimum Flow		Maximum Flow	
	u (m/s)	Q (L/min)	u (m/s)	Q (L/min)
21.4	0.17	3.62	2.5	53.95
28.4	0.13	4.80	2.5	95.02
36.4	0.1	6.24	2.5	156.09
44.4	0.1	9.29	2.5	232.25
57.4	0.1	15.53	2.5	388.15
69.4	0.1	22.70	2.5	567.41
83.0	0.1	32.46	2.5	811.59
93.0	0.1	40.76	2.5	1018.94

Chapter 6

SUMMARY AND CONCLUSIONS

The cross-correlation flowmeter measures flow by sensing the disturbances in the flow at two suitable locations along the pipe and by finding the transit time of the disturbance pattern between the two locations from the peak in the cross-correlation function of the signals. In case of single-phase flow, the only disturbance is the turbulence present in the flow.

Sensing the disturbances in the flow using ultrasound can be non-intrusive in cross-correlation flowmeters. Continuous wave ultrasound is most commonly used for sensing the disturbances. The disturbances modulate the ultrasonic beam transmitted across the diameter of the pipe. For clean fluids the dominant modulation of continuous wave ultrasound is caused by turbulent eddies which modulate the phase but not the amplitude. However, some problems arise in this technique. The use of continuous wave ultrasound generates standing waves in the pipe. The problem of the standing waves has been studied in Chapter 2. The standing wave pattern alters with the variations in fluid properties, and environmental factors, especially temperature. This results in erroneous detection of the phase of the received ultrasound; unless a feedback control system is employed to correct the undesired variations in the standing wave pattern. In addition, the acoustic short circuit noise through the pipe wall tends to swamp the liquid-borne signal. The acoustic short circuit noise has been studied theoretically and experimentally and a clamping method to minimize the acoustic short circuit has been suggested in Chapter 2. Yet another source of interference studied in Chapter 2 is the multiple reflections of ultrasound within the pipe wall.

Considering these difficulties, viability of pulsed ultrasound in place of continuous wave ultrasound has been investigated. Subsequently, a new technique that detects modulation in time of flight of the pulsed ultrasound, due to the turbulence has been developed. Two ultrasonic transducers, both of which act as transmitter and receiver, are mounted diametrically opposite to each other on the pipe wall. They transmit ultrasonic pulses at the same instant and in opposite directions. The pulses after passing through the fluid are received by the opposite transducers which now act as the receivers. The turbulent velocity components in the flow alter the velocity of the pulses, and the time of flight of the pulses is changed. Since the two pulses travel in opposite directions, the relative variation in the time of flight is twice that would be obtained with single

transmitter-receiver. In addition, the double pulse method facilitates obtaining variations in time of flight by processing the two received signals, and eliminates the need of a stable time reference that would be essential in the one pulse method. The peak value of the voltage output after subtraction of the received signals, is a function of the line integral of the turbulent velocity component, as derived in Chapter 4. The pulse repetition period should be longer than the transit time of the pulse across the pipe, and this pulse repetition frequency should exceed twice the bandwidth of the flow turbulence signal, in order to give an accurate reconstruction of the flow turbulence. A sample-and-hold circuit is employed to approximate the reconstruction of the flow turbulence between subsequent pulses. The working of the entire circuit has been tested by detecting water currents artificially generated in a tank.

The development of the technique has been supported by a theoretical model of the ultrasonic pulse transmission and reception process. A numerical simulation of the flowmeter based on the theoretical model has been carried out. The ultrasonic transducer is modeled as a second order underdamped system with $\zeta = 0.15$ which corresponds to 6 dB bandwidth of 48 %. The change in time of flight (Δt) of the pulses caused by the turbulent velocity component is modeled as a random variable. For each excitation pulse the value of Δt is obtained from a pseudo random number generator. The two receiver outputs and the differential amplifier output are calculated. The sampled value of the differential amplifier output at appropriate instant gives the value of turbulence signal for the particular excitation pulse. Successive values for a sequence of excitation pulses are used to obtain the discretized version of the turbulence signal at the upstream sensing location. Assuming that the turbulence pattern is unchanged between the two sensing locations, the signal at the downstream location is obtained as a delayed version of the upstream signal, and the cross-correlation function is calculated. In the cross-correlation function, a distinct peak is found at the position corresponding to the delay between the upstream and downstream signals. The effect of dispersion in the turbulence pattern as it moves along the pipe has been studied by adding various proportions of random noise in the downstream signal. It has been observed that the peak in the cross-correlation function becomes less dominant with more dispersion in the turbulence pattern. This implies that the dispersion in the turbulence pattern determines the upper limit of sensor spacing. For very large sensor spacings the peak in the cross-correlation function may be indistinct and may have a flat top causing errors in the estimation of the peak position. On the other hand small sensor spacings give large peak in the cross-correlation function. In actual implementation of the scheme, the sensed signals will be digitized using a fixed number of bits, n . The effect of quantization errors has been studied by adding random noise to the two sensed waveforms of 1024 sample length. The random

noise is added in proportion corresponding to the quantization error for various number of bits, viz. $n = 8, 4, 2, 1$. It has been found that the sharpness of the peak decreases as the number of quantization bits decreases, and that the cross-correlation function with $n = 8$ is almost identical to that obtained without quantization. Therefore, 8-bit quantization is adequate for digitizations.

A system has been built for sensing turbulence at two locations on a pipe. This system is employed for flow measurement non-intrusively, using ultrasonic transducers clamped on a PVC pipe in a water circulation system. Transducers with resonant frequency of 2.2 MHz have been used. The turbulence signals sensed at the two locations were sampled and cross-correlated with the help of a signal analyzer. The sampling rate was fixed at 1 k samples/s and record length of 1000 samples was used for computing the cross-correlation function. The cross-correlation function gave unique and consistent peak. The volumetric flow measured by the cross-correlation meter was calculated assuming uniform flow profile and compared with that of a venturimeter. The graphs of the flow measured by cross-correlation versus that of the venturimeter were plotted for various sensor spacings. It has been observed that at smaller sensor spacing, the deviation from the best fit line is more because of poor flow resolution due to smaller transit time. On the other hand, for larger sensor spacing the deviation is because of the decrease in the correlation due to break-up in turbulence pattern, as it gives broad and less distinct peak and causes error in estimating the position of the peak. It is also noted that the cross-correlation flowmeter reads higher, the reason being that the eddies at the center of the pipe are more persistent and contribute more to the cross-correlation function.

In order to estimate the precision of the measurement, graphs of standard deviation of transit time of turbulence pattern σ_τ and corresponding standard deviation of the flow measured by cross-correlation σ_Q versus mean flow measured by cross-correlation \bar{Q}_C have been plotted (Fig. 5-5). From the graphs of σ_τ versus \bar{Q}_C , it is observed that in general σ_τ decreases at higher flow rates. The mean value $\bar{\sigma}_Q$ obtained over the flow range of 300–600 L/min for various sensor spacings (Table 5-4) shows that $\bar{\sigma}_Q$ is minimum (7 L/min) for the sensor spacing of 101 mm, and maximum (19 L/min) for the sensor spacing of 35 mm. The mean relative error, $\bar{\sigma}_Q/\bar{Q}$ over the full flow range is minimum (1.45 %) for the sensor spacing of 101 mm. Thus, it may be concluded that the best precision over the flow range of 300–600 L/min for pipe diameter of 90 mm is obtained for sensor spacing of about 100 mm. The relative error for this spacing was found to be in the range of 0.7–2.6 %.

In the water circulation set-up built in the laboratory, fluctuations up to 20 L/min, comparable to the values of σ_o , have been observed. The fluctuations may have been generated by the pump, pipe bends, and pipe vibrations. These fluctuations could have degraded the precision in the flow measurement. The fluctuations at the measurement location can be reduced by increasing the upstream straight pipe length, and adding a flow straightener at an appropriate place in the pipeline [3], [31]–[33]. It will help in better estimation of the precision of the measurement set-up.

The range of the cross-correlation flowmeter can be calculated based on the following criteria: The position of the peak in the cross-correlation function is between 100 ms and 333 ms, so that the resolution is better than 1 % and at least two third samples contribute to the cross-correlation function near the peak. Thus, the minimum velocity that can be measured by the system is 0.1 m/s, and maximum velocity is 2.5 m/s for all sizes of pipes except for those with inner diameter less than 36 mm, as the Reynolds number falls below 4000 and the flow is not turbulent. For pipes with inner diameter less than 36 mm, the lower flow velocity limit is decided by the Reynolds number.

As discussed in Chapter 5, the precision of the measurement is affected by the relative resolution of the measurement of the turbulence transit time τ_m . Since the resolution of τ_m is dependent on the sampling rate, the sampling rate should be so adjusted that the relative resolution of τ_m remains unchanged.

In the system used for flow measurement, a signal analyzer has been used for data acquisition and cross-correlation function calculation. A dedicated instrument may be developed that involves hardware for ultrasound transmission and reception, and digital signal processing hardware interfaced to a 2-channel ADC and display. The author has developed a cross-correlator with adjustable sampling rate in order to get optimum resolution for given sensor spacing and flow rate. The cross-correlator uses a DSP (TMS320C25) add-on board in a PC. The DSP board samples the signals using the on-board ADC and calculates the cross-correlation function, while the PC finds the location of the peak in the cross-correlation function, calculates the volumetric flow and decides the optimum sampling rate. A trial run of this system has been satisfactory as tested on the modified water circulation system that included a flow straightener and longer straight pipes. Experiments with the set-up and analysis of the test results need to be carried out. The system explained above may be developed as a stand alone unit consisting of the DSP processor interfaced to ADC, microcontroller, and display.

The experiments have been carried out on a PVC pipe, as PVC has an acoustic impedance ($3.2 \times 10^6 \text{ kg/m}^2\text{s}$) close to that of water ($1.5 \times 10^6 \text{ kg/m}^2\text{s}$) and the coupling of ultrasound is good. Since steel has the acoustic impedance ($45 \times 10^6 \text{ kg/m}^2\text{s}$) much higher than that of water, the coupling of ultrasound is poor in steel pipes, and the instrumentation set-up may require high power ultrasonic transmitters and high gain receiver amplifiers.

In the system developed for sensing turbulence, shown as a block diagram in Fig. 3-1, the differential amplifier output is sampled by the sample-and-hold, and the sampling instant is derived by a preset delay from the instant of pulse transmission. The delay is generated by a monostable multivibrator and set equal to the time of flight of the received pulses at no flow. A change in temperature of fluid will alter the time of flight of the pulses and affect the sensitivity of measurement. As the turbulent velocity components alter the time of flight of the pulses by equal amount but in opposite directions, the pulse obtained by addition represents the pulse at no flow. In order to reduce the effect of temperature, the sampling instant should be derived from the addition of the two received pulses.

In summary, the problems associated with the use of continuous wave ultrasound for non-intrusive measurement of single-phase fluid flow by cross-correlation have been studied, a new technique for sensing naturally occurring turbulence in the flow has been developed, and the technique has been applied for flow measurement by using cross-correlation of the turbulence patterns sensed at two locations on the pipe. A theoretical model of the technique has been developed, and a numerical simulation of the flowmeter based on the model has been carried out. The technique has been experimentally verified by building the hardware, and employing it for the measurement of water flow non-intrusively on a PVC pipe in a water circulation system for various sensor spacings.

The technique can be used for flow measurement with high precision. The sensors of the meter are non-intrusively clamped on the pipe, and the meter does not introduce any pressure drop in the flow line. The flowmeter does not have any mechanical inertia and the response time is governed by the record length for cross-correlation which can be of the order of a second or less. The turbulence sensing hardware need not be calibrated, and the variations in the characteristics of the ultrasonic transducers does not degrade the performance of the flowmeter. The issues related to the flow range as a function of pipe diameter, choice of sampling rate and sensor spacing, effect of temperature, and development of dedicated instrumentation have been discussed.

Appendix A

ABSTRACT OF DATA SHEETS

- A.1 LM733C Differential Video Amplifier
(National Semiconductor Corporation, Santa Clara, CA, 1988)

- A.2 SHC605 High-Speed Operational Track-And-Hold Amplifier
(Burr-Brown Corporation, Tucson, AZ, 1992)

- A.3 SHC5320 High Speed Bipolar Monolithic Sample/ Hold Amplifier
(Burr-Brown Corporation, Tucson, AZ, 1992)

A.1 LM733C Differential Video Amplifier

Absolute Maximum Ratings

Differential Input Voltage	±5V
Common Mode Input Voltage	±6V
V _{CC}	±8V
Output Current	10 mA
Power Dissipation	500 mW

Electrical Characteristics (T_A=25°C, V_S=±6.0V)

Parameter	Test Conditions	Min	Typ	Max	Units	
Differential Voltage Gain						
Gain 1 (Note 1)	R _L =2kΩ, V _{OUT} =3V _{P-P}	250	400	600		
Gain 2 (Note 2)		80	100	120		
Gain 3 (Note 3)		8	10	12		
Bandwidth						
Gain 1	V _{OUT} =1V _{P-P}		40		MHz	
Gain 2			90		MHz	
Gain 3			120		MHz	
Rise Time						
Gain 1			10.5		12	ns
Gain 2			4.5			ns
Gain 3		2.5			ns	
Propagation Delay						
Gain 1	V _{OUT} =1V _{P-P}		7.5		ns	
Gain 2			6.0	10	ns	
Gain 3			3.6		ns	
Input Resistance						
Gain 1	Gain 2	10	4.0		kΩ	
Gain 2			30		kΩ	
Gain 3			250		kΩ	
Input Capacitance			2.0		pF	
Input Offset Current			0.4	5.0	μA	
Input Bias Current			9.0	30	μA	
Input Noise Voltage	BW=1kHz to 10MHz		12		μV _{rms}	
Common Mode Rejection Ratio						
Gain 2	V _{CM} =±1V, f≤100kHz	60	86		dB	
Gain 2			60		dB	
Supply Voltage Rejection Ratio	V _{CM} =±1V, f=5MHz	50	70		dB	
Gain 2						
Output Offset Voltage						
Gain 1	R _L =∞		0.6	1.5	V	
Gain 2 and 3			0.35	1.5	V	
Output Common Mode Voltage	R _L =∞	2.4	2.9	3.4	V	
Output Voltage Swing (Diff.)	R _L =2kΩ	3.0	4.0		V _{P-P}	
Output Sink Current			2.5	3.6		mA
Output Resistance			20		Ω	

Note 1: Pins G1A and G1B connected together.

Note 2: Pins G2A and G2B connected together.

Note 3: Gain select pins open.

A.2 SHC605 High-Speed Operational Track-And-Hold Amplifier

Absolute Maximum Ratings

Power Supply	±7V
Input Voltage Range	±5V
Differential Input Range	±5.5V
Output Short Circuit	Continuous to Ground

Electrical Characteristics ($T_A=25^\circ\text{C}$, $V_S=\pm 6.0\text{V}$, $G=1\text{V/V}$, $R_L=100\Omega$, $C_L=5\text{pF}$)

Parameter	Test Conditions	Min	Typ	Max	Units
DC INPUT PARAMETERS					
Offset Voltage			±1	±7.5	mV
Power Supply Rejection	$V_S=\pm 4.5\text{V}$ to $\pm 5.5\text{V}$	60	85		dB
Input Bias Current	$V_{CM}=0\text{V}$		15	50	μA
Input Offset Current	$V_{CM}=0\text{V}$		±0.2	±5	μA
Common Mode Input Range		±2.0	±2.5		V
Common Mode Rejection	$V_{CM}=\pm 2\text{VDC}$		80		dB
Differential Input Impedance			13 1		kΩ pF
Common Mode Input Impedance			2 1		kΩ pF
Open Loop Voltage Gain	$V_O=\pm 2\text{V}$, $R_L=100\Omega$		100		dB
OUTPUT					
Voltage Output	$R_L=50\Omega$	±2.0	±2.5		V
Current Output		±40	±80		mA
Short Circuit Current			±140		mA
Output Resistance, Open Loop	DC		0.1		mΩ
TRACK-MODE RESPONSE					
Closed-Loop Bandwidth	Gain=1	100	200		MHz
	Gain=2		75		MHz
	Gain=5		20		MHz
	Gain=10		10		MHz
Full Power Response	±1V Input, -3dB Output		32		MHz
Slew Rate	Gain=1, 2V Step	140	200		V/μs
Acquisition Time to 1%	2V Step		15	25	ns
0.1%	2V Step		23	35	ns
0.012%	2V Step		30	45	ns
0.012%	4V Step		40	60	ns
TRACK-TO-HOLD SWITCHING					
Aperture Delay	$V_{IN}=0\text{V}$		1.7		ns
Aperture Jitter			2.4		ps rms
Pedestal Offset			±5	±20	mV
Transient Amplitude			±5		mV
Settling Time to 1mV			8	15	ns
100μV			15		ns
HOLD-MODE RESPONSE					
Droop Rate			±1	±8	mV/μs
Hold Time				2	μs
Feedthrough Rejection			85		dB

A.3 SHC5320 High Speed Bipolar Monolithic Sample/ Hold Amplifier

Absolute Maximum Ratings

Voltage between +V _{CC} and -V _{CC}	40V
Input Voltage Range	Actual Supply Voltage
Differential Input Voltage	±24V
Digital Input Voltage	+15V, -1V
Output Current, Continuous	±20mA
Output Short Circuit Duration	None

Electrical Characteristics (At 25°C, rated power supplies, with internal hold capacitor)

Parameter	Test Conditions	Min	Typ	Max	Units
INPUT CHARACTERISTICS					
ANALOG					
Voltage Range		±10			V
Common-Mode Range		±10			V
Input Resistance		1	5		MΩ
Input Capacitance				3	pF
OUTPUT CHARACTERISTICS					
Voltage Range		±10			V
Current		±10			mA
Output Impedance	Hold Mode		1		Ω
Noise, DC to 10MHz			125	200	μVrms
DC ACCURACY/STABILITY					
Gain, Open Loop, DC		3×10 ⁵	2×10 ⁶		V/V
Input Offset Voltage			±0.5		mV
Input Offset Voltage Drift			±5	±20	μV/°C
CMRR	V _{CM} =±5VDC	72	90		dB
HOLD-TO-SAMPLE MODE					
DYNAMIC CHARACTERISTICS					
Acquisition Time to ±0.01% ±0.1%	Gain=-1, V _O =10V Step		1 0.8	1.5 1.2	μs μs
SAMPLE MODE					
Gain-Bandwidth Product	V _O =200mVp-p, C _H =100pF		2		MHz
	C _H =1000pF		180		kHz
Full Power Bandwidth	V _{IN} =±20Vp-p		600		kHz
Slew Rate	V _O =20V Step		45		V/μs
SAMPLE-TO-HOLD MODE					
DYNAMIC CHARACTERISTICS					
Aperture Time	Simulated		25		ns
Effective Aperture Time		-50	-25	0	ns
Aperture Uncertainty			0.3		ns
Charge Offset (Adjustable to 0)	V _{IN} =0V		1	5	mV
Settling Time to ±0.01% of FSR			165	350	ns
HOLD MODE					
Droop	V _{IN} =0V		0.08	0.5	μV/μs
Feedthrough	V _{IN} =10Vp-p, 100kHz sine		2		mV
POWER SUPPLIES					
+V _{CC}		+12	+15	+18	V
-V _{CC}		-12	-15	-18	V

Appendix B

SPECIFICATIONS OF THE SIGNAL ANALYZER (*Analogic model DATA6000 with plug in module 620*)

Specifications of DATA6000 Mainframe:

CPU	: 16 bit, 8 MHz
Memory	: 48K ROM 64K RAM
Display	: 9 in. CRT: X, Y, Z, type
Screen Resolution	: 1024 X 512
Display modes	: 1 trace (Full screen) 2 traces (Half screen per trace) 4 traces (Quarter screen per trace)
Overlaid	: 2 traces overlaid (Full screen) 4 traces overlaid (full screen) X vs Y
Data Format	: Block Floating Point. 16 bit integer array values. 32 bit real scale.
Data Records	: up to 64 K data points.
Record Operations	: Assign, delete, add, subtract, multiply, divide, spectrum magnitude plus phase for real and complex inputs, cross correlation, auto correlation, differentiation, integration, n-point convolution (averaging).
Interfaces	: Dual floppy (1.5 MB of storage for data, text, control set-ups, programs, and extensions). RS232 IEEE488 X-Y plotter PLOT-10 plotter
Remote Control	: All functions are readable and programmable over RS232 or IEEE488 I/O.

Specifications of Model 620 (100 Megasamples/second plug-in):

Basic System Accuracy	: +(0.5% of inp + lsd)
Automatic Calibration	: Every 200 seconds with override. Once every 15 minutes (default) User selectable 1/frame, 5 min, 15min, 1 hour, off.
System Drift Rate	: <(0.1% + 1 mV) 4 hours after calibration
Number of channels	: 2 independent
Maximum Safe Voltage	
Any input Hi	
to Input Common	: 120 Vrms indefinitely
Input isolation	: Double guarded
Input Impedance	: 1 Megohm 47 pF
Input range	: +1V (+1.2V), resolution 10 mV +3V (+3.6V), resolution 30 mV
Power Bandwidth (3dB)	: 20 MHz
Rise/Fall Time	
(settling to 1%)	: <20ns
Slew Rate	: Linear front end over specified bandwidth with no slew rate limitations
Overshoot	: <1%
Input coupling	: dc or ac
CMRR	: >60 dB dc to 1 kHz >30 dB 1 kHz to 10 kHz
Filter (Fixed)	: 20 MHz, 3 dB
Noise	
(Referenced to Input)	: +1/3 LSB rms, typical +1/2 LSB rms, maximum
Signal to Noise Ratio	
Full Scale 5 kHz	: 44 dB
Full Scale 1 MHz	: 42 dB
Full Scale 5 MHz	: 40 dB
Full Scale 20 MHz	: 32 dB
Offset Voltage	
(Referenced to Input)	: <1/2 LSB (with autocal).

References

- [1] B. G. Liptak, *Instrument Engineers' Handbook, vol. 1 – Process Measurement and Analysis*. London: Butterworth-Heinemann, 1995.
- [2] D. M. Considine, *Process Instruments and Control Handbook*. Toronto: McGraw-Hill, 1985.
- [3] R. W. Miller, *Flow Measurement Engineering Handbook*. New York: McGraw-Hill, 1989.
- [4] E. O. Doebelin, *Measurement Systems – Application and Design*. New York: McGraw-Hill, 1990.
- [5] C. S. Rangan, G. R. Sarma, and V. S. mani, *Instrumentation – Devices and Systems*. New Delhi: Tata McGraw-Hill, 1983.
- [6] Y. L. Arora, *Flow Measurement Techniques*. Bombay: U.B.S., 1978.
- [7] D. Patranabis, *Principles of Industrial Instrumentation*. New Delhi: Tata McGraw-Hill, 1986.
- [8] M. S. Beck and A. Plaskowski, *Cross Correlation Flowmeters – Their Design and Application*. Bristol, UK: Adam Hilger, 1987.
- [9] W. Balchandran and M. S. Beck, "Solids concentration measurement and flow measurement of slurries and sludges using ultrasonic sensors with random data analysis, Part 1: Solids-concentration measurement," *Transactions of the Institute of Measurement and Control*, vol. 2, No. 4, pp. 181–197, Dec. 1980.
- [10] L. A. Xu, R. G. Green, A. Plaskowski, and M. S. Beck, "The pulsed ultrasonic cross-correlation flowmeter for two-phase flow measurement," *Journal of Physics E: Scientific Instruments*, vol. 21, pp. 406–414, 1988.
- [11] M. S. Beck, "Correlation in instruments: Cross correlation flowmeter," *Journal of Physics E : Scientific Instruments*, vol. 14, pp. 7–19, 1981.
- [12] J. G. Proakis and D. G. Manolakis, *Digital Signal Processing – Principles, Algorithms, and Applications*. New Delhi: Prentice-Hall of India, 1997.

- [13] B. P. Lathi, *Modern Digital and Analog Communication Systems*. San Francisco: Holt, Rinehart and Winston, 1989.
- [14] J. Coulthard, "Cross-correlation flow measurement – a history and the state of the art," *Measurement and Control*, vol. 16, pp. 214–218, Jun. 1983.
- [15] J. Coulthard and Y. Yan, "Ultrasonic cross-correlation flowmeters," *Measurement+Control*, vol. 26, pp. 164–167, Aug. 1993.
- [16] K. H. Ong and M. S. Beck , "Slurry flow velocity, concentration and particle size measurement using flow noise and correlation technique," *Measurement and Control*, vol. 8, pp. 453–463, 1975.
- [17] L. E. Kinsler and A. R. Frey, *Fundamentals of Acoustics*. New York: John Wiley, 1962.
- [18] L. C. Lynnworth, *Ultrasonic Measurement for Process Control – Theory, Techniques, Applications*. San Diego, CA: Academic, 1989.
- [19] J. O. Hinze, *Turbulence: An Introduction to Its Mechanism and Theory*. New York: McGraw-Hill, 1975.
- [20] J. Krautkramer and H. Krautkramer, *Ultrasonic Testing of Materials*. Berlin: Springer-Verlag, 1990.
- [21] *Intersil Applications Handbook*. Cupertino, CA: Intersil Inc., 1988.
- [22] *Linear IC Databook*. Santa Clara, CA: National Semiconductor Corporation, 1988.
- [23] *Burr-Brown Integrated Circuits Data Book*. Tucson, AZ: Burr-Brown Corporation, 1992.

- [24] H. B. Nemade, T. Anjaneyulu, and P. C. Pandey, "Sensing turbulence transit time by pulsed ultrasound for single-phase fluid flow measurement," *IEEE Transactions on Instrumentation and Measurement*, vol. 47, no. 1, pp. 265–269, Feb. 1998.
- [25] A. K. Sawhney, *A course in Electrical and Electronic Measurements and Instrumentation*. Delhi: Dhanpat Rai & Sons, 1985.
- [26] K. Ogata, *Modern Control Engineering*. New Delhi: Prentice-Hall of India, 1986.
- [27] W. B. Andrews and H. B. Williams, *Applied Instrumentation in Process Industries, vol. 3, Engineering Data and Resource Material*. Houston, TX: Gulf, 1982.
- [28] J. F. Douglas, J. M. Gasiorek, and J. A. Swaffield, *Fluid Mechanics*. Harlow, UK: Addison-Wesley, 1999.
- [29] N. P. Cheremisinoff, *Fluid flow – Pumps, Pipes and Channels*. Ann Arbor, MI: Ann Arbor Science, 1981.
- [30] M. S. Beck, "Recent developments and the future of cross-correlation flowmeters," *Proceedings of International Conference on Advances in Flow Measurement Techniques* (Warwick, UK), Sep. 1981. Bedford: BHRA, 1981, pp. 241–253.
- [31] *Shell Flow Meter Engineering Handbook*. London: McGraw-Hill, 1985.
- [32] H. P. Kallen, *Handbook of Instrumentation and Controls*. New York: McGraw-Hill, 1961.
- [33] C. J. Benard, *Handbook of Fluid Flowmetering*. Surrey, UK: Trade & Technical Press, 1988.

Synopsis

Flow measurement by cross-correlation involves sensing disturbances in the flow at two locations on a pipe, and estimating the transit time of the tagging markers between the two locations, with the help of the cross-correlation function of the signals. If $x(t)$ and $y(t)$ are the two signals derived from the upstream and downstream sensors, respectively, the cross-correlation function $r_{yx}(\tau)$ relating these signals in terms of the time delay τ is given by the expression

$$r_{yx}(\tau) = \lim_{T \rightarrow \infty} \frac{1}{T} \int_0^T x(t-\tau) y(t) dt$$

where T represents the period of integration. The transit time of the disturbances τ_m is determined as the delay corresponding to the peak in the cross-correlation function. The flow velocity u is calculated from

$$u = \frac{L}{\tau_m}$$

where L represents the sensor spacing. Since only the transit time is measured between two fixed locations, the flowmeter is largely unaffected by wide variations in the fluid properties and environmental factors. In addition, the sensors do not need to be linear, and the DC stability of the sensors is not important. However, phase delay does need careful consideration.

Ultrasonic sensing facilitates non-intrusive flow measurement and the pressure drop due to the flowmeter is nil. The research is aimed at applying the cross-correlation principle using ultrasonic sensing for the flow measurement of single-phase fluid, like clean water.

The most common method of sensing disturbances in fluid flow using ultrasound is by detecting modulation of a continuous wave ultrasonic beam transmitted across the diameter of the pipe. Usually two continuous wave type ultrasonic transducers are mounted diametrically opposite to each other on the pipe. One transducer transmits the ultrasound into the fluid and the other one placed opposite receives the signal modulated by the fluid disturbances. The only disturbance present in a single-phase fluid flow is the turbulence. The turbulent eddies cause phase modulation of the ultrasound. The major drawback of using continuous wave ultrasound is that the fluid-borne signal is superimposed by reflections from the inner pipe wall, reflections within the pipe wall, and acoustic short circuit through the pipe wall. We studied these sources

of interference and deduced that the continuous wave ultrasound would be unsuitable for single-phase flow measurement. As an alternative, the viability of pulsed ultrasound for sensing turbulence was investigated .

A steady turbulent flow can be regarded as a mean flow vector, with additional fluctuating velocities that are mainly the result of irregular motions of the eddies. Thus, the turbulent component normal to the flow-axis can be sensed as the variation in time of flight (TOF) of an ultrasonic pulse, transmitted along the pipe diameter. However, the variation is extremely small (a few ns) compared with the TOF of the pulse across the pipe diameter, and, therefore, difficult to measure reliably. Besides, the uncertainty in detecting the exact instant of arrival of the pulse is considerably large. A new technique for sensing turbulence using pulsed ultrasound has been developed to overcome these difficulties. Two ultrasonic transducers, both of which act as the transmitters and receivers, are mounted diametrically opposite to each other on the pipe wall. The transducers facing each other transmit ultrasonic pulses at the same instant and in the opposite directions. The pulses, after traveling through the fluid in the pipe, are received by the transducers which now act as the receivers, and the receiver outputs are fed to a differential amplifier.

The turbulent velocity components, along the axis of placement of the transducers, alter the velocity of the pulses and the instants of arrival of the pulses at the receivers are different. The output of the differential amplifier is sampled at the peak, in order to maximize the sensitivity to the turbulent velocity component. The sampled value is a function of the line integral of the turbulent velocity components encountered by the pulses. Since the turbulent velocity component alters the TOFs of the two pulses by the same magnitude but in opposite directions, the magnitude of the turbulent velocity component does not alter the sampling instant and it can be derived from the instant of pulse transmission with the help of a preset delay. A train of pulses is used for periodically sampling the turbulent velocity component. The pulse repetition frequency should exceed twice the bandwidth of the flow turbulence signal, in order to obtain proper reconstruction of the turbulence signal. A sample-and-hold amplifier and a low pass filter is employed for this purpose. The working of the entire circuit has been tested by detecting water currents artificially generated in a tank. The turbulence pattern sensed at two locations on the pipe can be cross-correlated and flow velocity can be obtained from the position of the peak in the cross-correlation function.

The development of the technique has been supported by a theoretical model of the ultrasonic pulse transmission and reception process. A numerical simulation of the flowmeter based on the theoretical model has been carried out.

The ultrasonic transducer is modeled as a second order underdamped system with $\zeta = 0.15$ which corresponds to 6 dB bandwidth of 48 %. The change in time of flight (Δt) of the pulses caused by the turbulent velocity component is modeled as a random variable. For each excitation pulse the value of Δt is obtained from a pseudo random number generator. The two receiver outputs and the differential amplifier output are calculated. The sampled value of the differential amplifier output at appropriate instant gives the value of turbulence signal for the particular excitation pulse. Successive values for a sequence of excitation pulses are used to obtain the discretized version of the turbulence signal at the upstream sensing location. Assuming that the turbulence pattern is unchanged between the two sensing locations, the signal at the downstream location is obtained as a delayed version of the upstream signal, and the cross-correlation function is calculated. The effect of dispersion in the turbulence pattern as it moves along the pipe has been studied by adding various proportions of random noise in the downstream signal. It has been observed that the peak in the cross-correlation function becomes less dominant with more dispersion in the turbulence pattern. This implies that the dispersion in the turbulence pattern determines the upper limit of sensor spacing. For very large sensor spacings the peak in the cross-correlation function may be indistinct and may have a flat top causing errors in the estimation of the peak position. On the other hand small sensor spacings give large peak in the cross-correlation function. In practice, the sensed signals are quantized using fixed number of bits. The effect of quantization error on the peak in the cross-correlation function has been studied for various number of quantization bits. Random noise in proportion corresponding to the quantization is added in both the sensed signals error and the cross-correlation function is calculated. For a signal length of 1024 samples, it has been found that the sharpness of the peak in the cross-correlation function decreases as the number of quantization bits decreases, and that 8-bit quantization is adequate for digitizing the signals, as it does not result in any appreciable broadening of the peak.

A system has been built for sensing turbulence at two locations on a pipe and employed for the measurement of flow non-intrusively, using ultrasonic transducers clamped on a PVC pipe in a water circulation system. The transducers with resonant frequency of 2.2 MHz have been used. The turbulence signals sensed at the two locations were sampled and cross-correlated with the help of a signal analyzer. The sampling rate was fixed at 1 k samples/s and record length of 1000 samples was used for computing the cross-correlation function. The cross-correlation function gave unique and consistent peak. The volumetric flow measured by the cross-correlation meter was calculated assuming uniform flow profile and compared with that of a venturimeter. The graphs of the flow measured by cross-correlation versus that of the venturimeter

were plotted for various sensor spacings. It has been observed that at smaller sensor spacing, the deviation from the best fit line is more because of poor flow resolution due to smaller transit time. On the other hand, for larger sensor spacing the deviation is because of the decrease in the correlation due to break-up in turbulence pattern, as it gives broad and less distinct peak and causes error in estimating the position of the peak. It is also noted that the cross-correlation flowmeter reads higher, the reason being that the eddies at the center of the pipe are more persistent and contribute more to the cross-correlation function.

In order to estimate the precision of the measurement, graphs of standard deviation of transit time of turbulence pattern σ_τ and corresponding standard deviation of the flow measured by cross-correlation σ_Q versus mean flow measured by cross-correlation \bar{Q}_C have been plotted. From the graphs of σ_τ versus \bar{Q}_C , it is observed that in general σ_τ decreases at higher flow rates. The mean values $\bar{\sigma}_Q$ obtained over the flow range of 300–600 L/min for various sensor spacings show that $\bar{\sigma}_Q$ is minimum (7 L/min) for the sensor spacing of 101 mm, and maximum (19 L/min) for the sensor spacing of 35 mm. The mean relative error, $\bar{\sigma}_Q/\bar{Q}$ over the full flow range is minimum (1.45 %) for the sensor spacing of 101 mm. Thus, it may be concluded that the best precision over the flow range of 300–600 L/min for pipe diameter of 90 mm is obtained for sensor spacing of about 100 mm. The relative error for this spacing was found to be in the range of 0.7–2.6 %.

In summary, the problems associated with the use of continuous wave ultrasound for non-intrusive measurement of single-phase fluid flow by cross-correlation have been studied, a new technique for sensing naturally occurring turbulence in the flow has been developed, and the technique has been applied for flow measurement by using cross-correlation of the turbulence patterns sensed at two locations on the pipe. A theoretical model of the technique has been developed, and a numerical simulation of the flowmeter based on the model has been carried out. The technique has been experimentally verified by building the hardware, and employing it for the measurement of water flow non-intrusively on a PVC pipe in a water circulation system for various sensor spacings.
